



This is a repository copy of *Charged-hadron and identified-hadron ($K^0 S, \bar{K}^0, \pi^\pm$) yield measurements in photonuclear $Pb+Pb$ and $p+Pb$ collisions at $\sqrt{s_{NN}} = 5.02\text{TeV}$ with ATLAS*.

White Rose Research Online URL for this paper:

<https://eprints.whiterose.ac.uk/228973/>

Version: Published Version

Article:

Aad, G. orcid.org/0000-0002-6665-4934, Aakvaag, E. orcid.org/0000-0001-7616-1554, Abbott, B. orcid.org/0000-0002-5888-2734 et al. (2906 more authors) (2025) Charged-hadron and identified-hadron ($K^0 S, \bar{K}^0, \pi^\pm$) yield measurements in photonuclear $Pb+Pb$ and $p+Pb$ collisions at $\sqrt{s_{NN}} = 5.02\text{TeV}$ with ATLAS. *Physical Review C*, **111** (6). 064908. ISSN 2469-9985

<https://doi.org/10.1103/7lx4-x8rw>

Reuse

This article is distributed under the terms of the Creative Commons Attribution (CC BY) licence. This licence allows you to distribute, remix, tweak, and build upon the work, even commercially, as long as you credit the authors for the original work. More information and the full terms of the licence here:
<https://creativecommons.org/licenses/>

Takedown

If you consider content in White Rose Research Online to be in breach of UK law, please notify us by emailing eprints@whiterose.ac.uk including the URL of the record and the reason for the withdrawal request.

Charged-hadron and identified-hadron (K_S^0 , Λ , Ξ^-) yield measurements in photonuclear $\text{Pb} + \text{Pb}$ and $p + \text{Pb}$ collisions at $\sqrt{s_{NN}} = 5.02 \text{ TeV}$ with ATLAS

G. Aad *et al.**
(ATLAS Collaboration)



(Received 12 March 2025; accepted 5 May 2025; published 17 June 2025)

This paper presents the measurement of charged-hadron and identified-hadron (K_S^0 , Λ , Ξ^-) yields in photonuclear collisions using 1.7 nb^{-1} of $\sqrt{s_{NN}} = 5.02 \text{ TeV}$ $\text{Pb} + \text{Pb}$ data collected in 2018 with the ATLAS detector at the Large Hadron Collider. Candidate photonuclear events are selected using a combination of tracking and calorimeter information, including the zero-degree calorimeter. The yields as a function of transverse momentum and rapidity are measured in these photonuclear collisions as a function of charged-particle multiplicity. These photonuclear results are compared with 0.1 nb^{-1} of $\sqrt{s_{NN}} = 5.02 \text{ TeV}$ $p + \text{Pb}$ data collected in 2016 by ATLAS using similar charged-particle multiplicity selections. These photonuclear measurements shed light on potential quark-gluon plasma formation in photonuclear collisions via observables sensitive to radial flow, enhanced baryon-to-meson ratios, and strangeness enhancement. The results are also compared with the Monte Carlo DPMJET-III generator and hydrodynamic calculations to test whether such photonuclear collisions may produce small droplets of quark-gluon plasma that flow collectively.

DOI: [10.1103/7lx4-x8rw](https://doi.org/10.1103/7lx4-x8rw)

I. INTRODUCTION

When ultrarelativistic beams of lead nuclei are brought into collision, the processes often studied are those for which the nuclei have an impact parameter smaller than twice the nuclear radius. Such collisions are now understood to create droplets of quark-gluon plasma (QGP) that flow as a nearly perfect fluid, i.e., hydrodynamically [1]. However, the strong electromagnetic (EM) fields of the fully ionized nuclei can also induce interactions when the nuclei have significantly larger impact parameters [2,3]. In the equivalent photon approximation, these strong EM fields correspond to a flux of quasi-real, high-energy photons. Importantly, the nuclei can produce high-energy photons coherently from the entire nucleus, resulting in an enhancement to the photon spectrum over a broad energy range which is proportional to Z^2 (e.g., atomic number $Z = 82$ for Pb).

As a result, the rates for EM interactions (which include photon–photon and photon–nucleus scatterings) are large enough to be measurable in $\text{Pb}+\text{Pb}$ collisions at the Large Hadron Collider (LHC). Such collisions are commonly referred to as “ultraperipheral collisions” (UPCs) because they can occur when the impact parameters between the incoming nuclei are large enough such that there is no hadronic interaction between the nuclei. The ATLAS Collaboration has measured UPC events where the basic interactions are

photon–photon collisions [4–7], including light-by-light scattering and scattering where two leptons in the final state are produced. The ATLAS Collaboration has also measured UPC photonuclear collisions, for example, in the case of dijet production [8]. In photonuclear reactions, the photon could act as a pointlike particle interacting with a parton in the nucleus (the “direct” case). However, the vector-meson dominance picture suggests that the photon could fluctuate to a vector meson, for example, a ρ meson, which then interacts with the Pb nucleus (the “resolved” case) [2,9]. Therefore, some subset of these collisions could be considered as ρ –nucleus collisions, albeit at a lower center-of-mass collision energy than the nucleon-nucleon $\sqrt{s_{NN}}$, depending on the ρ energy. Hence, such events will have an overall rapidity boost of the center-of-mass frame in the direction of the nucleus.

Two-particle azimuthal correlations have been measured in photonuclear ($\gamma + \text{Pb}$) events by ATLAS [10]. These results indicate significant nonzero elliptic (v_2) and triangular (v_3) flow coefficients. These coefficients have been interpreted in terms of a hydrodynamically flowing medium [11], and alternatively in terms of scattering diagrams in the glasma framework [12]. The v_2 values are significantly smaller in photonuclear events compared with $p + \text{Pb}$ events at the same charged particle multiplicity $N_{\text{ch}}^{\text{rec}}$. The lower elliptic flow in photonuclear events may be explained by the stronger longitudinal decorrelations in the rapidity-shifted photonuclear events in hydrodynamic calculations [11]. These authors make the specific prediction that the radial flow [13] is essentially the same in photonuclear and $p + \text{Pb}$ collisions, as measured via the mean transverse momentum, p_T , of charged and identified particles. The formation of a small QGP droplet may also lead to other manifestations of QGP seen in heavy-ion collisions such as a baryon/meson enhancement [14] and strangeness enhancement [15,16]. A measurement by CMS

*Full author list given at the end of the article.

of two-particle correlations in the lower-multiplicity $\gamma + p$ system did not find evidence for collective effects when compared to the expectation from event generators [17].

This paper presents the yields of charged hadrons and identified strange hadrons (K_S^0 , Λ , Ξ^-) in photonuclear collisions using 1.7 nb^{-1} of $\sqrt{s_{NN}} = 5.02 \text{ TeV}$ Pb+Pb data collected in 2018 with the ATLAS detector at the LHC. The results are compared with measurements in $p + \text{Pb}$ collisions specifically to test the predictions of Ref. [11]. Additionally, these photonuclear data are compared with the photonuclear Monte Carlo (MC) DPMJET-III [18,19] generator and with hydrodynamic calculations [11] to test the hypothesis of a small QGP droplet formation.

II. ATLAS DETECTOR

The ATLAS detector [20] at the LHC [21] covers nearly the entire solid angle around the collision point.¹ It consists of an inner tracking detector surrounded by a thin superconducting solenoid, electromagnetic and hadronic calorimeters, and a muon spectrometer incorporating three large superconducting magnets. The inner-detector system (ID) is immersed in a 2 T axial magnetic field and provides charged-particle tracking in the range $|\eta| < 2.5$.

The high-granularity silicon pixel detector covers the vertex region and typically provides three measurements per track. An innermost insertable B-layer [22] has been operating as a part of the pixel detector since 2015. It is followed by the silicon microstrip tracker (SCT) which usually provides four two-dimensional measurement points per track. These silicon detectors are complemented by the transition radiation tracker (TRT), which enables radially extended track reconstruction up to $|\eta| = 2.0$.

The calorimeter system covers the pseudorapidity range $|\eta| < 4.9$. Within the region $|\eta| < 3.2$, electromagnetic calorimetry is provided by barrel and endcap high-granularity lead/liquid-argon (LAr) electromagnetic calorimeters, with an additional thin LAr presampler covering $|\eta| < 1.8$, to correct for energy loss in material upstream of the calorimeters. Hadronic calorimetry is provided by the steel/scintillating-tile calorimeter, segmented into three barrel structures within $|\eta| < 1.7$, and two copper/LAr hadronic endcap calorimeters covering $1.5 < |\eta| < 3.2$. The angular coverage is completed with forward copper/LAr and tungsten/LAr calorimeter modules optimized for electromagnetic and hadronic measurements, respectively. The muon spectrometer (MS) surrounds the calorimeters and is based on three large air-core toroidal

superconducting magnets with eight coils each. The MS includes a system of precision tracking chambers and fast detectors for triggering. The minimum-bias trigger scintillator, reconfigured for Run 2, detects charged particles over $2.07 < |\eta| < 3.86$ using two hodoscopes of 12 counters positioned at $z = \pm 3.6 \text{ m}$. The zero-degree calorimeters (ZDCs) play a key role in identifying UPC events in heavy-ion collisions. They are located at $z = \pm 140 \text{ m}$ from the interaction point, just beyond the point where the common straight-section vacuum-pipe divides back into two independent beam-pipes. The ZDC modules consist of layers of alternating quartz rods and tungsten plates that measure neutral particles at pseudorapidities $|\eta| > 8.3$.

A two-level trigger system [23] is used to select events. The first-level trigger (L1) is implemented in hardware and uses a subset of the detector information to reduce the accepted rate to at most 100 kHz. This is followed by the software-based high-level trigger (HLT) that reduced the accepted event rate to 1–4 kHz depending on the data-taking conditions during 2018 Pb+Pb collisions.

A software suite [24] is used in data simulation, in the reconstruction and analysis of real and simulated data, in detector operations, and in the trigger and data acquisition systems of the experiment.

III. EVENT SELECTION AND SIMULATIONS

Photonuclear interactions are selected via event topologies where one of the Pb nuclei remains intact, resulting in no spectator neutrons and very sparse particle production downstream of the given nucleus. This is taken to be the photon-going direction. The datasets and event selection for photonuclear collisions are identical to those used in a previous measurement of two-particle azimuthal correlations [10], and are briefly summarized below.

The measurements presented in this paper were performed using the $\sqrt{s_{NN}} = 5.02 \text{ TeV}$ Pb+Pb dataset collected with a variety of triggers in 2018, with a total integrated luminosity of 1.7 nb^{-1} . The 25-track high-multiplicity trigger (HMT), 15-track HMT, and the minimum-bias (MB) trigger were configured with progressively higher prescale factors, sampling 1.6 nb^{-1} , 0.13 nb^{-1} , and $1.0 \mu\text{b}^{-1}$ of data, respectively. Photonuclear candidate events were first selected by the trigger requiring one ZDC side (referred to as the Pb-going side and corresponding to $\eta < 0$) to have a minimum amount of energy at L1, $E > 1 \text{ TeV}$, consistent with the presence of one or more neutrons. The other side (referred to as the photon-going side and corresponding to $\eta > 0$) was required to have energy below a maximum-energy cutoff, $E < 1 \text{ TeV}$, consistent with no neutrons. The per-nucleon energy is 2.5 TeV, leading to a single neutron peak energy well above this 1 TeV threshold [4]. The selected topology is referred to as “OnXn.” Events were also required to satisfy an upper bound of 200 GeV on the total transverse energy deposited across all central calorimeters at L1, for further rejection of hadronic Pb + Pb events.

Reconstructed pseudorapidity gap quantities, constructed using charged-particle tracks and clusters of energetic calorimeter cells in each event, are used to distinguish between different physics processes such as photonuclear col-

¹ATLAS uses a right-handed coordinate system with its origin at the nominal interaction point (IP) in the center of the detector and the z axis along the beam pipe. The x axis points from the IP to the center of the LHC ring, and the y axis points upwards. Cylindrical coordinates (r, Φ) are used in the transverse plane, Φ being the azimuthal angle around the z axis. The pseudorapidity is defined in terms of the polar angle θ as $\eta = -\ln \tan(\theta/2)$. Angular distance is measured in units of $\Delta R \equiv \sqrt{(\Delta\eta)^2 + (\Delta\Phi)^2}$. Both the rapidity and pseudorapidity are calculated in the center-of-mass frame per nucleon pair.

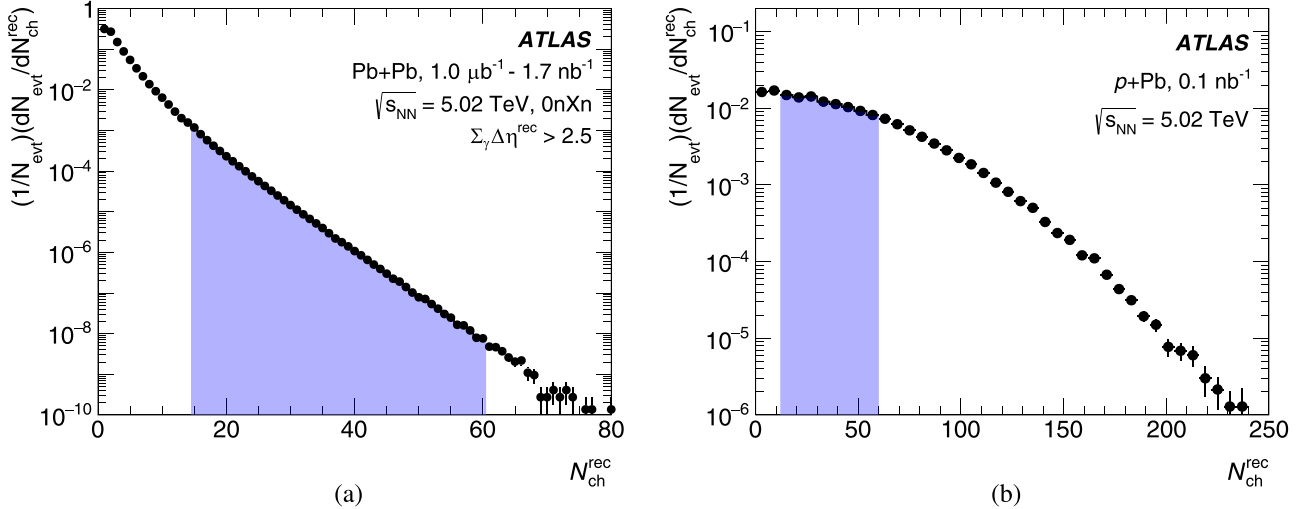


FIG. 1. Multiplicity distributions ($N_{\text{ch}}^{\text{rec}}$) from (a) Pb+Pb photonuclear and (b) $p + \text{Pb}$ collisions. The $N_{\text{ch}}^{\text{rec}}$ range utilized in this paper, $15 \leq N_{\text{ch}}^{\text{rec}} \leq 60$, is highlighted.

lisions, low-activity (peripheral) hadronic $\text{Pb} + \text{Pb}$ collisions, and $\gamma\gamma \rightarrow X$ processes. The requirement of a rapidity gap above a minimum value in the photon-going direction can efficiently remove peripheral $\text{Pb} + \text{Pb}$ events. Rather than the traditional pseudorapidity gap quantity [25], which determines the pseudorapidity difference between the edge of the detector and the closest particle, an alternative “sum-of-gaps” definition is used, which adds together contiguous gaps separated by particle production concentrated in a narrow pseudorapidity region. This alternative definition is used to retain a large selection efficiency for resolved photon events where a large contiguous pseudorapidity gap may otherwise be spoiled by a hadronic fragment on the photon-going side. The quantity $\sum_{\gamma} \Delta\eta^{\text{rec}}$ corresponds to the sum-of-gaps calculated in the photon-going half of the detector, and is constructed using tracks with $p_{\text{T}} > 0.4 \text{ GeV}$, $|\eta| < 2.5$ and clusters with $p_{\text{T}} > 0.2 \text{ GeV}$, $|\eta| < 4.9$ in each event. It is calculated by first sorting the tracks and clusters in η . The differences in η between adjacent particles, $\Delta\eta$, are included in the sum if they are larger than 0.5. The value of 0.5 was observed in the simulation to retain good efficiency for resolved photon events. The gap calculation is computed as always starting from mid rapidity to the edge of the detector; thus, $\sum_{\gamma} \Delta\eta^{\text{rec}}$ ranges from 0 to 4.9. UPC events with $\sum_{\gamma} \Delta\eta^{\text{rec}} > 2.5$ are utilized in this paper following the procedure in Ref. [10].

Despite the OnXn ZDC and $\sum_{\gamma} \Delta\eta^{\text{rec}}$ selections, a residual contamination of the photonuclear events by $\text{Pb}+\text{Pb}$ peripheral inelastic collisions remains, which is smaller than 3%. To account for this, a small purity correction factor and associated systematic uncertainties are applied, as performed in Ref. [10]. No other backgrounds, such as from $\gamma\gamma$ processes, were found to be significant after the event selection.

This paper includes comparisons with the 2016 $p + \text{Pb}$ collision data collected at $\sqrt{s_{\text{NN}}} = 5.02 \text{ TeV}$, with an integrated luminosity of 0.1 nb^{-1} , obtained using a minimum-bias trigger as detailed in Ref. [26]. In the $p + \text{Pb}$ system,

positive and negative (pseudo)rapidities denote the proton- and nucleus-going directions, respectively.

Each event is characterized by the number of reconstructed tracks with $p_{\text{T}} > 0.4 \text{ GeV}$ and $|\eta| < 2.5$, referred to as the reconstructed charged-particle multiplicity ($N_{\text{ch}}^{\text{rec}}$). This standard ATLAS heavy-ion event class definition utilizes reconstructed tracks that are not corrected for track acceptance and efficiency; see, for example, Refs. [27–30]. Monte Carlo studies indicate that selections on $N_{\text{ch}}^{\text{rec}}$ correspond to equivalent selections on truth-level charged particles with $p_{\text{T}} > 0.4 \text{ GeV}$ and $|\eta| < 2.5$ as well, but with an average value of $N_{\text{ch}}^{\text{truth}} \approx 1.2 \times N_{\text{ch}}^{\text{rec}}$. Figure 1 shows the $N_{\text{ch}}^{\text{rec}}$ distributions in photonuclear $\text{Pb}+\text{Pb}$ and $p + \text{Pb}$ events. The $N_{\text{ch}}^{\text{rec}}$ range utilized in this paper, $15 \leq N_{\text{ch}}^{\text{rec}} \leq 60$, is highlighted. The $N_{\text{ch}}^{\text{rec}}$ differential results are presented in the range $15 \leq N_{\text{ch}}^{\text{rec}} \leq 60$ and $N_{\text{ch}}^{\text{rec}}$ integrated results are shown for $25 \leq N_{\text{ch}}^{\text{rec}} \leq 60$. The $p + \text{Pb}$ events are then reweighted to have effectively the same $N_{\text{ch}}^{\text{rec}}$ distribution as the UPC $\text{Pb}+\text{Pb}$ events.

The simulated event sample for the photonuclear analysis is generated with DPMJET-III + STARLIGHT. Events were generated with different minimum requirements on $N_{\text{ch}}^{\text{rec}}$ to provide a good statistical coverage over the $N_{\text{ch}}^{\text{rec}}$ range accessed in data. First, the distribution of photon flux for Pb beams at the LHC was calculated using STARLIGHT [31]. The flux distribution was passed to a multipurpose generator based on the Dual Parton Model (DPM) and referred to as DPMJET-III [18,19], which simulates direct and resolved photon-lead ($\gamma + \text{Pb}$) interactions at the generator level.

The DPM model is a diagrammatic way of describing particle production in hadron–hadron collisions [32]. There are two major concepts that underlie the dual-parton model. The first is the dual resonance model [33], which assumes that there are two alternative (or “dual”) descriptions of hadron–hadron interactions—the t -channel diagram where particles can be exchanged as a form of interaction and the s -channel diagram where the two incoming particles fluctuate into an intermediate state and then interact. The second is the Veneziano

scattering amplitude, which allows for a convergent calculation of the scattering amplitude for the exchange of a large set of particles. These two concepts enable calculations in soft hadron physics through *pomeron* exchange. The pomeron is a particle with vacuum quantum numbers analogous to a closed string and can be exchanged between hadrons as a form of interaction. Thus, through the dual resonance model there are intermediate states in elastic hadron–hadron collisions with a large number of pomerons. These diagrams can be “cut” to calculate the amplitude of the inelastic process of hadrons interacting to form a large number of primarily meson final states. The DPMJET-III MC generator combines the DPM with perturbative QCD (pQCD), as well as other features, to attempt a full description of hadron–hadron, hadron–photon, and photon–photon collisions [19]. The full set of particles was then run through a full GEANT4 [34] simulation of the ATLAS detector. A sample of thirteen million $\gamma + \text{Pb}$ events were generated.

The simulated event sample for the $p + \text{Pb}$ analysis is generated with HIJING [35]. The HIJING model combines pQCD inspired models for multiple-jet production with low- p_T multistring phenomenology. The model thus extends the PYTHIA string picture [36] to include modeling of both high-energy pp collisions, as well as p –nucleus and nucleus–nucleus collisions. The geometry for multiple collisions in p –nucleus and nucleus–nucleus collisions is provided by MC Glauber [37]. The model also includes multiple mini-jet production, nuclear shadowing of parton distribution functions, and a schematic mechanism of jet interactions in dense matter. The phenomenological parameters are adjusted to reproduce essential features of pp multiparticle production data for a wide energy range ($\sqrt{s_{NN}} = 5 \text{ GeV}$ to 2 TeV). For the sample used here the so-called “jet quenching” feature is turned off. A sample of five million $p + \text{Pb}$ HIJING events was generated.

IV. ANALYSIS

This paper reports charged-hadron and identified-strange-hadron yields reconstructed using tracks in the inner tracker with $p_T > 0.1 \text{ GeV}$ and $|\eta| < 2.5$. Both utilize the same event selection criteria detailed above. Additionally, the yields are determined in both photonuclear $\text{Pb}+\text{Pb}$ and $p + \text{Pb}$ using identical track reconstruction and extraction methods.

A. Charged hadrons

The charged-hadron analysis utilizes tracks that originate from the collision, referred to as primaries. Primary particles are defined as charged particles with a lifetime $\tau > 3 \times 10^{-10} \text{ s}$, either directly produced in the collision or from subsequent decays of directly produced particles with $\tau < 3.0 \times 10^{-11} \text{ s}$. This definition excludes charged strange baryons that have a very small probability to actually traverse the tracker before decaying (for example, the Ξ^- with $\tau = 1.6 \times 10^{-10} \text{ s}$ and Ω^- with $\tau = 0.8 \times 10^{-10} \text{ s}$). However, it includes charged hadrons from the decay of Δ resonances and ρ mesons with lifetimes shorter than $3.0 \times 10^{-8} \text{ s}$. The contribution of charged leptons is negligible and thus the tracks represent charged hadrons. The track reconstruction

follows that utilized for low pileup pp data-taking [38,39]. The reconstructed tracks are required to satisfy quality criteria as detailed in Ref. [40]. Tracks are further required to have $p_T > 0.1 \text{ GeV}$, $|\eta| < 2.5$, and a distance of closest approach to the reconstructed vertex in both the longitudinal and transverse directions of less than 1.5 mm.

The reconstructed tracks are then used to calculate charged-hadron yields as functions of p_T in different η slices:

$$Y_1(\eta, p_T) = \frac{1}{N_{\text{ev}}} \frac{dN_{\text{ch}}^2}{dp_T d\eta} \quad (1)$$

and then yields integrated over p_T as a function of η :

$$Y_2(\eta) = \frac{1}{N_{\text{ev}}} \frac{dN_{\text{ch}}}{d\eta}, \quad (2)$$

where N_{ev} is the number of selected events and N_{ch} is the number of charged particles.

The tracks entering these observables in bins of p_T and η are corrected for reconstruction and selection inefficiency, as well as for contributions from tracks that are not associated with primary particles, on a per-track basis using simulation-derived correction factors.

The reconstruction efficiency is defined as the ratio of the number of truth primary charged particles whose associated reconstructed track has a truth-matched primary charged particle $N_{\text{truth}}^{\text{matched}}$ (as defined in Ref. [41]) to the total number of truth primary charged particles, N_{truth} , as a function of both p_T and η :

$$\varepsilon(\eta, p_T) = \frac{N_{\text{truth}}^{\text{matched}}(\eta, p_T)}{N_{\text{truth}}(\eta, p_T)}. \quad (3)$$

The contributions to reconstructed tracks that are not associated with primary particles are classified into fake tracks and secondary tracks. To correct for these contributions, tracks are weighted on a track-by-track basis by the “primary fraction,” f_{primary} , which is estimated as a function of reconstructed kinematics in simulated events by taking the ratio of the number of primary tracks $N_{\text{ch}}^{\text{primary}}$ to the number of reconstructed tracks N_{ch} :

$$f_{\text{primary}}(\eta, p_T) = \frac{N_{\text{ch}}^{\text{primary}}(\eta, p_T)}{N_{\text{ch}}(\eta, p_T)}. \quad (4)$$

The yields as a function of η are measured for $p_T > 0.1 \text{ GeV}$ and extrapolated using the DPMJET-III MC down to $p_T = 0 \text{ GeV}$, i.e., correcting the yields by the fraction of DPMJET-III charged particles with $p_T > 0.1 \text{ GeV}$ to charged particles down to $p_T = 0 \text{ GeV}$. These correction factors are 5–15% in photonuclear $\text{Pb}+\text{Pb}$ and 5–7% in $p + \text{Pb}$ collisions.

Finally, using the yields detailed above, the $\langle p_T \rangle$ in η intervals are calculated as a function of $N_{\text{ch}}^{\text{rec}}$. When calculating $\langle p_T \rangle$ the extrapolation down to $p_T = 0 \text{ GeV}$ is performed using a Modified Hagedorn fit [42]:

$$\frac{1}{N} \frac{dN}{dp_T} = A_1 \frac{p_T^2}{\sqrt{p_T^2 + m_0^2}} \left(1 + \frac{p_T}{p_1}\right)^{-n_1}, \quad (5)$$

where m_0 is the rest mass of considered particle, p_1 and n_1 are the free parameters, and A_1 is the normalization constant. The

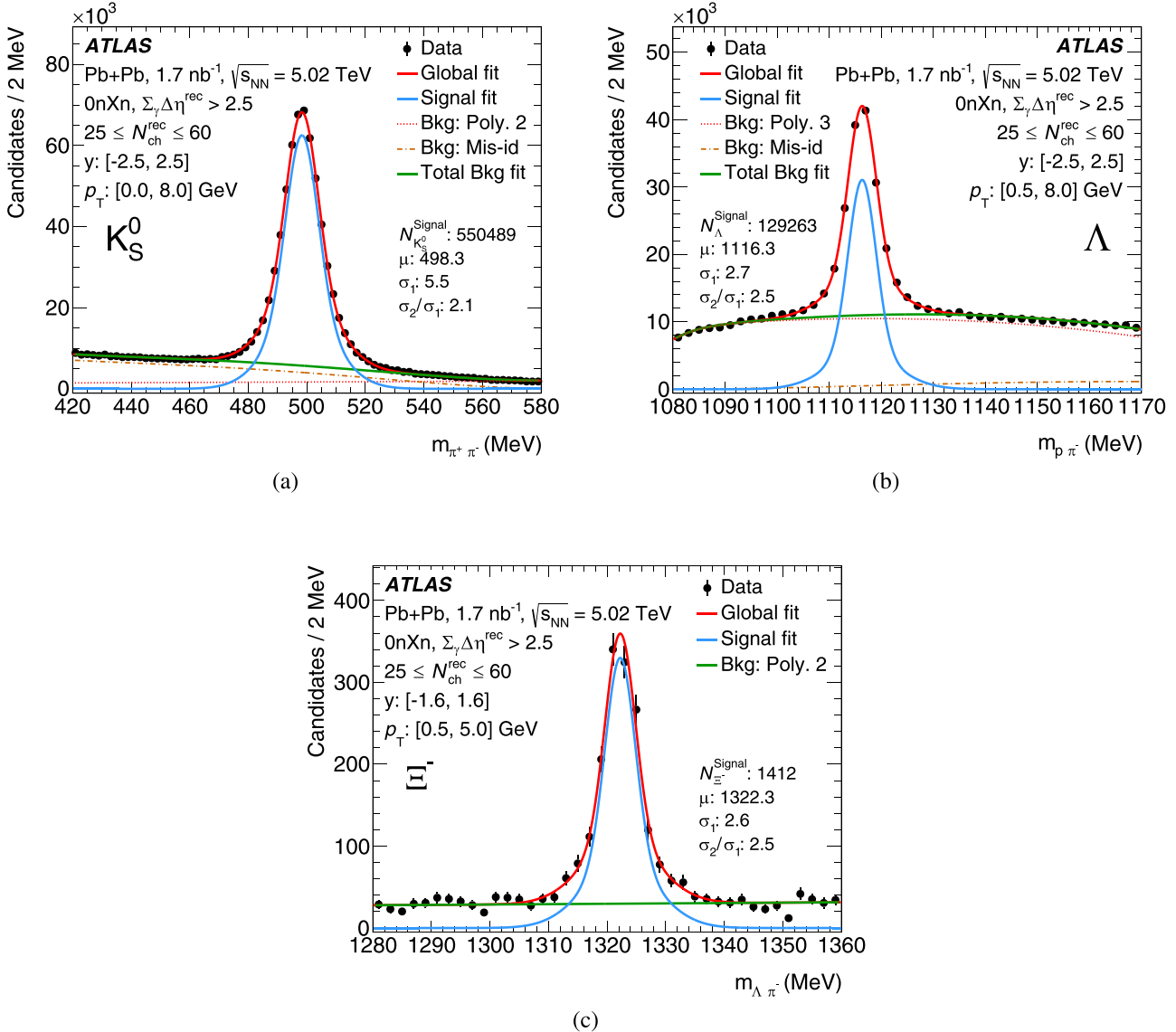


FIG. 2. Invariant-mass distributions of (a) K_S^0 , (b) Λ , and (c) Ξ^- in $\text{Pb}+\text{Pb}$ photonuclear collisions. The data are fitted to a signal (double Gaussian) and a background component (detailed in the text). The signal counts, and fit parameters for the mean μ and widths σ_1 and σ_2 of the double Gaussian are also shown in units of MeV.

$\langle p_T \rangle$ in each η bin and in each $N_{\text{ch}}^{\text{rec}}$ bin is calculated by finding the mean value of the fit results for $p_T > 0$ GeV.

B. Identified strange hadrons

Only the K_S^0 , Λ , and Ξ^- originating from the primary vertex are considered. The contribution of secondary Λ from Σ^0 decay is included, while contributions from the decay products of heavy baryons (Ξ^- , Ω^-) are excluded from the definition of primary Λ . For Λ and Ξ^- , the definition includes only the baryon state and does not represent an average of baryons and antibaryons. Antibaryons have an additional acceptance correction due to annihilation processes, and GEANT4 is known to not model this correctly [43,44].

Identified strange hadrons are reconstructed using oppositely charged tracks with $p_T > 0.1$ GeV and $|\eta| < 2.5$, which are fitted to a common secondary vertex using a Kalman

filter [45]. The K_S^0 candidates in the $\pi^+ + \pi^-$ decay mode (branching ratio of 69.2%) are required to satisfy the following criteria:

- The χ^2 of the two-track vertex fit is required to be less than 15 (with one degree of freedom).
- The cosine of the pointing angle in the transverse plane ($\cos \theta$) between the K_S^0 momentum vector and the K_S^0 flight direction, defined as the line connecting the reconstructed primary vertex to the decay direction, is required to fulfill the requirements:
 - $\cos \theta > 0.999$ for $\text{Pb}+\text{Pb}$ photonuclear collisions, except in the most backward rapidity bin, $y: [-2.5, -1.6]$, $\cos \theta > 0.999$.
 - $\cos \theta > 0.995$ for $p + \text{Pb}$, except in the most backward and forward rapidity bins of $p + \text{Pb}$, $y: [-2.5, -1.6]$ and $y: [1.6, 2.5]$, $\cos \theta > 0.99$

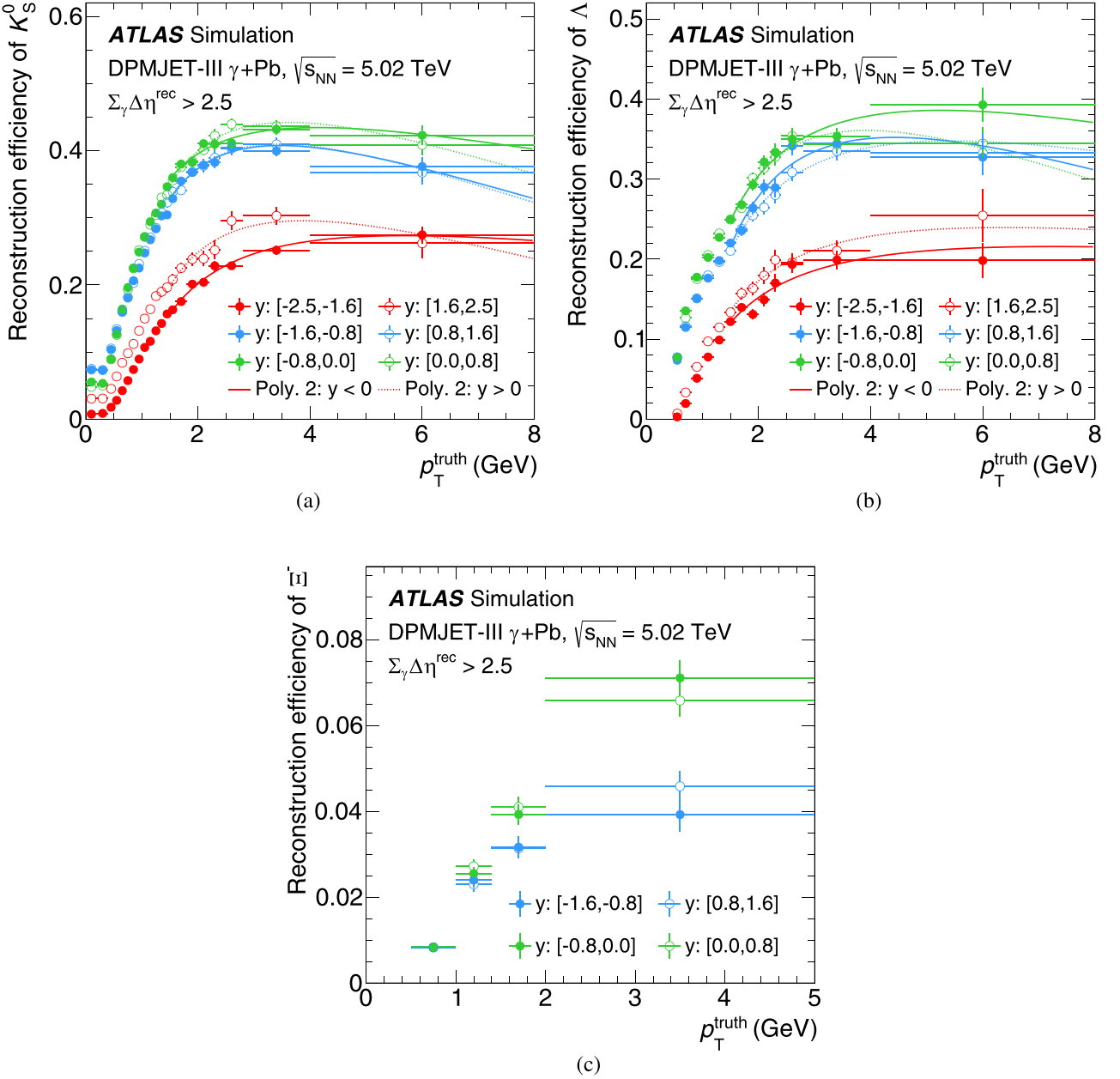


FIG. 3. Reconstruction efficiencies of (a) K_S^0 , (b) Λ , and (c) Ξ^- as a function of p_T^{truth} in intervals of y^{truth} as determined using DPMJET-III. The efficiencies are fitted using polynomial functions for K_S^0 and Λ . Statistical uncertainties are shown as vertical lines.

(c) Requirements on the minimum values of the variables $|\frac{L_{xy}}{\sigma_{L_{xy}}}|$ and $|\frac{p_T}{\sigma_{p_T}}|$, in bins of p_T and y . These are optimized using the Toolkit for Multivariate Data Analysis (TMVA) package within the ROOT framework [46], where L_{xy} is the distance from the reconstructed primary vertex to the reconstructed secondary vertex (decay vertex of the K_S^0 candidate) in the transverse plane, $\sigma_{L_{xy}}$ is the uncertainty on L_{xy} reconstruction, p_T is the reconstructed momentum of the K_S^0 candidate and σ_{p_T} is the uncertainty in the p_T reconstruction.

The Λ candidates in the $p + \pi^-$ decay mode (branching ratio of 63.9%) are required to satisfy the following criteria:

- The p_T of the Λ candidate is greater than 0.5 GeV.
- The χ^2 of the two-track vertex fit is required to be less than 15 (with one degree of freedom).
- The cosine of the pointing angle ($\cos \theta$) is required to be greater than 0.999.
- Requirements on the minimum values of the variables $|\frac{L_{xy}}{\sigma_{L_{xy}}}|$ and $|\frac{p_T}{\sigma_{p_T}}|$, in bins of p_T and y , determined using the TMVA package as above.

The Ξ^- candidates in the $\Lambda + \pi^-$ decay mode (branching ratio of 99.5%) are required to satisfy the following criteria:

- The p_T of the Ξ^- candidate is greater than 1 GeV, and $|y| < 1.6$.

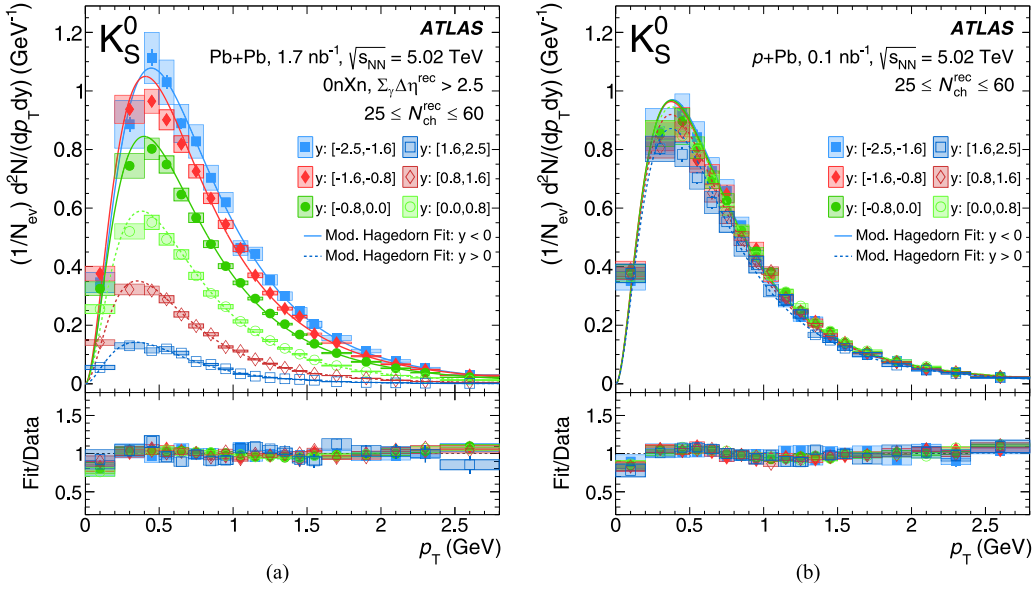


FIG. 4. K_S^0 yields as a function of p_T in different y selections in (a) $\text{Pb}+\text{Pb}$ photonuclear and (b) $p+\text{Pb}$ collisions. The bottom panels show the ratio of the Modified Hagedorn fit results to the data. Statistical uncertainties are shown as vertical lines and systematic uncertainties are shown as colored boxes.

- (ii) The χ^2 of the two-track vertex fit for reconstructing both Λ and Ξ^- is required to be less than 15 (with one degree of freedom).
- (iii) The cosine of the pointing angle ($\cos \theta$) associated with Ξ^- vertex is required to be greater than 0.9992.
- (iv) The cosine of the pointing angle associated with Λ vertex is required to be greater than 0.99999.
- (v) Requirements on the minimum values of the variables $|\frac{L_{xy}}{\sigma_{L_{xy}}}|$ associated with vertex fit for reconstructing Λ

and Ξ^- , in bins of p_T and y , determined using the TMVA package as above.

Below the minimum p_T value for Λ and Ξ^- , the efficiency is very low due to the slow pions. In contrast, the K_S^0 can be measured down to $p_T = 0 \text{ GeV}$. The tight selection criteria for the pointing angle and the minimum value of $|\frac{L_{xy}}{\sigma_{L_{xy}}}|$ significantly improve the signal significance in all kinematic regions.

Figure 2 shows the resulting invariant-mass distributions for K_S^0 , Λ , and Ξ^- in $\text{Pb}+\text{Pb}$ photonuclear collisions. The

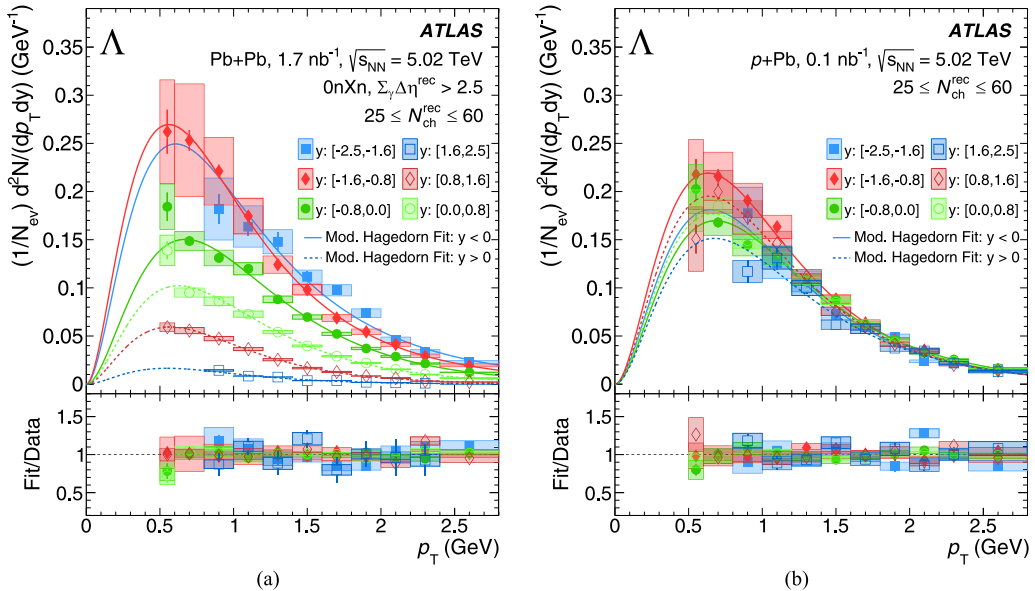


FIG. 5. Λ yields as a function of p_T in different y selections in (a) $\text{Pb}+\text{Pb}$ photonuclear and (b) $p+\text{Pb}$ collisions. The bottom panels show the ratio of the Modified Hagedorn fit results to the data. Statistical uncertainties are shown as vertical lines and systematic uncertainties are shown as colored boxes.

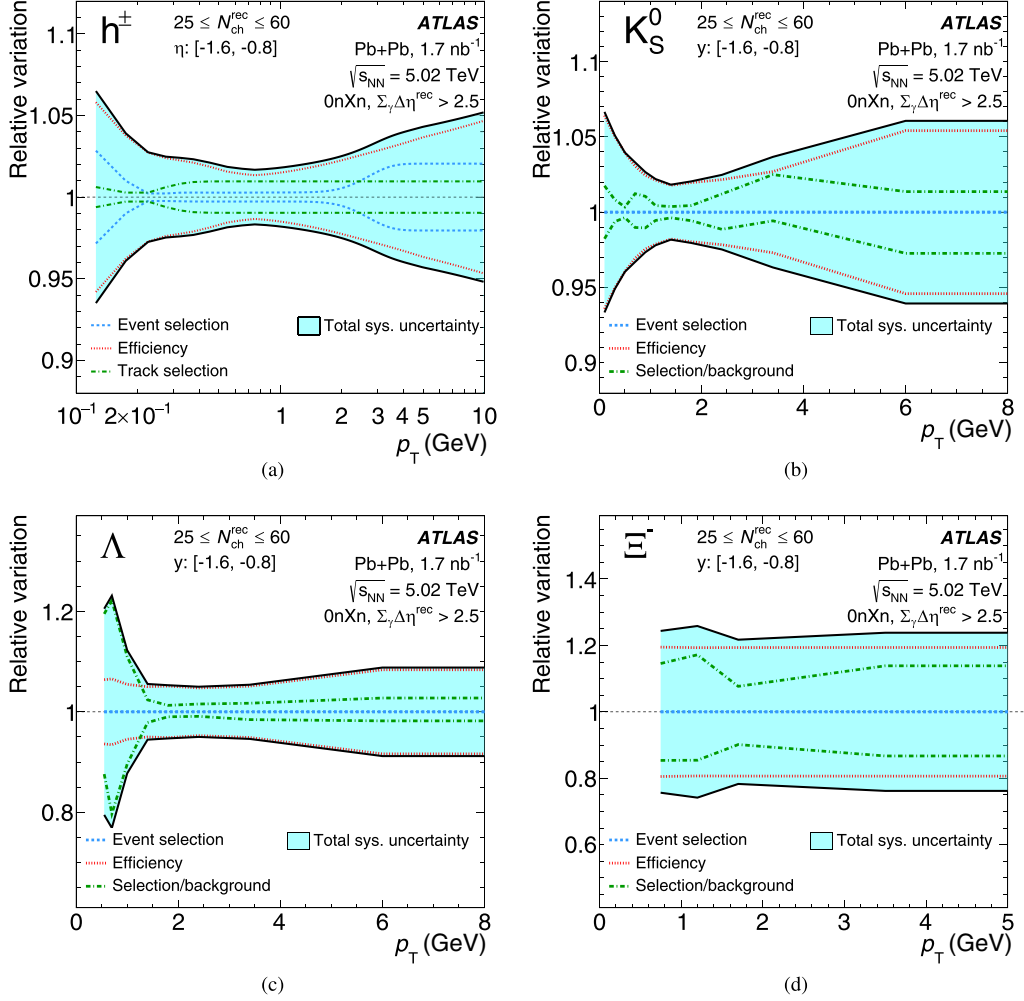


FIG. 6. Relative systematic uncertainties in (a) charged hadrons, (b) K_S^0 , (c) Λ , and (d) Ξ^- yields in photonuclear collisions as a function of p_T . All uncertainty contributions are added in quadrature and the result is symmetrized to obtain the full systematic uncertainty.

number of signal candidates in a given p_T and y bin is determined by fitting the invariant-mass distribution of the strange hadron candidates in that bin. The fit utilizes a double Gaussian for the signal peak and a second-order (third-order for Λ) polynomial for the combinatorial background. The background component also includes a functional form modeling the cases where the particles are mis-identified, e.g., a truth K_S^0 that has its decay products fit under the assumption of a parent Λ particle. These functional forms are determined from DPMJET-III MC. The ratio of the widths and amplitudes of the two Gaussian distributions is constrained based on the MC truth-matched invariant-mass distributions within the corresponding p_T - y bin. The fit ranges utilized in this analysis are [420, 580] MeV for K_S^0 , [1080, 1170] MeV for Λ , and [1280, 1360] MeV for Ξ^- . The quality of the fit is evaluated based on reasonable χ^2 values.

The signal candidates, obtained in bins of p_T and y , are corrected for reconstruction and selection inefficiencies, using Eq. (3) on the secondary vertex candidates, and for signal inefficiency, which accounts for the missed fraction of reconstructed candidates due to the TMVA-optimized selection requirements. Furthermore, signal candidates are corrected for

the contributions of secondaries, as defined by Eq. (4). The largest sources of secondaries are from hadronic interactions of particles with the detector material and the decay products of heavier strange baryons, which contribute to the Λ yield at the 10% level [47]. Figure 3 shows the reconstruction efficiencies for K_S^0 , Λ , and Ξ^- calculated using DPMJET-III $\gamma + \text{Pb}$ simulations. High- p_T neutral strange particles start to have a sufficiently large relativistic boost that the decay occurs after some of the silicon-detector components, leading to missing hits and an efficiency drop.

The corrected number of signal candidates is used to calculate the identified-hadron yield as a function of p_T in different rapidity bins using Eq. (1), and as a function of y using Eq. (2).

The minimum p_T values are 0 GeV for K_S^0 , and 0.5 GeV for Ξ^- . For Λ , the minimum p_T is 0.5 GeV for $|y| < 1.6$ and 0.8 GeV for $1.6 < |y| < 2.5$. Thus the p_T -integrated yields for K_S^0 are simply calculated by summing the yields as a function of p_T , whereas for Λ and Ξ^- the yield below the minimum p_T must be accounted for. Hence, an extrapolation procedure is performed for Λ and Ξ^- , using the Modified Hagedorn functional fit, given by Eq. (5). Figures 4 and 5 show the K_S^0 and Λ

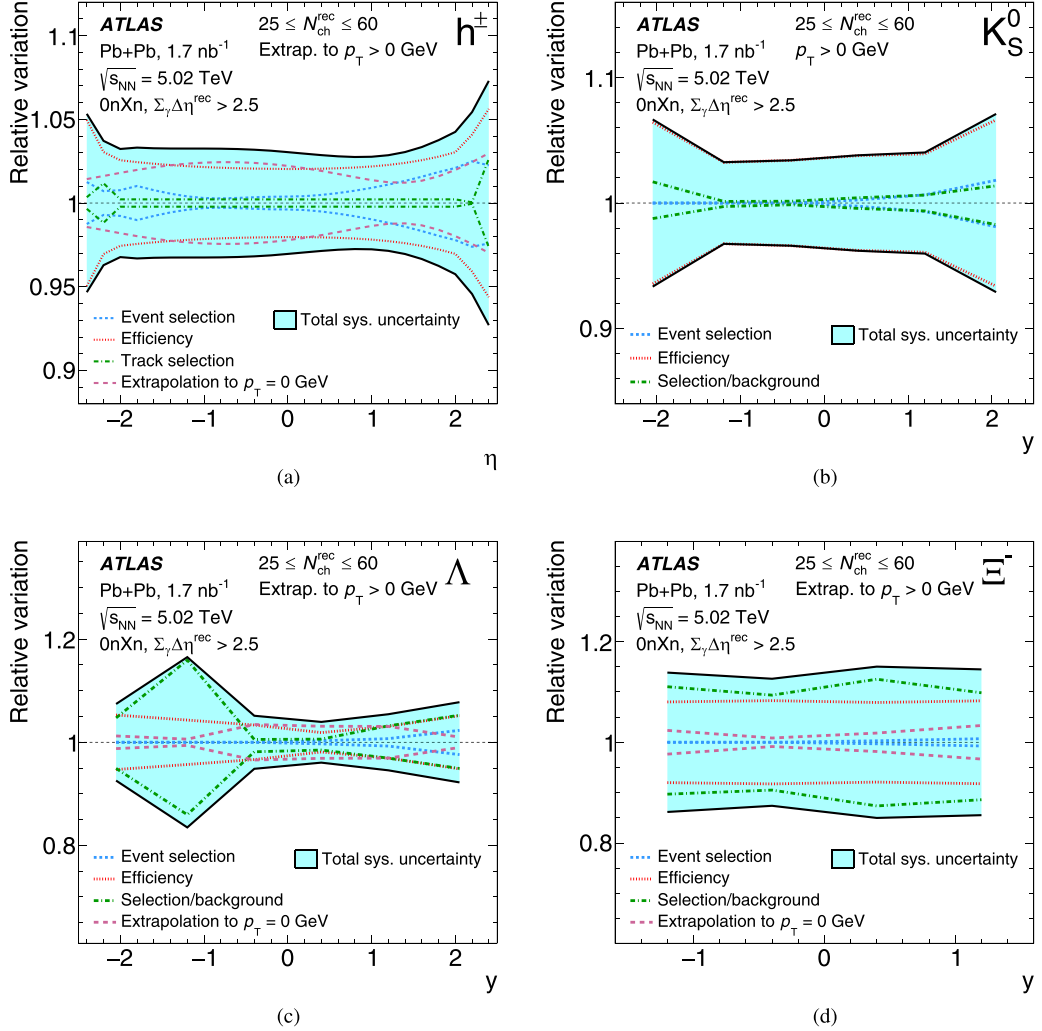


FIG. 7. Relative systematic uncertainties in (a) charged hadrons, (b) K_S^0 , (c) Λ , and (d) Ξ^- yields in photonuclear collisions as a function of (pseudo) rapidity. The yield of K_S^0 is measured down to $p_T = 0$ GeV. For charged hadrons, Λ and Ξ^- , the measured yield is extrapolated to $p_T = 0$ GeV. All uncertainty contributions are added in quadrature and the result is symmetrized to obtain the full systematic uncertainty.

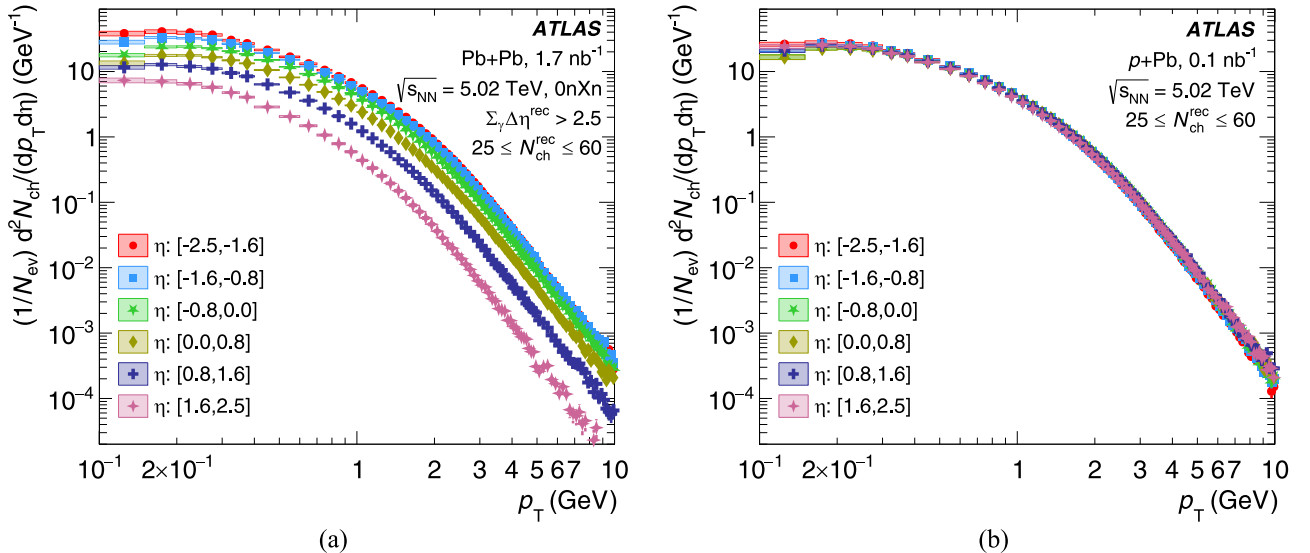


FIG. 8. Charged-hadron yields as a function of p_T in six η selections for (a) Pb+Pb photonuclear and (b) $p + Pb$ collisions. Statistical uncertainties are shown as vertical lines and systematic uncertainties are shown as colored boxes.

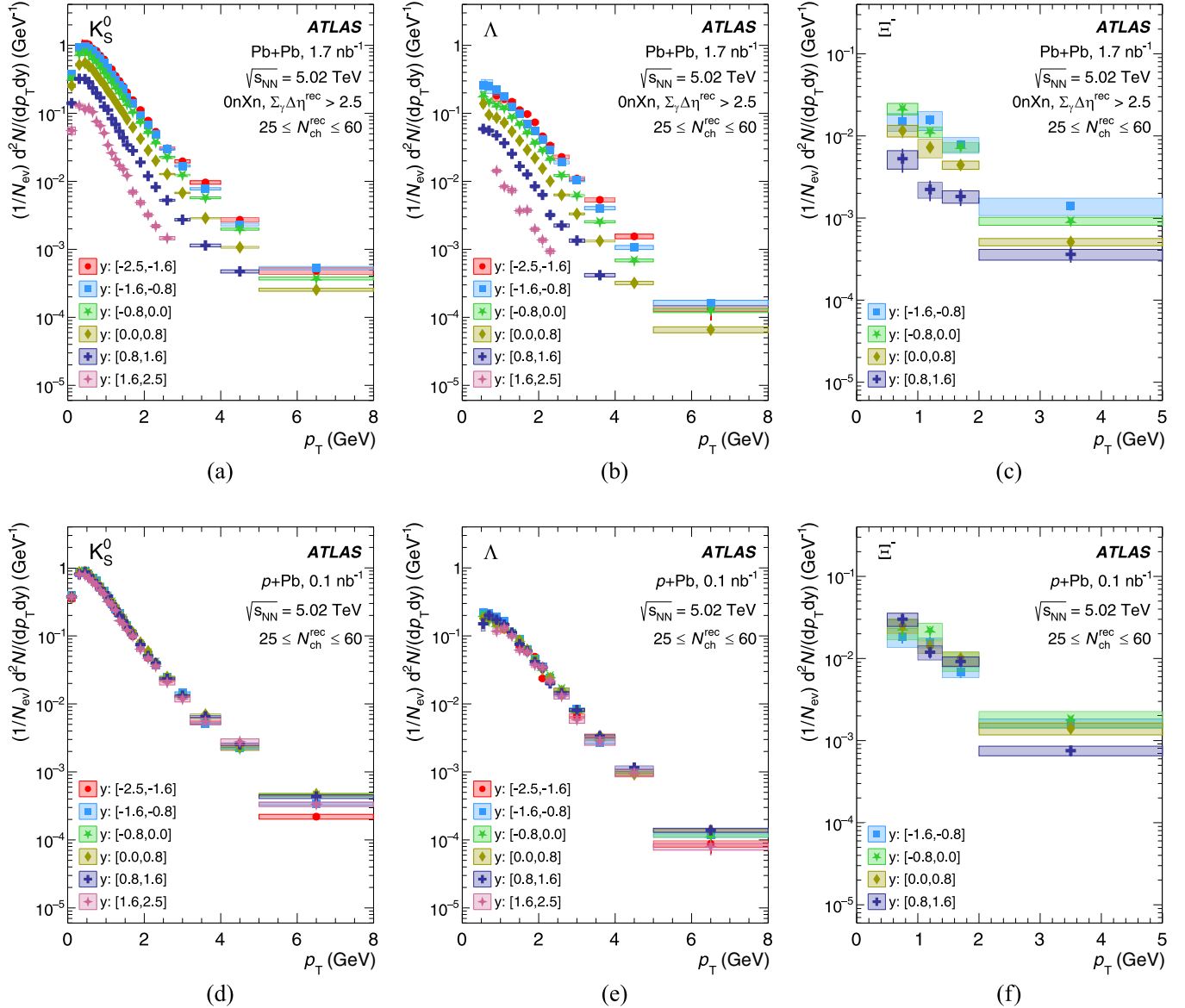


FIG. 9. (a) K_S^0 , (b) Λ , and (c) Ξ^- yields are shown as a function of p_T in six y selections in $\text{Pb}+\text{Pb}$ photonuclear collisions. The (d) K_S^0 , (e) Λ , and (f) Ξ^- yields are shown as a function of p_T in six y selections in $p+\text{Pb}$ collisions. Statistical uncertainties are shown as vertical lines and systematic uncertainties are shown as colored boxes.

yields in $\text{Pb}+\text{Pb}$ photonuclear and $p+\text{Pb}$ collisions as a function of p_T across six y selections, with the Modified Hagedorn fit results. The fit to the K_S^0 yield, where measurements extend down to $p_T = 0 \text{ GeV}$, shows that the function provides a good description of the data. This confirms that the same fit function can be used to extrapolate the Λ and Ξ^- yields down to $p_T = 0 \text{ GeV}$. The fit is performed using statistical uncertainties only and is then repeated for each systematic uncertainty variation. Approximately 20% of the total yield lies in the region of extrapolation ($p_T < 0.5 \text{ GeV}$) for Λ , and is larger for the most forward/backward rapidities (where $p_T < 0.8 \text{ GeV}$). Approximately 20–30% of the total yield lies in the region of extrapolation ($p_T < 0.5 \text{ GeV}$) for Ξ^- . Systematic uncertainties on these extrapolations, and from other sources, are discussed below.

Finally, using the p_T -integrated yields determined above, the $\langle p_T \rangle$ and the ratio of strange-hadron to charged-hadron yields are calculated as a function of $N_{\text{ch}}^{\text{rec}}$. These values are calculated after extrapolating down to $p_T = 0 \text{ GeV}$.

V. SYSTEMATIC UNCERTAINTIES

The sources of systematic uncertainties in this measurement are described in the following. For the event selection criteria in $\text{Pb}+\text{Pb}$ photonuclear events, the primary sources contributing to both the charged-hadron and identified-hadron yields include uncertainties associated with the purity estimation and pseudorapidity gap selection. In both $\text{Pb}+\text{Pb}$ photonuclear and $p+\text{Pb}$ collisions, uncertainties are assigned to track selection by relaxing specific hit requirements in turn,

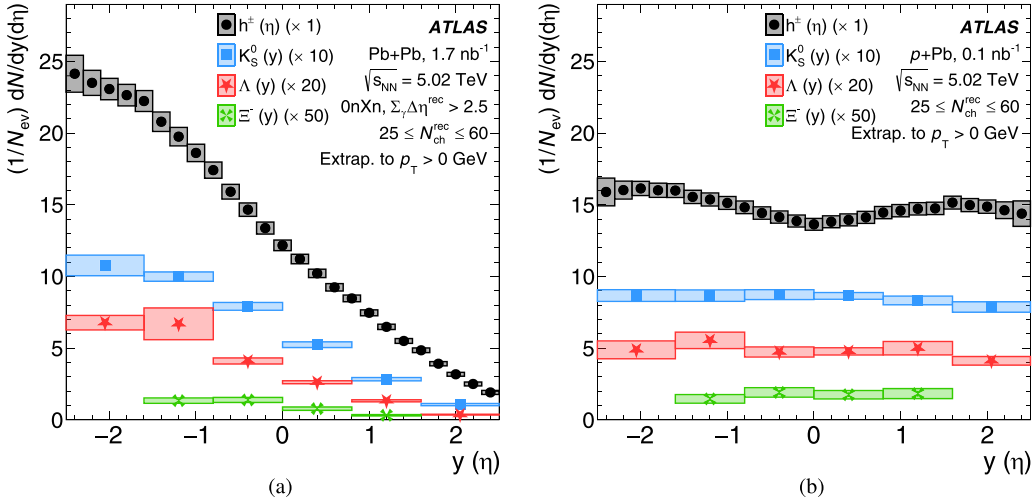


FIG. 10. Charged-hadron yields as a function of η and the K_s^0 , Λ , and Ξ^- yields as a function of y for (a) $\text{Pb}+\text{Pb}$ photonuclear and (b) $p + \text{Pb}$ collisions. Statistical uncertainties are shown as vertical lines and systematic uncertainties are shown as colored boxes.

to contributions from fake and secondary tracks by varying f_{primary} in Eq. (4) by 50% of the rate, and to the mis-modeling of the detector material [38,48]. An uncertainty is also assigned for bin migration due to track momentum resolution. This bin migration effect is quite small and the uncertainty is set by turning off the bin migration entirely. Furthermore, uncertainties on the fit values of the track reconstruction efficiency are included as systematic uncertainties.

For the identified-hadron analysis, specific uncertainties are assigned to the selection requirements by varying the specific requirements from the nominal values. The uncertainty in the signal extraction is further quantified by varying the fit range of invariant-mass distributions. Finally, to assess the uncertainty in the extrapolation to $p_T = 0$ GeV, a varied fit functional form for the p_T distribution based on Tsallis statistics [49] is utilized. The fitting procedure is redone for all other systematic variations.

In all cases, the ratio of the varied to nominal result is either smoothed via fit or directly used, and the values are assigned as the systematic uncertainty. All uncertainty contributions are added in quadrature and then symmetrized by taking the maximum variation at each point to determine the total systematic uncertainty. Other potential sources of uncertainty, such as those related to the trigger efficiency [10], were found to be negligible compared to the ones described above.

Figures 6 and 7 present the relative systematic uncertainties on charged hadrons, K_s^0 , Λ , and Ξ^- yields in photonuclear collisions as a function of p_T and (pseudo)rapidity, respectively. The dominant uncertainty in the low p_T region ($p_T < 1$ GeV) arises from variations in the detector materials and bin-migration effects. For identified hadrons, in addition to these uncertainties, the uncertainty in the background correction contributes significantly. For the $\langle p_T \rangle$ calculation, the total uncertainties are on the order of 3–5%. As a function of rapidity, a significant uncertainty for charged hadrons and Λ , Ξ^- particles comes from the extrapolation of the yield down to $p_T = 0$ GeV. For the K_s^0 there is no such uncertainty as the

yield is measured down to $p_T = 0$ GeV. The uncertainty is dominated by systematic rather than statistical effects.

VI. RESULTS

The resulting yields as a function of p_T for charged hadrons are shown in Fig. 8 in six pseudorapidity selections spanning $-2.5 < \eta < 2.5$ in $\text{Pb}+\text{Pb}$ photonuclear and $p + \text{Pb}$ collisions. The yields are calculated for collisions with $25 \leq N_{\text{ch}}^{\text{rec}} \leq 60$, with the $p + \text{Pb}$ $N_{\text{ch}}^{\text{rec}}$ distribution reweighted to match that of the photonuclear collision sample. The photonuclear collision yields have a strong pseudorapidity dependence, with much lower multiplicity in the photon-going direction (positive η). In contrast, the $p + \text{Pb}$ collision yields are nearly η -symmetric. Unlike in more central $p + \text{Pb}$ collisions [50], the yields in the low-multiplicity selection ($25 \leq N_{\text{ch}}^{\text{rec}} \leq 60$) are symmetric in rapidity; hence, the η distribution is more pp -like.

Figure 9 shows the yields as a function of p_T for identified strange hadrons K_s^0 , Λ , and Ξ^- in six rapidity selections spanning $-2.5 < y < 2.5$ in $\text{Pb}+\text{Pb}$ photonuclear and $p + \text{Pb}$ collisions for the same event selection as the charged-hadron yields. The Λ and Ξ^- yields are for baryons only and are not the average of baryons and antibaryons. The Λ yields include decays from Σ_0 , but otherwise are not inclusive of other baryon feed-down contributions, e.g., from Ξ^- and Ω . As in the charged-hadron case, the yields of all strange hadrons have a strong rapidity dependence in photonuclear collisions.

The yields as a function of p_T are then integrated over the p_T range of the measurements, and extrapolated to be inclusive over all p_T , i.e., $p_T > 0$. The resulting p_T -integrated yields as a function of pseudorapidity, for charged hadrons, and rapidity, for identified strange hadrons are shown in Fig. 10. The p_T -integrated yields again show a strong rapidity asymmetry in photonuclear collisions and are nearly rapidity symmetric in $p + \text{Pb}$ collisions.

Next, the p_T distributions are characterized in terms of the $\langle p_T \rangle$, calculated to correspond to the mean value for $p_T > 0$.

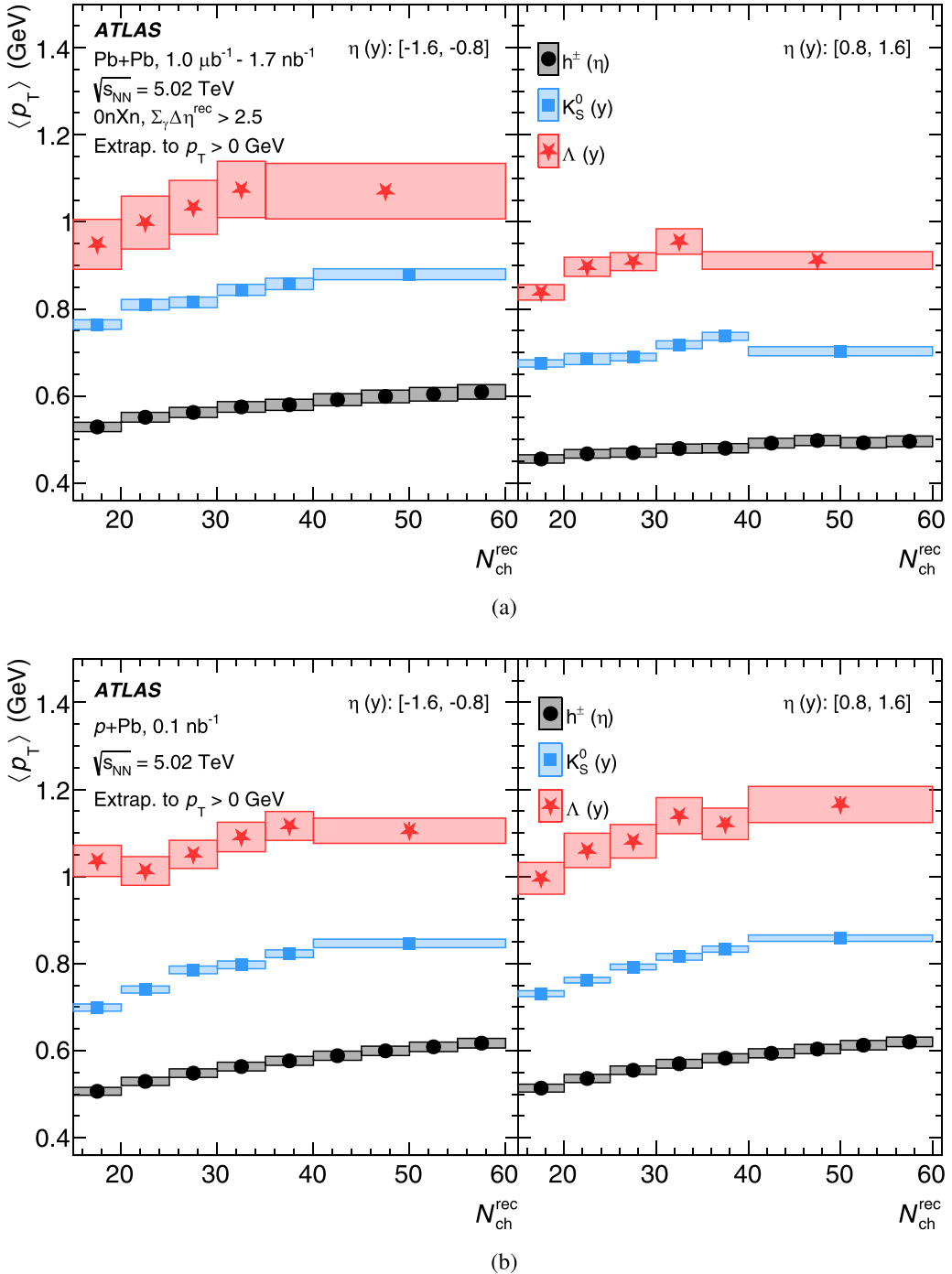


FIG. 11. $\langle p_T \rangle$ for charged hadrons, K_S^0 , and Λ in (a) $\text{Pb}+\text{Pb}$ photonuclear and (b) $p + \text{Pb}$ collisions as a function of $N_{\text{ch}}^{\text{rec}}$. The left (right) panels are for a backward (forward) rapidity interval. Statistical uncertainties are shown as vertical lines and systematic uncertainties are shown as colored boxes.

These $\langle p_T \rangle$ values for charged hadrons, K_S^0 , and Λ particles, in two rapidity intervals, as a function of finer intervals of $N_{\text{ch}}^{\text{rec}}$ are shown in Fig. 11. The top (bottom) subfigures correspond to photonuclear $\text{Pb}+\text{Pb}$ ($p + \text{Pb}$) collisions, with the left (right) panels corresponding to backward (forward) rapidity. In both photonuclear and $p + \text{Pb}$ collisions, the $\langle p_T \rangle$ increases with increasing $N_{\text{ch}}^{\text{rec}}$ and there is a distinct ordering

with $\langle p_T \rangle$ (charged hadrons) $<$ $\langle p_T \rangle$ (K_S^0) $<$ $\langle p_T \rangle$ (Λ). Under the assumption that charged hadrons are dominated by pions, the pattern follows a distinct mass ordering. In photonuclear collisions, the $\langle p_T \rangle$ show a large rapidity asymmetry, with much lower values for all particles at forward rapidity. In contrast, the $p + \text{Pb}$ results are consistent with being rapidity symmetric.

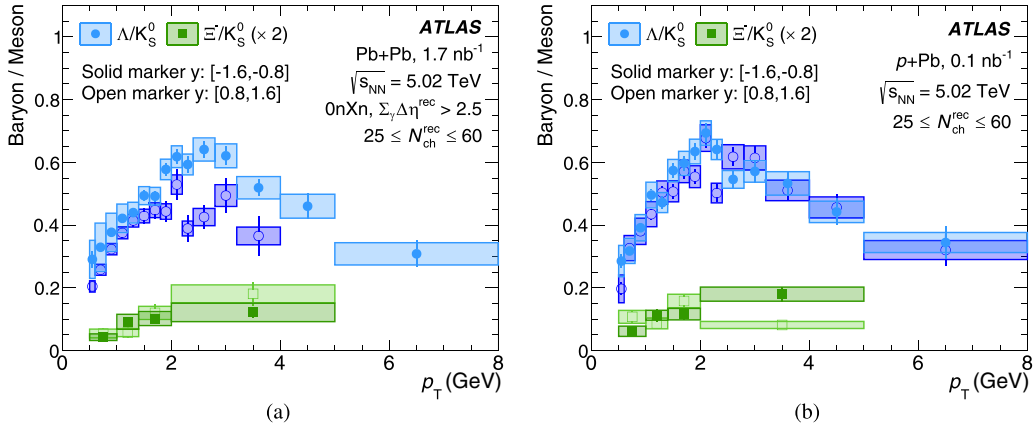


FIG. 12. Ratio of Λ/K_S^0 and Ξ^-/K_S^0 yields as a function of p_T in two rapidity intervals for (a) $\text{Pb}+\text{Pb}$ photonuclear and (b) $p+\text{Pb}$ collisions. Statistical uncertainties are shown as vertical lines and systematic uncertainties are shown as colored boxes.

For the Ξ^- , the $\langle p_T \rangle$ can only be calculated in one selection of $N_{\text{ch}}^{\text{rec}}$, $25 \leq N_{\text{ch}}^{\text{rec}} \leq 60$, and correspond to values of $1.60 \pm 0.02(\text{stat}) \pm 0.24(\text{sys}) \text{ GeV}$ [$1.04 \pm 0.01(\text{stat}) \pm 0.12(\text{sys}) \text{ GeV}$] for photonuclear collisions and $1.33 \pm 0.03(\text{stat}) \pm 0.18(\text{sys}) \text{ GeV}$ [$1.06 \pm 0.02(\text{stat}) \pm 0.25(\text{sys}) \text{ GeV}$] for $p+\text{Pb}$ collisions, at backward (forward) rapidity. These values suggest that the Ξ^- may have a slightly higher $\langle p_T \rangle$ than Λ particles, although consistent within large uncertainties.

To further elucidate the data trends, the ratios of Λ/K_S^0 and Ξ^-/K_S^0 as a function of p_T , for two rapidity intervals, in $\text{Pb}+\text{Pb}$ photonuclear and $p+\text{Pb}$ collisions are shown in Fig. 12. The most striking observation is the larger Λ/K_S^0 ratio at intermediate $p_T \approx 1.5\text{--}4.0 \text{ GeV}$ when measured at backward rapidity compared to forward rapidity in photonuclear collisions. This baryon enhancement at intermediate p_T is reminiscent of the “baryon anomaly” observed in $p+\text{Pb}$ and $\text{Pb}+\text{Pb}$ collisions [51] and is often associated with quark recombination as the dominant hadronization mechanism [52]. The ratios in $p+\text{Pb}$ in both rapidity intervals are comparable to the backward rapidity photonuclear values. For the Ξ^- , the uncertainties preclude any strong conclusions.

Finally, the ratio of identified-strange-hadron yields relative to charged-hadron yields is calculated as a function of $N_{\text{ch}}^{\text{rec}}$. The resulting ratios at backward and forward rapidities are shown as a function of $N_{\text{ch}}^{\text{rec}}$ in Fig. 13 for photonuclear and $p+\text{Pb}$ collisions. In photonuclear collisions, there is a clear increase in strange hadron yields relative to charged hadrons between backward and forward rapidity. If there is strangeness enhancement due to final-state interactions, this would be consistent with the larger ratios in the Pb-going direction. The ratios are similar between backward rapidity photonuclear yields and the $p+\text{Pb}$ yields in both rapidity intervals. Overall, the ratios are generally consistent with being flat, i.e., not exhibiting an $N_{\text{ch}}^{\text{rec}}$ dependence over the given range, with a hint of a rise in the Λ to charged-hadron ratios. It is notable that the large strangeness enhancement observed in pp , $p+\text{Pb}$, and $\text{Pb}+\text{Pb}$ collisions in Ref. [15] is actually quite small for K_S^0 and Λ in the multiplicity range corresponding to the measurements presented here.

VII. DISCUSSION

These experimental results are now compared with DPMJET-III MC for photonuclear collisions and HIJING for $p+\text{Pb}$ collisions, respectively, neither of which includes any final-state interactions or QGP formation. Comparisons are also made to the so-called “hybrid” model that explicitly includes a hydrodynamic modeling of QGP formation in both photonuclear and $p+\text{Pb}$ collisions [11]. The hybrid model incorporates initial conditions by an extension of MC Glauber to three-dimensions, time evolution via viscous hydrodynamics using the publicly available package MUSIC [53], and finally hadronic scattering via the publicly available package URQMD [54]. For the photonuclear case, following Ref. [9], a parametrization is used for the photon energy and hence the center-of-mass energy distribution. The $\gamma+\text{Pb}$ collisions are treated via the vector meson dominance picture, i.e., the virtual photon state may be decomposed into a set of vector meson states, like ρ , ω , and ϕ , in a low virtuality regime, $Q^2 = 0.0625 \text{ GeV}^2$. The virtual photon is treated as a vector meson with two “partonic participants” in the MC Glauber calculation (in contrast to the three “partonic participants” for the proton projectile in the $p+\text{Pb}$ case).

When making such comparisons to the data, the event selection criteria used here are important to incorporate. In particular, the yields presented here are characterized by specific $N_{\text{ch}}^{\text{rec}}$ intervals, e.g., $25 \leq N_{\text{ch}}^{\text{rec}} \leq 60$. As discussed earlier, MC studies indicate that the selections on $N_{\text{ch}}^{\text{rec}}$ correspond to equivalent selections on truth-level charged particles with $p_T > 0.4 \text{ GeV}$ and $|\eta| < 2.5$ as well, but with an average value of $N_{\text{ch}}^{\text{truth}} \approx 1.2 \times N_{\text{ch}}^{\text{rec}}$. Each event is additionally characterized by the sum-of-gaps using reconstructed tracks and energy clusters. Monte Carlo studies indicate that this selection corresponds to equivalent selections on truth-level particles with $p_T > 0.45 \text{ GeV}$ and $|\eta| < 4.9$. Differences between the reconstruction and truth level selections are less than 2–3%. For the DPMJET-III and HIJING simulations, the exact event selection criteria used in this measurement are applied through a full GEANT4 simulation of the detector

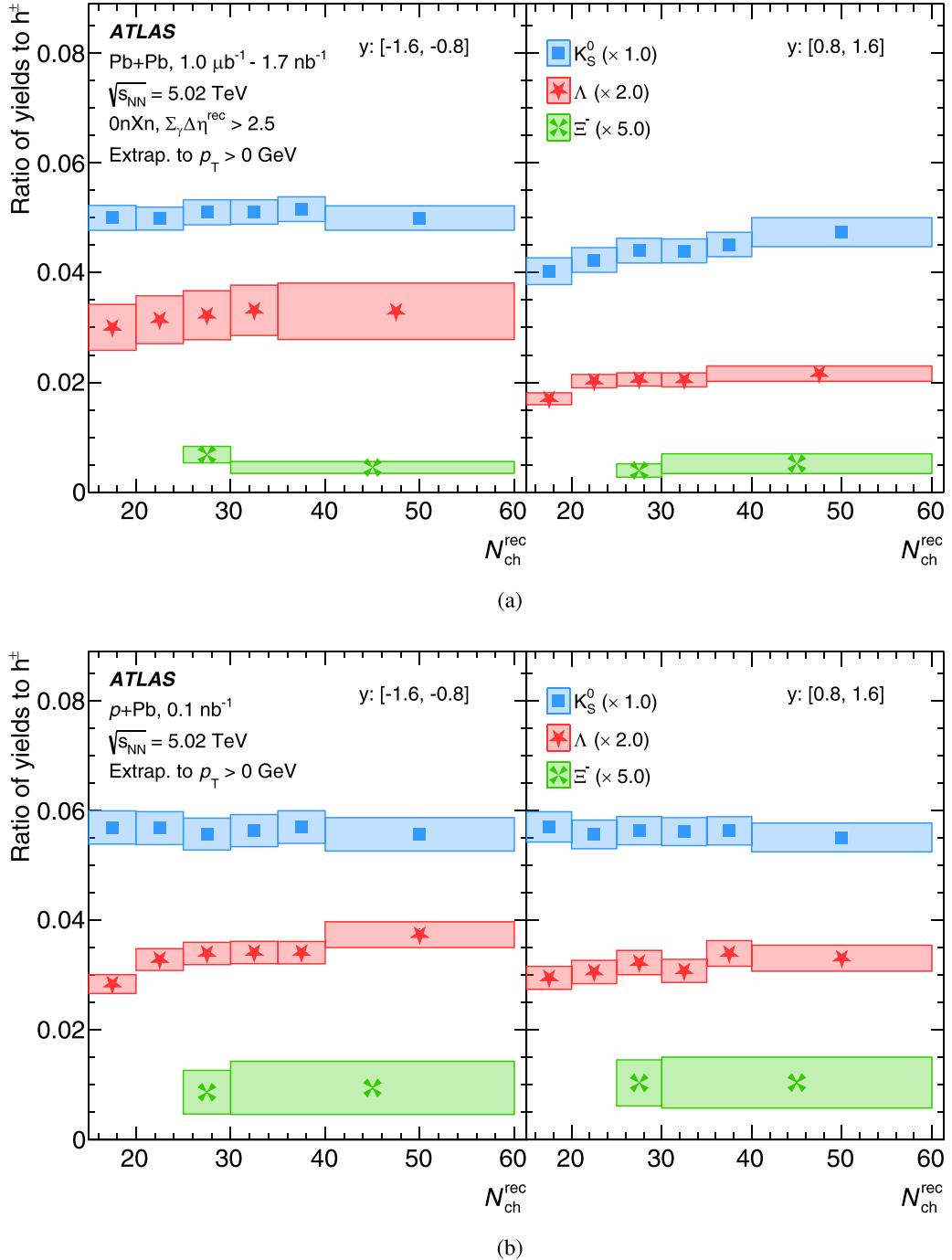


FIG. 13. Ratios of identified-strange-hadron yields to charged-hadron yields as a function of $N_{\text{ch}}^{\text{rec}}$ for (a) Pb+Pb photonuclear collisions and (b) $p + \text{Pb}$ collisions. The left (right) panels are for a backward (forward) rapidity interval. Statistical uncertainties are shown as vertical lines and systematic uncertainties are shown as colored boxes.

response and reconstruction, i.e., to match the experimental event selection of $N_{\text{ch}}^{\text{rec}}$ and $\sum_y \Delta\eta^{\text{rec}}$. Once an event satisfies these criteria, its truth-level particles are included in the yield calculation. In the hybrid model case, the model framework was calibrated with $p + \text{Pb}$ measurements at a center-of-mass energy of 5.02 TeV and then made predictions for $\gamma + \text{Pb}$ collisions.

Figure 14 shows the measured charged hadron, K_S^0 , Λ , and Ξ^- yields as a function of rapidity, compared to MC results from DPMJET-III for photonuclear collisions and HIJING for $p + \text{Pb}$ collisions. Both calculations describe the charged hadron and K_S^0 rapidity dependence and the overall normalization at the 15–25% level. In contrast, the Λ and Ξ^- yields are poorly described with HIJING under-predicting the strange

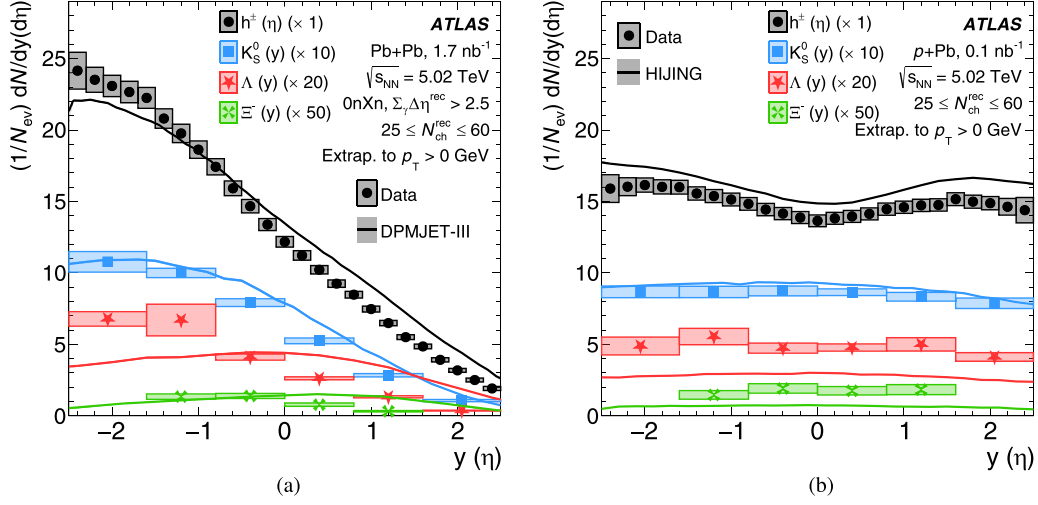


FIG. 14. Charged-hadron yields as a function of η and the K_s^0 , Λ , and Ξ^- yields as a function of y for (a) $\text{Pb}+\text{Pb}$ photonuclear collisions, with comparisons to the MC model DPMJET-III, and (b) $p+\text{Pb}$ collisions, with comparisons to HIJING. Statistical uncertainties are shown as vertical lines and systematic uncertainties are shown as colored boxes. The statistical uncertainties in the MC simulations are represented by colored bands, though they are negligible.

baryon yields by almost a factor of two and DPMJET-III over-predicting the yields at forward rapidity and under-predicting at backward rapidity.

Figure 15 shows the same ATLAS results now compared with calculations from the hybrid model. The charged-hadron yields are well described in $p+\text{Pb}$ collisions, and only qualitatively described in photonuclear collisions. For both collision systems, the K_s^0 are over-predicted, the Λ under-predicted, and the Ξ^- well described. Since the level of disagreement for strange hadrons (K_s^0 and Λ) is similar in both $p+\text{Pb}$ and photonuclear collisions, it is likely a generic failing of the modeling for strangeness and/or baryons in general in the hadronization of the hydrodynamic QGP.

It is also instructive to compare the experimental results for $\langle p_T \rangle$ as a function of $N_{\text{ch}}^{\text{rec}}$ as shown in Fig. 16 with the MC models DPMJET-III and HIJING and Fig. 17 with the hybrid model. Both MC models substantially under-predict the $\langle p_T \rangle$ for all particles, and also under-predict the difference in $\langle p_T \rangle$ between hadrons of different masses. Strikingly, DPMJET-III predicts a higher $\langle p_T \rangle$ for Λ particles at forward rapidity compared to backward rapidity, exactly opposite to the trend in data.

In contrast, the hybrid model provides a reasonable description of the $\langle p_T \rangle$ of charged hadrons and Λ particles in both photonuclear and $p+\text{Pb}$ collisions, including the higher $\langle p_T \rangle$ values at backward rapidity compared to forward rapidity in photonuclear collisions. However, the $\langle p_T \rangle$ values for K_s^0

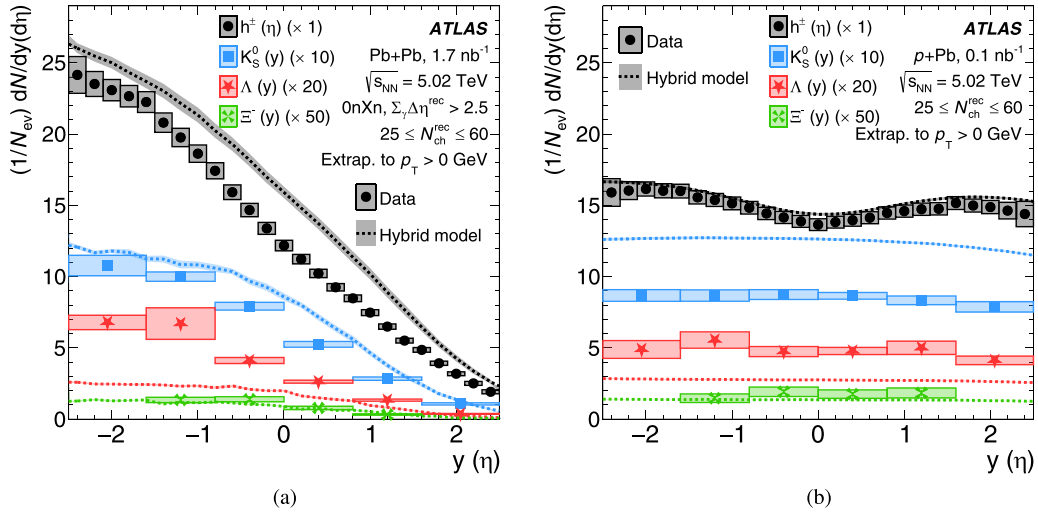


FIG. 15. Charged-hadron yields as a function of η and the K_s^0 , Λ , and Ξ^- yields as a function of y for (a) $\text{Pb}+\text{Pb}$ photonuclear collisions and (b) $p+\text{Pb}$ collisions. Both are compared to the hybrid model calculations. Statistical uncertainties are shown as vertical lines and systematic uncertainties are shown as colored boxes. The statistical uncertainties of the model calculations are shown by colored bands.

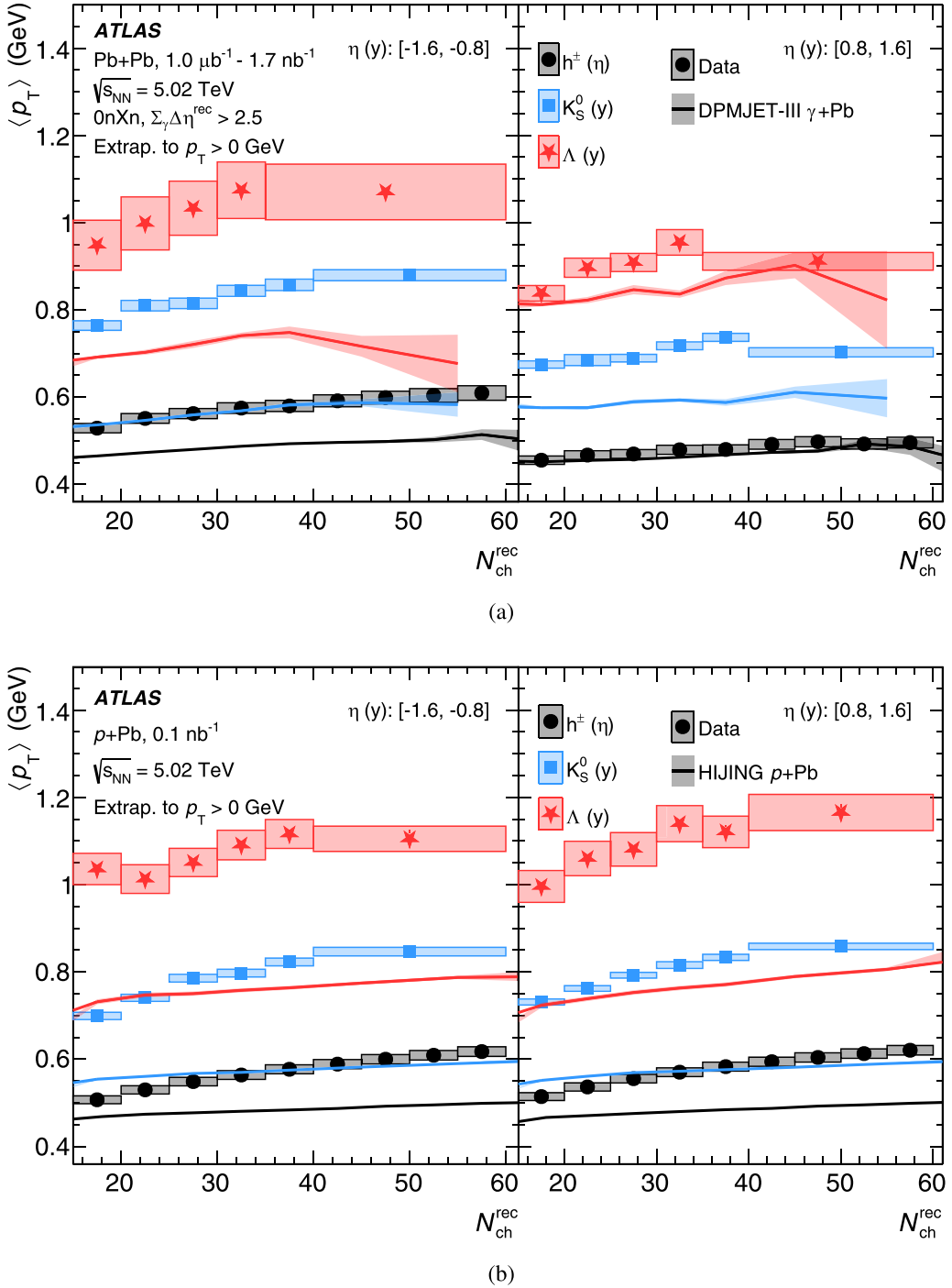


FIG. 16. $\langle p_T \rangle$ for charged hadrons, K_S^0 , and Λ in (a) Pb+Pb photonuclear and (b) $p + \text{Pb}$ collisions as a function of N_{ch}^{rec} . The left (right) panels are for a backward (forward) rapidity selection. Statistical uncertainties are shown as vertical lines and systematic uncertainties are shown as colored boxes. Also shown are comparisons to the MC model DPMJET-III and HIJING for Pb+Pb photonuclear and $p + \text{Pb}$ collisions, respectively, with the shaded bands indicating the statistical uncertainties.

are under-predicted in all cases. Until these deficiencies in the hybrid model are resolved, first in the $p + \text{Pb}$ case, stronger conclusions regarding QGP formation in photonuclear events remains premature.

VIII. CONCLUSION

This paper reports a measurement of the yields of charged hadrons and identified K_S^0 , Λ , Ξ^- in high-energy photonuclear collisions. Events are selected from 1.7 nb^{-1} of

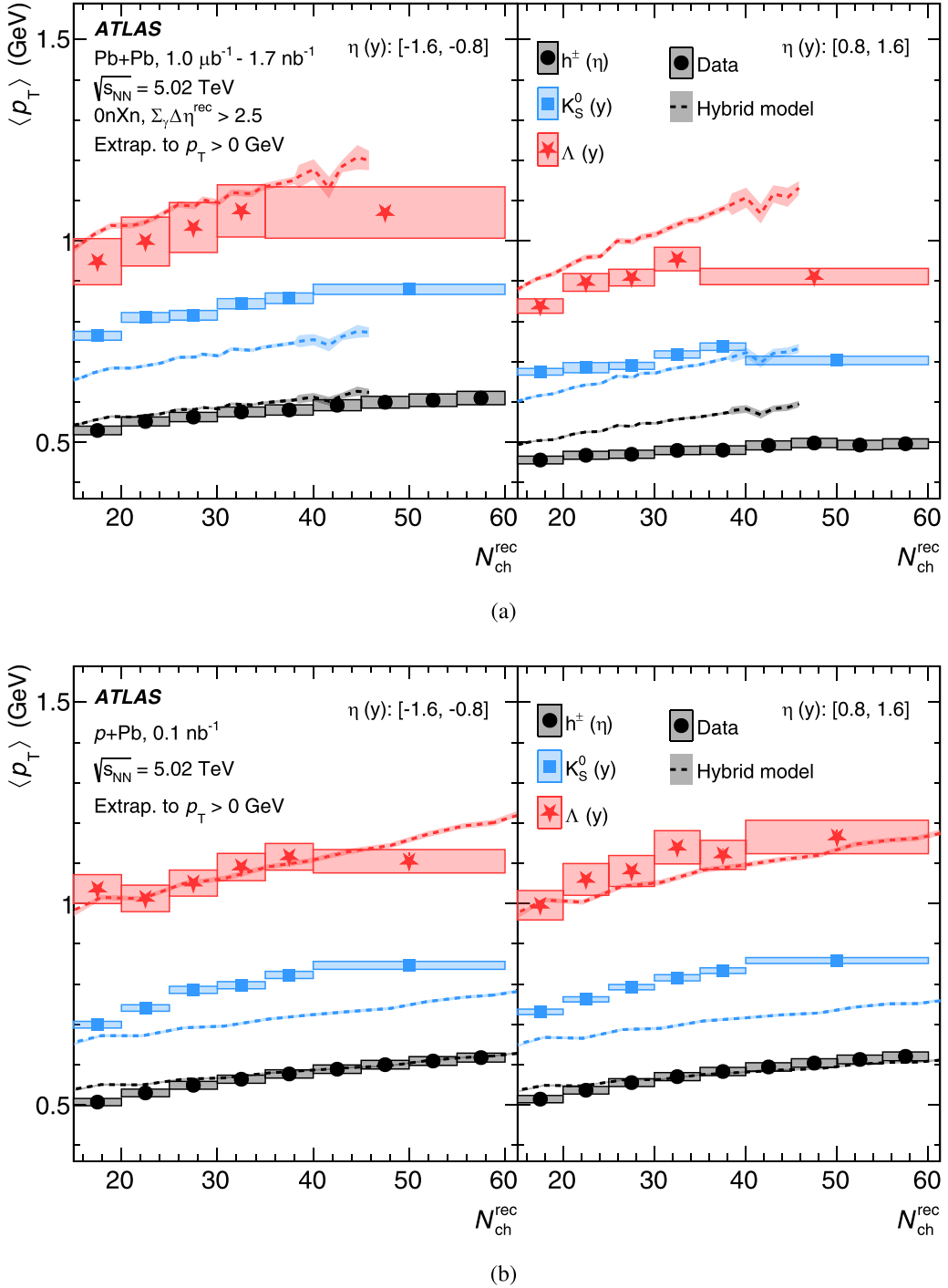


FIG. 17. $\langle p_T \rangle$ for charged hadrons, K_S^0 , and Λ in (a) p + Pb photonuclear and (b) p + Pb collisions as a function of N_{ch}^{rec} . The left (right) panels are for a backward (forward) rapidity selection. Statistical uncertainties are shown as vertical lines and systematic uncertainties are shown as colored boxes. Also shown are comparisons to the hybrid hydrodynamic model for both collision types.

$\sqrt{s_{NN}} = 5.02$ TeV $Pb+Pb$ data collected by the ATLAS detector at the LHC in 2018. The yields are measured as a function of p_T and rapidity for different N_{ch}^{rec} intervals. The results are compared with $p+Pb$ collision data at comparable N_{ch}^{rec} intervals. These photonuclear events reveal a strong rapidity asymmetry in all particle yields, with fewer particles in the photon-going direction as expected. In

the Pb -going direction, the particles exhibit larger average transverse momentum that increases for higher mass particles. There is also a significant enhancement of the Λ/K_S^0 (baryon/meson) ratio, and a hint of an enhancement of overall strange particle production. These observations in the Pb -going direction are generally consistent with what is observed in the $p+Pb$ Pb -going direction, giving credence to the

hypothesis that the photonuclear collisions are dominated by vector meson dominance, i.e., hadronic ρ meson–Pb collisions. Comparisons with MC models reveal a very incomplete modeling of the physics processes. The hybrid model, based on the assumption of QGP formation and hydrodynamic expansion, captures some features such as the larger mean p_T at backward rapidity in photonuclear events, but fails to quantitatively describe the yields of identified strange particles.

ACKNOWLEDGMENTS

We thank CERN for the very successful operation of the LHC and its injectors, as well as the support staff at CERN and at our institutions worldwide without whom ATLAS could not be operated efficiently. The crucial computing support from all WLCG partners is acknowledged gratefully, in particular from CERN, the ATLAS Tier-1 facilities at TRIUMF/SFU (Canada), NDGF (Denmark, Norway, Sweden), CC-IN2P3 (France), KIT/GridKA (Germany), INFN-CNAF (Italy), NL-T1 (Netherlands), PIC (Spain), RAL (UK) and BNL (USA), the Tier-2 facilities worldwide, and large non-WLCG resource providers. Major contributors of computing resources are listed in Ref. [55]. We gratefully acknowledge the support of ANPCyT, Argentina; YerPhI, Armenia; ARC, Australia; BMWFW and FWF, Austria; ANAS, Azerbaijan; CNPq and FAPESP, Brazil; NSERC, NRC and CFI, Canada; CERN; ANID, Chile; CAS, MOST and NSFC, China; Minciencias, Colombia; MEYS CR, Czech Republic; DNRF and DNSRC, Denmark; IN2P3-CNRS and CEA-DRF/IRFU, France; SRNSFG, Georgia; BMBF, HGF and MPG, Germany; GSRI, Greece; RGC and Hong Kong SAR, China; ICHEP and Academy of Sciences and Humanities, Israel; INFN, Italy; MEXT and JSPS, Japan; CNRST, Morocco; NWO, Netherlands; RCN, Norway; MNiSW, Poland; FCT, Portugal; MNE/IFA, Romania; MSTDI, Serbia; MSSR, Slovakia; ARIS and MVZI, Slovenia; DSI/NRF, South Africa; MICU/AEI, Spain; SRC and Wallenberg Foundation, Sweden; SERI, SNSF and Cantons of Bern and Geneva, Switzerland; NSTC, Taipei; TENMAK, Türkiye; STFC/UKRI, United Kingdom; DOE and NSF, USA. Individual groups and members have received support from BCKDF, CANARIE, CRC and DRAC, Canada; CERN-CZ, FORTE and PRIMUS, Czech Republic; COST, ERC, ERDF, Horizon 2020, ICSC-NextGenerationEU and Marie Skłodowska-Curie Actions, European Union; Investissements d’Avenir Labex, Investissements d’Avenir Idex and ANR, France; DFG and AvH Foundation, Germany; Herakleitos, Thales and Aristeia programmes co-financed by EU-ESF and the Greek NSRF, Greece; BSF-NSF and MINERVA, Israel; NCN and NAWA, Poland; La Caixa Banking Foundation, CERCA Programme Generalitat de Catalunya and PROMETEO and GenT Programmes Generalitat Valenciana, Spain; Göran Gustafssons Stiftelse, Sweden; The Royal Society and Leverhulme Trust, United Kingdom. In addition, individual members acknowledge support from Armenia: Yerevan Physics Institute (FAPERJ); CERN: European Organization for Nuclear Research (CERN DOCT);

Chile: Agencia Nacional de Investigación y Desarrollo (Grants No. FONDECYT 1230812, No. FONDECYT 1230987, and No. FONDECYT 1240864); China: Chinese Ministry of Science and Technology (Grants No. MOST-2023YFA1605700 and No. MOST-2023YFA1609300), National Natural Science Foundation of China (Grants No. NSFC 12175119 and No. NSFC 12275265); Czech Republic: Czech Science Foundation (Grant No. GACR 24-11373S), Ministry of Education Youth and Sports (ERC-CZ-LL2327, FORTE CZ.02.01.01/00/22_008/0004632), PRIMUS Research Programme (PRIMUS/21/SCI/017); EU: H2020 European Research Council (Grant No. ERC 101002463); European Union: European Research Council (Grants No. ERC 948254, No. ERC 101089007, and No. ERC, BARD, 101116429), European Regional Development Fund (SMASH COFUND 101081355, SLO ERDF), Horizon 2020 Framework Programme (MUCCA—CHIST-ERA-19-XAI-00), European Union, Future Artificial Intelligence Research (FAIR-NextGenerationEU PE00000013), Horizon 2020 (EuroHPC—EHPC-DEV-2024D11-051), Italian Center for High Performance Computing, Big Data and Quantum Computing (ICSC, NextGenerationEU); France: Agence Nationale de la Recherche (Grants No. ANR-21-CE31-0013, No. ANR-21-CE31-0022, and No. ANR-22-EDIR-0002); Germany: Baden-Württemberg Stiftung (BW Stiftung-Postdoc Eliteprogramme), Deutsche Forschungsgemeinschaft (Grants No. DFG-469666862 and No. DFG-CR 312/5-2); China: Research Grants Council (GRF); Italy: Istituto Nazionale di Fisica Nucleare (ICSC, NextGenerationEU), Ministero dell’Università e della Ricerca (NextGenEU PRIN20223N7F8K M4C2.1.1); Japan: Japan Society for the Promotion of Science (Grants No. JSPS KAKENHI JP22H01227, No. JSPS KAKENHI JP22H04944, No. JSPS KAKENHI JP22KK0227, and No. JSPS KAKENHI JP23KK0245); Norway: Research Council of Norway (Grant No. RCN-314472); Poland: Ministry of Science and Higher Education (IDUB AGH, POB8, D4 No. 9722), Polish National Science Centre (Grants No. NCN 2021/42/E/ST2/00350, No. NCN OPUS 2023/51/B/ST2/02507, No. NCN OPUS nr 2022/47/B/ST2/03059, No. NCN UMO-2019/34/E/ST2/00393, No. UMO-2020/37/B/ST2/01043, No. UMO-2022/47/O/ST2/00148, No. UMO-2023/49/B/ST2/04085, No. UMO-2023/51/B/ST2/00920, and No. UMO-2024/53/N/ST2/00869); Portugal: Foundation for Science and Technology (FCT); Spain: Generalitat Valenciana (Artemisa, FEDER, Grant No. IDIFEDER/2018/048), Ministry of Science and Innovation (MCIN & NextGenEU Grant No. PCI2022-135018-2, MICIN & FEDER Grants No. PID2021-125273NB, No. RYC2019-028510-I, No. RYC2020-030254-I, No. RYC2021-031273-I, and No. RYC2022-038164-I); Sweden: Carl Trygger Foundation (Carl Trygger Foundation CTS Grant No. 22:2312), Swedish Research Council (Swedish Research Council Grants No. 2023-04654, No. VR 2021-03651, No. VR 2022-03845, No. VR 2022-04683, No. VR 2023-03403, No. VR 2024-05451), Knut and Alice Wallenberg Foundation (Grants No. KAW 2018.0458, No. KAW 2022.0358, and No. KAW 2023.0366); Switzerland: Swiss National Science Foundation

(Grant No. SNSF PCEFP2_194658); United Kingdom: Leverhulme Trust (Leverhulme Trust Grant No. RPG-2020-004), Royal Society (Grant No. NIF-R1-231091); United States of America: U.S. Department of Energy (Grant No. ECA DE-AC02-76SF00515), Neubauer Family Foundation.

DATA AVAILABILITY

The public release of data supporting the findings of this article will follow the CERN Open Data Policy [56]. The values of relevant plots and tables associated with this article are stored in HEPData [57].

-
- [1] J. W. Harris and B. Muller, “QGP signatures” revisited, *Eur. Phys. J. C* **84**, 247 (2024).
 - [2] C. A. Bertulani, S. R. Klein, and J. Nystrand, Physics of ultra-peripheral nuclear collisions, *Annu. Rev. Nucl. Part. Sci.* **55**, 271 (2005).
 - [3] S. R. Klein and H. Mantysaari, Imaging the nucleus with high-energy photons, *Nat. Rev. Phys.* **1**, 662 (2019).
 - [4] ATLAS Collaboration, Exclusive dimuon production in ultra-peripheral Pb+Pb collisions at $\sqrt{s_{NN}} = 5.02$ TeV with ATLAS, *Phys. Rev. C* **104**, 024906 (2021).
 - [5] ATLAS Collaboration, Evidence for light-by-light scattering in heavy-ion collisions with the ATLAS detector at the LHC, *Nat. Phys.* **13**, 852 (2017).
 - [6] ATLAS Collaboration, Observation of light-by-light scattering in ultraperipheral Pb+Pb collisions with the ATLAS detector, *Phys. Rev. Lett.* **123**, 052001 (2019).
 - [7] ATLAS Collaboration, Observation of the $\gamma\gamma \rightarrow \tau\tau$ process in Pb+Pb collisions and constraints on the τ -lepton anomalous magnetic moment with the ATLAS detector, *Phys. Rev. Lett.* **131**, 151802 (2023).
 - [8] ATLAS Collaboration, Measurement of photonuclear jet production in ultraperipheral Pb+Pb collisions at $\sqrt{s_{NN}} = 5.02$ TeV with the ATLAS detector, *Phys. Rev. D* **111**, 052006 (2025).
 - [9] A. J. Baltz *et al.*, The physics of ultraperipheral collisions at the LHC, *Phys. Rep.* **458**, 1 (2008).
 - [10] ATLAS Collaboration, Two-particle azimuthal correlations in photonuclear ultraperipheral Pb+Pb collisions at 5.02 TeV with ATLAS, *Phys. Rev. C* **104**, 014903 (2021).
 - [11] W. Zhao, C. Shen and B. Schenke, Collectivity in ultraperipheral Pb+Pb collisions at the large hadron collider, *Phys. Rev. Lett.* **129**, 252302 (2022).
 - [12] Y. Shi, L. Wang, S.-Y. Wei, B.-W. Xiao, and L. Zheng, Exploring collective phenomena at the electron-ion collider, *Phys. Rev. D* **103**, 054017 (2021).
 - [13] U. Heinz and R. Snellings, Collective flow and viscosity in relativistic heavy-ion collisions, *Annu. Rev. Nucl. Part. Sci.* **63**, 123 (2013).
 - [14] R. J. Fries, B. Muller, C. Nonaka, and S. A. Bass, Hadronization in heavy ion collisions: Recombination and fragmentation of partons, *Phys. Rev. Lett.* **90**, 202303 (2003).
 - [15] ALICE Collaboration, Enhanced production of multi-strange hadrons in high-multiplicity proton-proton collisions, *Nat. Phys.* **13**, 535 (2017).
 - [16] ATLAS Collaboration, Underlying-event studies with strange hadrons in pp collisions at $\sqrt{s} = 13$ TeV with the ATLAS detector, *Eur. Phys. J. C* **84**, 1335 (2024).
 - [17] CMS Collaboration, Two-particle azimuthal correlations in γp interactions using $p\text{Pb}$ collisions at $\sqrt{s_{NN}} = 8.16$ TeV, *Phys. Lett. B* **844**, 137905 (2023).
 - [18] R. Engel, Photoproduction within the two-component dual parton model: Amplitudes and cross sections, *Z. Phys. C* **66**, 203 (1995).
 - [19] S. Roesler, R. Engel, and J. Ranft, The Monte Carlo event generator DPMJET-III, in *Proceedings of the International Conference on Advanced Monte Carlo for Radiation Physics, Particle Transport Simulation, and Applications* (Springer-Verlag Berlin Heidelberg, 2001), p. 1033.
 - [20] ATLAS Collaboration, The ATLAS experiment at the CERN Large Hadron Collider, *JINST* **3** S08003 (2008).
 - [21] L. Evans and P. Bryant, LHC Machine, *JINST* **3**, S08001 (2008).
 - [22] ATLAS Collaboration, ATLAS Insertable B-Layer: Technical Design Report, ATLAS-TDR-19; CERN-LHCC-2010-013 (2010), <https://cds.cern.ch/record/1291633>; Addendum: ATLAS-TDR-19-ADD-1; CERN-LHCC-2012-009 (2012), <https://cds.cern.ch/record/1451888>.
 - [23] ATLAS Collaboration, Performance of the ATLAS trigger system in 2015, *Eur. Phys. J. C* **77**, 317 (2017).
 - [24] ATLAS Collaboration, Software and computing for Run 3 of the ATLAS experiment at the LHC, *EPJC* **85**, 234 (2025).
 - [25] ATLAS Collaboration, Rapidity gap cross sections measured with the ATLAS detector in pp collisions at $\sqrt{s} = 7$ TeV, *Eur. Phys. J. C* **72**, 1926 (2012).
 - [26] ATLAS Collaboration, Correlated long-range mixed-harmonic fluctuations measured in pp , $p + \text{Pb}$, and low-multiplicity Pb+Pb collisions with the ATLAS detector, *Phys. Lett. B* **789**, 444 (2019).
 - [27] ATLAS Collaboration, Measurement of the sensitivity of two-particle correlations in pp collisions to the presence of hard scatterings, *Phys. Rev. Lett.* **131**, 162301 (2023).
 - [28] ATLAS Collaboration, Measurement of long-range two-particle azimuthal correlations in Z-boson tagged pp collisions at $\sqrt{s} = 8$ and 13 TeV, *Eur. Phys. J. C* **80**, 64 (2020).
 - [29] ATLAS Collaboration, Measurements of long-range azimuthal anisotropies and associated Fourier coefficients for pp collisions at $\sqrt{s} = 5.02$ and 13 TeV and $p + \text{Pb}$ collisions at $\sqrt{s_{NN}} = 5.02$ TeV with the ATLAS detector, *Phys. Rev. C* **96**, 024908 (2017).
 - [30] ATLAS Collaboration, Measurement of forward-backward multiplicity correlations in lead-lead, proton-lead, and proton-proton collisions with the ATLAS detector, *Phys. Rev. C* **95**, 064914 (2017).
 - [31] S. R. Klein, J. Nystrand, J. Seger, Y. Gorbunov, and J. Butterworth, STARlight: A Monte Carlo simulation program for ultra-peripheral collisions of relativistic ions, *Comput. Phys. Commun.* **212**, 258 (2017).
 - [32] C. Y. Wong, *Introduction to High-Energy Heavy-Ion Collisions* (WSPC, Singapore, 1994).

- [33] Z. Koba and H. B. Nielsen, Reaction amplitude for n mesons: A generalization of the Veneziano-Bardakci-Ruegg-Virasora model, *Nucl. Phys. B* **10**, 633 (1969).
- [34] S. Agostinelli *et al.*, GEANT4—A simulation toolkit, *Nucl. Instrum. Methods Phys. Res., Sect. A* **506**, 250 (2003).
- [35] X.-N. Wang and M. Gyulassy, HIJING: A Monte Carlo model for multiple jet production in pp, pA and AA collisions, *Phys. Rev. D* **44**, 3501 (1991).
- [36] C. Bierlich *et al.*, A comprehensive guide to the physics and usage of PYTHIA8.3, *SciPost Phys. Codebases* **2022**, 8 (2022).
- [37] M. L. Miller, K. Reygers, S. J. Sanders, and P. Steinberg, Glauber modeling in high energy nuclear collisions, *Annu. Rev. Nucl. Part. Sci.* **57**, 205 (2007).
- [38] ATLAS Collaboration, Charged-particle multiplicities in pp interactions measured with the ATLAS detector at the LHC, *New J. Phys.* **13**, 053033 (2011).
- [39] A. Salzburger, Optimisation of the ATLAS Track Reconstruction Software for Run-2, ATL-SOFT-PROC-2015-056 (2015), <https://cds.cern.ch/record/2018442>.
- [40] ATLAS Collaboration, Charged-particle distributions at low transverse momentum in $\sqrt{s} = 13$ TeV pp interactions measured with the ATLAS detector at the LHC, *Eur. Phys. J. C* **76**, 502 (2016).
- [41] ATLAS Collaboration, Modelling of Track Reconstruction Inside Jets with the 2016 ATLAS $\sqrt{s} = 13$ TeV pp Dataset, ATL-PHYS-PUB-2017-016 (2017), <https://cds.cern.ch/record/2275639>.
- [42] M. Biyajima, T. Mizoguchi, N. Nakajima, N. Suzuki, and G. Wilk, Modified Hagedorn formula including temperature fluctuation: Estimation of temperatures at RHIC experiments, *Eur. Phys. J. C* **48**, 597 (2006).
- [43] ALICE Collaboration, Strange particle production in proton-proton collisions at $\sqrt{s} = 0.9$ TeV with ALICE at the LHC, *Eur. Phys. J. C* **71**, 1594 (2011).
- [44] ALICE Collaboration, Midrapidity antiproton-to-proton ratio in pp collisions at $\sqrt{s} = 0.9$ and 7 TeV measured by the ALICE experiment, *Phys. Rev. Lett.* **105**, 072002 (2010).
- [45] R. Fröhwirth, Application of Kalman filtering to track and vertex fitting, *Nucl. Instrum. Methods Phys. Res., Sect. A* **262**, 444 (1987).
- [46] A. Hoecker *et al.*, TMVA—Toolkit for multivariate data analysis, Report No. CERN-OPEN-2007-007 (2007).
- [47] ATLAS Collaboration, K_S^0 and Λ production in pp interactions at $\sqrt{s} = 0.9$ and 7 TeV measured with the ATLAS detector at the LHC, *Phys. Rev. D* **85**, 012001 (2012).
- [48] ATLAS Collaboration, Charged-particle distributions in $\sqrt{s} = 13$ TeV pp interactions measured with the ATLAS detector at the LHC, *Phys. Lett. B* **758**, 67 (2016).
- [49] T. S. Biro and B. Muller, Almost exponential transverse spectra from power law spectra, *Phys. Lett. B* **578**, 78 (2004).
- [50] ATLAS Collaboration, Transverse momentum, rapidity, and centrality dependence of inclusive charged-particle production in $\sqrt{s_{NN}} = 5.02$ TeV $p + Pb$ collisions measured by the ATLAS experiment, *Phys. Lett. B* **763**, 313 (2016).
- [51] ALICE Collaboration, K_S^0 and Λ production in $Pb-Pb$ collisions at $\sqrt{s_{NN}} = 2.76$ TeV, *Phys. Rev. Lett.* **111**, 222301 (2013).
- [52] R. J. Fries, V. Greco, and P. Sorensen, Coalescence models For hadron formation from quark gluon plasma, *Annu. Rev. Nucl. Part. Sci.* **58**, 177 (2008).
- [53] B. Schenke, S. Jeon, and C. Gale, (3+1)D hydrodynamic simulation of relativistic heavy-ion collisions, *Phys. Rev. C* **82**, 014903 (2010).
- [54] M. Bleicher *et al.*, Relativistic hadron-hadron collisions in the ultra-relativistic quantum molecular dynamics model, *J. Phys. G* **25**, 1859 (1999).
- [55] ATLAS Collaboration, *ATLAS Computing Acknowledgements*, ATL-SOFT-PUB-2025-001 (2025), <https://cds.cern.ch/record/2922210>.
- [56] CERN, CERN Open Data Policy for the LHC Experiments, CERN-OPEN-2020-013, 2020, <https://cds.cern.ch/record/2745133>.
- [57] <https://www.hepdata.net/record/158635>.

G. Aad¹⁰⁴ E. Aakvaag¹⁷ B. Abbott¹²³ S. Abdelhameed^{119a} K. Abeling¹⁵⁵ N. J. Abicht¹⁵⁹ S. H. Abidi^{27b} M. Aboelela⁴⁵ A. Aboulhorma^{36e} H. Abramowicz¹⁵⁷ Y. Abulaiti¹²⁰ B. S. Acharya^{169a,69b,a} A. Ackermann^{163a} C. Adam Bourdarios⁴ L. Adamczyk^{86a} S. V. Addepalli¹⁴⁹ M. J. Addison¹⁰³ J. Adelman¹¹⁸ A. Adiguzel^{22c} T. Adye¹³⁷ A. A. Affolder¹³⁹ Y. Afik⁴⁰ M. N. Agaras¹⁰ A. Aggarwal¹⁰² C. Agheorghiesei^{129c} F. Ahmadov^{139,b} S. Ahuja⁹⁷ X. Ai^{143b} G. Aielli^{76a,76b} A. Aikot¹⁶⁹ M. Ait Tamlihat^{36e} B. Aitbenchikh^{36a} M. Akbiyik¹⁰² T. P. A. Åkesson¹⁰⁰ A. V. Akimov¹⁵¹ D. Akiyama¹⁰ T. Albert¹⁷¹ P. Albicocco⁵³ G. L. Albouy⁶⁰ S. Alderweireldt⁵² Z. L. Alegria¹²⁴ M. Aleksa³⁷ I. N. Aleksandrov³⁹ C. Alexa^{29b} T. Alexopoulos¹⁰ F. Alfonsi^{24b} M. Algren⁵⁶ M. Alhroob¹⁷³ B. Ali¹³⁵ H. M. J. Ali^{93,c} S. Ali³² S. W. Alibocus⁹⁴ M. Aliev^{34c} G. Alimonti^{71a} W. Alkakhi⁵⁵ C. Allaire⁶⁶ B. M. M. Allbrooke¹⁵² J. S. Allen¹⁰³ J. F. Allen⁵² P. P. Allport²¹ A. Aloisio^{72a,72b} F. Alonso⁹² C. Alpigiani¹⁴² Z. M. K. Alsolami⁹³ A. Alvarez Fernandez¹⁰² M. Alves Cardoso⁵⁶ M. G. Alviggi^{72a,72b} M. Aly¹⁰³ Y. Amaral Coutinho^{83b} A. Ambler¹⁰⁶ C. Ameling³⁷ M. Amerl¹⁰³ C. G. Ames¹¹¹ T. Amezza¹³⁰ D. Amidei¹⁰⁸ B. Amini⁵⁴ K. Amirie¹⁶¹ A. Amirkhanov³⁹ S. P. Amor Dos Santos^{133a} K. R. Amos¹⁶⁹ D. Amperiadou¹⁵⁸ S. An⁸⁴ C. Anastopoulos¹⁴⁵ T. Andeen¹¹ J. K. Anders⁹⁴ A. C. Anderson⁵⁹ A. Andreazza^{71a,71b} S. Angelidakis⁹ A. Angerami⁴² A. V. Anisenkov³⁹ A. Annovi^{74a} C. Antel⁵⁶ E. Antipov¹⁵¹ M. Antonelli⁵³ F. Anulli^{75a} M. Aoki⁸⁴ T. Aoki¹⁵⁹ M. A. Aparo¹⁵² L. Aperio Bella⁴⁸ M. Apicella³¹ C. Appelt¹⁵⁷ A. Apyan²⁸ S. J. Arbiol Val⁸⁷ C. Arcangeletti⁵³ A. T. H. Arce⁵¹ J.-F. Arguin¹¹⁰ S. Argyropoulos¹⁵⁸ J.-H. Arling⁴⁸ O. Arnaez⁴ H. Arnold¹⁵¹ G. Artoni^{75a,75b} H. Asada¹¹³ K. Asai¹²¹ S. Asai¹⁵⁹ N. A. Asbah³⁷ R. A. Ashby Pickering¹⁷³ A. M. Aslam⁹⁷ K. Assamagan^{27b} R. Astalos^{30a} K. S. V. Astrand¹⁰⁰ S. Atashi¹⁶⁵

- R. J. Atkin^{13a} H. Atmani^{36f} P. A. Atmasiddha¹³¹ K. Augsten¹³⁵ A. D. Auriol⁴¹ V. A. Austrup¹⁰³ G. Avolio³⁷
 K. Axiotis⁵⁶ G. Azuelos^{110,d} D. Babal^{30b} H. Bachacou¹³⁸ K. Bachas^{158,e} A. Bachiu³⁵ E. Bachmann⁵⁰
 M. J. Backes^{63a} A. Badea⁴⁰ T. M. Baer¹⁰⁸ P. Bagnaia^{75a,75b} M. Bahmani¹⁹ D. Bahner⁵⁴ K. Bai¹²⁶
 J. T. Baines¹³⁷ L. Baines⁹⁶ O. K. Baker¹⁷⁸ E. Bakos¹⁶ D. Bakshi Gupta⁸ L. E. Balabram Filho^{83b}
 V. Balakrishnan¹²³ R. Balasubramanian⁴ E. M. Baldin³⁸ P. Balek^{86a} E. Ballabene^{24b,24a} F. Balli¹³⁸
 L. M. Baltes^{63a} W. K. Balunas³³ J. Balz¹⁰² I. Bamwidhi^{119b} E. Banas⁸⁷ M. Bandieramonte¹³²
 A. Bandyopadhyay²⁵ S. Bansal²⁵ L. Barak¹⁵⁷ M. Barakat⁴⁸ E. L. Barberio¹⁰⁷ D. Barberis^{18b} M. Barbero¹⁰⁴
 M. Z. Barel¹¹⁷ T. Barillari¹¹² M-S. Barisits³⁷ T. Barklow¹⁴⁹ P. Baron¹²⁵ D. A. Baron Moreno¹⁰³
 A. Baroncelli⁶² A. J. Barr¹²⁹ J. D. Barr⁹⁸ F. Barreiro¹⁰¹ J. Barreiro Guimaraes da Costa¹⁴
 M. G. Barros Teixeira^{133a} S. Barsov³⁸ F. Bartels^{63a} R. Bartoldus¹⁴⁹ A. E. Barton⁹³ P. Bartos^{30a} A. Basan¹⁰²
 M. Baselga⁴⁹ S. Bashiri⁸⁷ A. Bassalat^{66,f} M. J. Basso^{162a} S. Batajou⁴⁵ R. Bate¹⁷⁰ R. L. Bates⁵⁹ S. Batlamous¹⁰¹
 M. Battaglia¹³⁹ D. Battulga¹⁹ M. Bauche^{75a,75b} M. Bauer⁷⁹ P. Bauer²⁵ L. T. Bayer⁴⁸ L. T. Bazzano Hurrell³¹
 J. B. Beacham¹¹² T. Beau¹³⁰ J. Y. Beauchamp⁹² P. H. Beauchemin¹⁶⁴ P. Bechtle²⁵ H. P. Beck^{20,g} K. Becker¹⁷³
 A. J. Beddall⁸² V. A. Bednyakov³⁹ C. P. Bee¹⁵¹ L. J. Beemster¹⁶ M. Begalli^{83d} M. Begel^{27b} J. K. Behr⁴⁸
 J. F. Beirer³⁷ F. Beisiegel²⁵ M. Belfkir^{119b} G. Bella¹⁵⁷ L. Bellagamba^{24b} A. Bellerive³⁵ C. D. Bellgraph⁶⁸
 P. Bellos²¹ K. Beloborodov³⁸ D. Benchekroun^{36a} F. Bendebba^{36a} Y. Benhammou¹⁵⁷ K. C. Benkendorfer⁶¹
 L. Beresford⁴⁸ M. Beretta⁵³ E. Bergeaas Kuutmann¹⁶⁷ N. Berger⁴ B. Bergmann¹³⁵ J. Beringer^{18a}
 G. Bernardi⁵ C. Bernius¹⁴⁹ F. U. Bernlochner²⁵ F. Bernon³⁷ A. Berrocal Guardia¹³ T. Berry⁹⁷ P. Berta¹³⁶
 A. Berthold⁵⁰ A. Berti^{133a} R. Bertrand¹⁰⁴ S. Bethke¹¹² A. Betti^{75a,75b} A. J. Bevan⁹⁶ L. Bezio⁵⁶
 N. K. Bhalla⁵⁴ S. Bharthuar¹¹² S. Bhatta¹⁵¹ P. Bhattarai¹⁴⁹ Z. M. Bhatti¹²⁰ K. D. Bhide⁵⁴ V. S. Bhopatkar¹²⁴
 R. M. Bianchi¹³² G. Bianco^{24b,24a} O. Biebel¹¹¹ M. Biglietti^{77a} C. S. Billingsley⁴⁵ Y. Bimgdi^{36f} M. Bind⁵⁵
 A. Bingham¹⁷⁷ A. Bingul^{22b} C. Bini^{75a,75b} G. A. Bird³³ M. Birman¹⁷⁵ M. Biros¹³⁶ S. Biryukov¹⁵²
 T. Bisanz⁴⁹ E. Bisceglie^{24b,24a} J. P. Biswal¹³⁷ D. Biswas¹⁴⁷ I. Bloch⁴⁸ A. Blue⁵⁹ U. Blumenschein⁹⁶
 J. Blumenthal¹⁰² V. S. Bobrovnikov³⁹ M. Boehler⁵⁴ B. Boehm¹⁷² D. Bogavac¹³ A. G. Bogdanchikov³⁸
 L. S. Boggia¹³⁰ V. Boisvert⁹⁷ P. Bokan³⁷ T. Bold^{86a} M. Bomben⁵ M. Bona⁹⁶ M. Boonekamp¹³⁸
 A. G. Borbely⁵⁹ I. S. Bordulev³⁸ G. Borissov⁹³ D. Bortoletto¹²⁹ D. Boscherini^{24b} M. Bosman¹³
 K. Bouaouda^{36a} N. Bouchhar¹⁶⁹ L. Boudet⁴ J. Boudreau¹³² E. V. Bouhova-Thacker⁹³ D. Boumediene⁴¹
 R. Bouquet^{57b,57a} A. Boveia¹²² J. Boyd³⁷ D. Boye^{27b} I. R. Boyko³⁹ L. Bozianu⁵⁶ J. Bracinik²¹ N. Brahimi¹⁷⁵
 G. Brandt¹⁷⁷ O. Brandt³³ B. Brau¹⁰⁵ J. E. Brau¹²⁶ R. Brener¹⁷⁵ L. Brenner¹¹⁷ R. Brenner¹⁶⁷ S. Bressler¹⁷⁵
 G. Brianti^{78a,78b} D. Britton⁵⁹ D. Blitzger¹¹² I. Brock²⁵ R. Brock¹⁰⁹ G. Brooijmans⁴² A. J. Brooks⁶⁸
 E. M. Brooks^{162b} E. Brost^{27b} L. M. Brown^{171,162a} L. E. Bruce⁶¹ T. L. Bruckler¹²⁹
 P. A. Bruckman de Renstrom⁸⁷ B. Brüers⁴⁸ A. Bruni^{24b} G. Bruni^{24b} D. Brunner^{47a,47b} M. Bruschi^{24b}
 N. Bruscino^{75a,75b} T. Buanes¹⁷ Q. Buat¹⁴² D. Buchin¹¹² A. G. Buckley⁵⁹ O. Bulekov⁸² B. A. Bullard¹⁴⁹
 S. Burdin⁹⁴ C. D. Burgard⁴⁹ A. M. Burger⁹¹ B. Burghgrave⁸ O. Burlayenko⁵⁴ J. Burleson¹⁶⁸ J. T. P. Burr³³
 J. C. Burzynski¹⁴⁸ E. L. Busch⁴² V. Büscher¹⁰² P. J. Bussey⁵⁹ J. M. Butler²⁶ C. M. Buttar⁵⁹
 J. M. Butterworth⁹⁸ W. Buttlinger¹³⁷ C. J. Buxo Vazquez¹⁰⁹ A. R. Buzykaev³⁹ S. Cabrera Urbán¹⁶⁹
 L. Cadamuro⁶⁶ D. Caforio⁵⁸ H. Cai¹³² Y. Cai^{24b,114c,24a} Y. Cai^{114a} V. M. M. Cairo³⁷ O. Cakir^{3a} N. Calace³⁷
 P. Calafiura^{18a} G. Calderini¹³⁰ P. Calfayan³⁵ G. Callea⁵⁹ L. P. Caloba^{83b} D. Calvet⁴¹ S. Calvet⁴¹
 R. Camacho Toro¹³⁰ S. Camarda³⁷ D. Camarero Munoz²⁸ P. Camarri^{76a,76b} C. Camincher¹⁷¹ M. Campanelli⁹⁸
 A. Camplani⁴³ V. Canale^{72a,72b} A. C. Canbay^{3a} E. Canonero⁹⁷ J. Cantero¹⁶⁹ Y. Cao¹⁶⁸ F. Capocasa²⁸
 M. Capua^{44b,44a} A. Carbone^{71a,71b} R. Cardarelli^{76a} J. C. J. Cardenas⁸ M. P. Cardiff²⁸ G. Carducci^{44b,44a}
 T. Carli³⁷ G. Carlino^{72a} J. I. Carlotto¹³ B. T. Carlson^{132,h} E. M. Carlson¹⁷¹ J. Carmignani⁹⁴
 L. Carminati^{71a,71b} A. Carnelli⁴ M. Carnesale³⁷ S. Caron¹¹⁶ E. Carquin^{140f} I. B. Carr¹⁰⁷ S. Carrá^{71a}
 G. Carrat^{24b,24a} A. M. Carroll¹²⁶ M. P. Casado^{13,i} M. Caspar⁴⁸ F. L. Castillo⁴ L. Castillo Garcia¹³
 V. Castillo Gimenez¹⁶⁹ N. F. Castro^{133a,133e} A. Catinaccio³⁷ J. R. Catmore¹²⁸ T. Cavaliere⁴ V. Cavaliere^{27b}
 L. J. Caviedes Betancourt^{23b} Y. C. Cekmecelioglu⁴⁸ E. Celebi⁸² S. Cella³⁷ V. Cepaitis⁵⁶ K. Cerny¹²⁵
 A. S. Cerqueira^{83a} A. Cerri^{74a,74b,j} L. Cerrito^{76a,76b} F. Cerutti^{18a} B. Cervato^{71a,71b} A. Cervelli^{24b} G. Cesarini⁵³
 S. A. Cetin⁸² P. M. Chabrillat¹³⁰ J. Chan^{18a} W. Y. Chan¹⁵⁹ J. D. Chapman³³ E. Chapon¹³⁸
 B. Chargeishvili^{155b} D. G. Charlton²¹ C. Chauhan¹³⁶ Y. Che^{114a} S. Chekanov⁶ S. V. Chekulaev^{162a}
 G. A. Chelkov^{39,k} B. Chen¹⁵⁷ B. Chen¹⁷¹ H. Chen^{114a} H. Chen^{27b} J. Chen^{144a} J. Chen¹⁴⁸ M. Chen¹²⁹
 S. Chen⁸⁹ S. J. Chen^{114a} X. Chen^{144a} X. Chen^{15,1} Z. Chen⁶² C. L. Cheng¹⁷⁶ H. C. Cheng^{64a} S. Cheong¹⁴⁹
 A. Cheplakov³⁹ E. Cheremushkina⁴⁸ E. Cherepanova¹¹⁷ R. Cherkaoui El Moursli^{36e} E. Cheu⁷ K. Cheung⁶⁵
 L. Chevalier¹³⁸ V. Chiarella⁵³ G. Chiarella^{74a} G. Chiodini^{70a} A. S. Chisholm²¹ A. Chitan^{29b} M. Chitishvili¹⁶⁹
 M. V. Chizhov^{39,m} K. Choi¹¹ Y. Chou¹⁴² E. Y. S. Chow¹¹⁶ K. L. Chu¹⁷⁵ M. C. Chu^{64a} X. Chu^{14,114c}
 Z. Chubinidze⁵³ J. Chudoba¹³⁴ J. J. Chwastowski⁸⁷ D. Cieri¹¹² K. M. Ciesla^{86a} V. Cindro⁹⁵ A. Ciocio^{18a}
 F. Cirotto^{72a,72b} Z. H. Citron¹⁷⁵ M. Citterio^{71a} D. A. Ciubotaru^{29b} A. Clark⁵⁶ P. J. Clark⁵² N. Clarke Hall⁹⁸
 C. Clarry¹⁶¹ S. E. Clawson⁴⁸ C. Clement^{47a,47b} Y. Coadou¹⁰⁴ M. Cobal^{69a,69c} A. Coccaro^{57b}
 R. F. Coelho Barrue^{133a} R. Coelho Lopes De Sa¹⁰⁵ S. Coelli^{71a} L. S. Colangeli¹⁶¹ B. Cole⁴² P. Collado Soto¹⁰¹

- J. Collot ⁶⁰ R. Coluccia ^{70a,70b} P. Conde Muiño ^{133a,133g} M. P. Connell ^{34c} S. H. Connell ^{34c} E. I. Conroy ¹²⁹
F. Conventi ^{72a,n} H. G. Cooke ²¹ A. M. Cooper-Sarkar ¹²⁹ L. Corazzina ^{75a,75b} F. A. Corchia ^{24b,24a}
A. Cordeiro Oudot Choi ¹⁴² L. D. Corpe ⁴¹ M. Corradi ^{75a,75b} F. Corriveau ^{106,o} A. Cortes-Gonzalez ¹⁹
M. J. Costa ¹⁶⁹ F. Costanza ⁴ D. Costanzo ¹⁴⁵ B. M. Cote ¹²² J. Couthures ⁴ G. Cowan ⁹⁷ K. Cranmer ¹⁷⁶
L. Cremer ⁴⁹ D. Cremonini ^{24b,24a} S. Crépé-Renaudin ⁶⁰ F. Crescioli ¹³⁰ T. Cresta ^{73a,73b} M. Cristinziani ¹⁴⁷
M. Cristoforetti ^{78a,78b} V. Croft ¹¹⁷ J. E. Crosby ¹²⁴ G. Crosetti ^{44b,44a} A. Cueto ¹⁰¹ H. Cui ⁹⁸ Z. Cui ⁷
W. R. Cunningham ⁵⁹ F. Curcio ¹⁶⁹ J. R. Curran ⁵² M. J. Da Cunha Sargedas De Sousa ^{57b,57a}
J. V. Da Fonseca Pinto ^{83b} C. Da Via ¹⁰³ W. Dabrowski ^{86a} T. Dado ³⁷ S. Dahbi ¹⁵⁴ T. Dai ¹⁰⁸ D. Dal Santo ²⁰
C. Dallapiccola ¹⁰⁵ M. Dam ⁴³ G. D'amen ^{27b} V. D'Amico ¹¹¹ J. Damp ¹⁰² J. R. Dandoy ³⁵ D. Dannheim ³⁷
G. D'anniballe ^{74a,74b} M. Danninger ¹⁴⁸ V. Dao ¹⁵¹ G. Darbo ^{57b} S. J. Das ^{27b} F. Dattola ⁴⁸ S. D'Auria ^{71a,71b}
A. D'Avanzo ^{72a,72b} T. Davidek ¹³⁶ J. Davidson ¹⁷³ I. Dawson ⁹⁶ K. De ⁸ C. De Almeida Rossi ¹⁶¹
R. De Asmundis ^{72a} N. De Biase ⁴⁸ S. De Castro ^{24b,24a} N. De Groot ¹¹⁶ P. de Jong ¹¹⁷ H. De la Torre ¹¹⁸
A. De Maria ^{114a} A. De Salvo ^{75a} U. De Sanctis ^{76a,76b} F. De Santis ^{70a,70b} A. De Santo ¹⁵²
J. B. De Vivie De Regie ⁶⁰ J. Debevc ⁹⁵ D. V. Dedovich ³⁹ J. Degens ⁹⁴ A. M. Deiana ⁴⁵ J. Del Peso ¹⁰¹
L. Delagrange ¹³⁰ F. Deliot ¹³⁸ C. M. Delitzsch ⁴⁹ M. Della Pietra ^{72a,72b} D. Della Volpe ⁵⁶ A. Dell'Acqua ³⁷
L. Dell'Asta ^{71a,71b} M. Delmastro ⁴ C. C. Delogu ¹⁰² P. A. Delsart ⁶⁰ S. Demers ¹⁷⁸ M. Demichev ³⁹
S. P. Denisov ³⁸ H. Denizli ^{22a,p} L. D'Eramo ⁴¹ D. Derendarz ⁸⁷ F. Derue ¹³⁰ P. Dervan ⁹⁴ K. Desch ²⁵
F. A. Di Bello ^{57b,57a} A. Di Ciaccio ^{76a,76b} L. Di Ciaccio ⁴ A. Di Domenico ^{75a,75b} C. Di Donato ^{72a,72b}
A. Di Girolamo ³⁷ G. Di Gregorio ³⁷ A. Di Luca ^{78a,78b} B. Di Micco ^{77a,77b} R. Di Nardo ^{77a,77b} K. F. Di Petrillo ⁴⁰
M. Diamantopoulou ³⁵ F. A. Dias ¹¹⁷ M. A. Diaz ^{140a,140b} A. R. Didenko ³⁹ M. Didenko ¹⁶⁹ S. D. Diefenbacher ^{18a}
E. B. Diehl ¹⁰⁸ S. Díez Cornell ⁴⁸ C. Diez Pardos ¹⁴⁷ C. Dimitriadi ¹⁵⁰ A. Dimitrieva ²¹ A. Dimri ¹⁵¹
J. Dingfelder ²⁵ T. Dingley ¹²⁹ I-M. Dinu ^{29b} S. J. Dittmeier ^{63b} F. Dittus ³⁷ M. Divisek ¹³⁶ B. Dixit ⁹⁴
F. Djama ¹⁰⁴ T. Djjobava ^{155b} C. Doglioni ^{103,100} A. Dohnalova ^{30a} Z. Dolezal ¹³⁶ K. Domijan ^{86a} K. M. Dona ⁴⁰
M. Donadelli ^{83d} B. Dong ¹⁰⁹ J. Donini ⁴¹ A. D'Onofrio ^{72a,72b} M. D'Onofrio ⁹⁴ J. Dopke ¹³⁷ A. Doria ^{72a}
N. Dos Santos Fernandes ^{133a} P. Dougan ¹⁰³ M. T. Dova ⁹² A. T. Doyle ⁵⁹ M. A. Draguet ¹²⁹ M. P. Drescher ⁵⁵
E. Dreyer ¹⁷⁵ I. Drivas-koulouris ¹⁰ M. Drnevich ¹²⁰ M. Drozdova ⁵⁶ D. Du ⁶² T. A. du Pree ¹¹⁷ Z. Duan ^{114a}
F. Dubinin ³⁹ M. Dubovsky ^{30a} E. Duchovni ¹⁷⁵ G. Duckeck ¹¹¹ P. K. Duckett ⁹⁸ O. A. Ducu ^{29b} D. Duda ⁵²
A. Dudarev ³⁷ E. R. Duden ²⁸ M. D'uffizi ¹⁰³ L. Duflot ⁶⁶ M. Dürhssen ³⁷ I. Dumincà ^{29g} A. E. Dumitriu ^{29b}
M. Dunford ^{63a} S. Dungs ⁴⁹ K. Dunne ^{47a,47b} A. Duperrin ¹⁰⁴ H. Duran Yildiz ^{3a} M. Düren ⁵⁸ A. Durglishvili ^{155b}
D. Duvnjak ³⁵ B. L. Dwyer ¹¹⁸ G. I. Dyckes ^{18a} M. Dyndal ^{86a} B. S. Dziedzic ³⁷ Z. O. Earnshaw ¹⁵²
G. H. Eberwein ¹²⁹ B. Eckerova ^{30a} S. Eggebrecht ⁵⁵ E. Egidio Purcino De Souza ^{83e} G. Eigen ¹⁷ K. Einsweiler ^{18a}
T. Ekelof ¹⁶⁷ P. A. Ekman ¹⁰⁰ S. El Farkh ^{36b} Y. El Ghazali ⁶² H. El Jarrari ³⁷ A. El Moussaoui ^{36a}
V. Ellajosyula ¹⁶⁷ M. Ellert ¹⁶⁷ F. Ellinghaus ¹⁷⁷ N. Ellis ³⁷ J. Elmsheuser ^{27b} M. Elsawy ^{119a} M. Elsing ³⁷
D. Emeliyanov ¹³⁷ Y. Enari ⁸⁴ I. Ene ^{18a} S. Epari ¹¹⁰ D. Ernani Martins Neto ⁸⁷ F. Ernst ³⁷ M. Errenst ¹⁷⁷
M. Escalier ⁶⁶ C. Escobar ¹⁶⁹ E. Etzion ¹⁵⁷ G. Evans ^{133a,133b} H. Evans ⁶⁸ L. S. Evans ⁹⁷ A. Ezhilov ³⁸
S. Ezzarqtouni ^{36a} F. Fabbri ^{24b,24a} L. Fabbri ^{24b,24a} G. Facini ⁹⁸ V. Fadeyev ¹³⁹ R. M. Fakhrutdinov ³⁸
D. Fakoudis ¹⁰² S. Falciano ^{75a} L. F. Falda Ulhoa Coelho ^{133a} F. Fallavollita ¹¹² G. Falsetti ^{44b,44a} J. Faltova ¹³⁶
C. Fan ¹⁶⁸ K. Y. Fan ^{64b} Y. Fan ¹⁴ Y. Fang ^{14,114c} M. Fanti ^{71a,71b} M. Faraj ^{69a,69b} Z. Farazpay ⁹⁹ A. Farbin ⁸
A. Farilla ^{77a} T. Farooque ¹⁰⁹ J. N. Farr ¹⁷⁸ S. M. Farrington ^{137,52} F. Fassi ^{36e} D. Fassouliotis ⁹ L. Fayard ⁶⁶
P. Federic ¹³⁶ P. Federicova ¹³⁴ O. L. Fedin ^{38,k} M. Feickert ¹⁷⁶ L. Feligioni ¹⁰⁴ D. E. Fellers ^{18a} C. Feng ^{143a}
Z. Feng ¹¹⁷ M. J. Fenton ¹⁶⁵ L. Ferencz ⁴⁸ B. Fernandez Barbadillo ⁹³ P. Fernandez Martinez ⁶⁷
M. J. V. Fernoux ¹⁰⁴ J. Ferrando ⁹³ A. Ferrari ¹⁶⁷ P. Ferrari ^{117,116} R. Ferrari ^{73a} D. Ferrere ⁵⁶ C. Ferretti ¹⁰⁸
M. P. Fewell ¹ D. Fiacco ^{75a,75b} F. Fiedler ¹⁰² P. Fiedler ¹³⁵ S. Filimonov ³⁹ M. S. Filip ^{29b,q} A. Filipčič ⁹⁵
E. K. Filmer ^{162a} F. Filthaut ¹¹⁶ M. C. N. Fiolhais ^{133a,133c,r} L. Fiorini ¹⁶⁹ W. C. Fisher ¹⁰⁹ T. Fitschen ¹⁰³
P. M. Fitzhugh ¹³⁸ I. Fleck ¹⁴⁷ P. Fleischmann ¹⁰⁸ T. Flick ¹⁷⁷ M. Flores ^{34d,s} L. R. Flores Castillo ^{64a}
L. Flores Sanz De Acedo ³⁷ F. M. Follega ^{78a,78b} N. Fomin ³³ J. H. Foo ¹⁶¹ A. Formica ¹³⁸ A. C. Forti ¹⁰³
E. Fortin ³⁷ A. W. Fortman ^{18a} L. Foster ^{18a} L. Fountas ^{9,t} D. Fournier ⁶⁶ H. Fox ⁹³ P. Francavilla ^{74a,74b}
S. Francescato ⁶¹ S. Franchellucci ⁵⁶ M. Franchini ^{24b,24a} S. Franchino ^{63a} D. Francis ³⁷ L. Franco ¹¹⁶
V. Franco Lima ³⁷ L. Franconi ⁴⁸ M. Franklin ⁶¹ G. Frattari ²⁸ Y. Y. Frid ¹⁵⁷ J. Friend ⁵⁹ N. Fritzsche ³⁷
A. Froch ⁵⁶ D. Froidevaux ³⁷ J. A. Frost ¹²⁹ Y. Fu ¹⁰⁹ S. Fuenzalida Garrido ^{140f} M. Fujimoto ¹⁰⁴ K. Y. Fung ^{64a}
E. Furtado De Simas Filho ^{83e} M. Furukawa ¹⁵⁹ J. Fuster ¹⁶⁹ A. Gaa ⁵⁵ A. Gabrielli ^{24b,24a} A. Gabrielli ¹⁶¹
P. Gadow ³⁷ G. Gagliardi ^{57b,57a} L. G. Gagnon ^{18a} S. Gaid ^{88b} S. Galantzan ¹⁵⁷ J. Gallagher ¹ E. J. Gallas ¹²⁹
A. L. Gallen ¹⁶⁷ B. J. Gallop ¹³⁷ K. K. Gan ¹²² S. Ganguly ¹⁵⁹ Y. Gao ⁵² A. Garabaglu ¹⁴²
F. M. Garay Walls ^{140a,140b} C. García ¹⁶⁹ A. Garcia Alonso ¹¹⁷ A. G. Garcia Caffaro ¹⁷⁸ J. E. García Navarro ¹⁶⁹
M. Garcia-Sciveres ^{18a} G. L. Gardner ¹³¹ R. W. Gardner ⁴⁰ N. Garelli ¹⁶⁴ R. B. Garg ¹⁴⁹ J. M. Gargan ⁵²
C. A. Garner ¹⁶¹ C. M. Garvey ^{34a} V. K. Gassmann ¹⁶⁴ G. Gaudio ^{73a} V. Gautam ¹³ P. Gauzzi ^{75a,75b} J. Gavranovic ⁹⁵
I. L. Gavrilenko ^{133a} A. Gavriluk ³⁸ C. Gay ¹⁷⁰ G. Gaycken ¹²⁶ E. N. Gazis ¹⁰ A. Gekow ¹²² C. Gemme ^{57b}
M. H. Genest ⁶⁰ A. D. Gentry ¹¹⁵ S. George ⁹⁷ T. Geralis ⁴⁶ A. A. Gerwin ¹²³ P. Gessinger-Befurt ³⁷

- M. E. Geyik ¹⁷⁷ M. Ghani ¹⁷³ K. Ghorbanian ⁹⁶ A. Ghosal ¹⁴⁷ A. Ghosh ¹⁶⁵ A. Ghosh ⁷ B. Giacobbe ^{24b}
 S. Giagu ^{75a,75b} T. Giani ¹¹⁷ A. Giannini ⁶² S. M. Gibson ⁹⁷ M. Gignac ¹³⁹ D. T. Gil ^{86b} A. K. Gilbert ^{86a}
 B. J. Gilbert ⁴² D. Gillberg ³⁵ G. Gilles ¹¹⁷ D. M. Gingrich ^{2,d} M. P. Giordani ^{69a,69c} P. F. Giraud ¹³⁸
 G. Giugliarelli ^{69a,69c} D. Giugni ^{71a} F. Giuli ^{76a,76b} I. Gkialas ^{9,t} L. K. Gladilin ³⁸ C. Glasman ¹⁰¹ M. Glazewska ²⁰
 G. Glemža ⁴⁸ M. Glisic ¹²⁶ I. Gnesi ^{44b} Y. Go ^{27b} M. Goblirsch-Kolb ³⁷ B. Gocke ⁴⁹ D. Godin ¹¹⁰ B. Gokturk ^{22a}
 S. Goldfarb ¹⁰⁷ T. Golling ⁵⁶ M. G. D. Gololo ^{34c} D. Golubkov ³⁸ J. P. Gombas ¹⁰⁹ A. Gomes ^{133a,133b}
 G. Gomes Da Silva ¹⁴⁷ A. J. Gomez Delegido ¹⁶⁹ R. Gonçalo ^{133a} L. Gonella ²¹ A. Gongadze ^{155c} F. Gonnella ²¹
 J. L. Gonski ¹⁴⁹ R. Y. González Andana ⁵² S. González de la Hoz ¹⁶⁹ M. V. Gonzalez Rodrigues ⁴⁸
 R. Gonzalez Suarez ¹⁶⁷ S. Gonzalez-Sevilla ⁵⁶ L. Goossens ³⁷ B. Gorini ³⁷ E. Gorini ^{70a,70b} A. Gorišek ⁹⁵
 T. C. Gosart ¹³¹ A. T. Goshaw ⁵¹ M. I. Gostkin ³⁹ S. Goswami ¹²⁴ C. A. Gottardo ³⁷ S. A. Gotz ¹¹¹
 M. Gouighri ^{36b} A. G. Goussiou ¹⁴² N. Govender ^{34c} R. P. Grabarczyk ¹²⁹ I. Grabowska-Bold ^{86a} K. Graham ³⁵
 E. Gramstad ¹²⁸ S. Grancagnolo ^{70a,70b} C. M. Grant ¹ P. M. Gravila ^{29f} F. G. Gravili ^{70a,70b} H. M. Gray ^{18a}
 M. Greco ¹¹² M. J. Green ¹ C. Grefe ²⁵ A. S. Grefsrud ¹⁷ I. M. Gregor ⁴⁸ K. T. Greif ¹⁶⁵ P. Grenier ¹⁴⁹
 S. G. Grewe ¹¹² A. A. Grillo ¹³⁹ K. Grimm ³² S. Grinstein ^{13,u} J.-F. Grivaz ⁶⁶ E. Gross ¹⁷⁵ J. Grosse-Knetter ⁵⁵
 L. Guan ¹⁰⁸ G. Guerrieri ³⁷ R. Guevara ¹²⁸ R. Gugel ¹⁰² J. A. M. Guhit ¹⁰⁸ A. Guida ¹⁹ E. Guilloton ¹⁷³
 S. Guindon ³⁷ F. Guo ^{14,114c} J. Guo ^{144a} L. Guo ⁴⁸ L. Guo ^{114b,v} Y. Guo ¹⁰⁸ A. Gupta ⁴⁹ R. Gupta ¹³²
 S. Gupta ²⁸ S. Gurbuz ²⁵ S. S. Gurdasani ⁴⁸ G. Gustavino ^{75a,75b} P. Gutierrez ¹²³ L. F. Gutierrez Zagazeta ¹³¹
 M. Gutsche ⁵⁰ C. Gutschow ⁹⁸ C. Gwenlan ¹²⁹ C. B. Gwilliam ⁹⁴ E. S. Haaland ¹²⁸ A. Haas ¹²⁰ M. Habedank ⁵⁹
 C. Haber ^{18a} H. K. Hadavand ⁸ A. Haddad ⁴¹ A. Hadef ⁵⁰ A. I. Hagan ⁹³ J. J. Hahn ¹⁴⁷ E. H. Haines ⁹⁸
 M. Haleem ¹⁷² J. Haley ¹²⁴ G. D. Hallewell ¹⁰⁴ L. Halser ²⁰ K. Hamano ¹⁷¹ M. Hamer ²⁵ S. E. D. Hammoud ⁶⁶
 E. J. Hampshire ⁹⁷ J. Han ^{143a} L. Han ^{114a} L. Han ⁶² S. Han ^{18a} K. Hanagaki ⁸⁴ M. Hance ¹³⁹ D. A. Hangal ⁴²
 H. Hanif ¹⁴⁸ M. D. Hank ¹³¹ J. B. Hansen ⁴³ P. H. Hansen ⁴³ D. Harada ⁵⁶ T. Harenberg ¹⁷⁷ S. Harkusha ¹⁷⁹
 M. L. Harris ¹⁰⁵ Y. T. Harris ²⁵ J. Harrison ¹³ N. M. Harrison ¹²² P. F. Harrison ¹⁷³ M. L. E. Hart ⁹⁸
 N. M. Hartman ¹¹² N. M. Hartmann ¹¹¹ R. Z. Hasan ^{97,137} Y. Hasegawa ¹⁴⁶ F. Haslbeck ¹²⁹ S. Hassan ¹⁷
 R. Hauser ¹⁰⁹ M. Haviernik ¹³⁶ C. M. Hawkes ²¹ R. J. Hawkings ³⁷ Y. Hayashi ¹⁵⁹ D. Hayden ¹⁰⁹ C. Hayes ¹⁰⁸
 R. L. Hayes ¹¹⁷ C. P. Hays ¹²⁹ J. M. Hays ⁹⁶ H. S. Hayward ⁹⁴ M. He ^{14,114c} Y. He ⁴⁸ Y. He ⁹⁸ N. B. Heatley ⁹⁶
 V. Hedberg ¹⁰⁰ C. Heidegger ⁵⁴ K. K. Heidegger ³⁵ J. Heilmann ⁴⁸ S. Heim ^{18a} T. Heim ^{18a} J. G. Heinlein ¹³¹
 J. J. Heinrich ¹²⁶ L. Heinrich ¹¹² J. Hejbal ¹³⁴ M. Helbig ⁵⁰ A. Held ¹⁷⁶ S. Hellesund ¹⁷ C. M. Helling ¹⁷⁰
 S. Hellman ^{47a,47b} L. Henkelmann ³³ A. M. Henriques Correia ³⁷ H. Herde ¹⁰⁰ Y. Hernández Jiménez ¹⁵¹
 L. M. Herrmann ²⁵ T. Herrmann ⁵⁰ G. Herten ⁵⁴ R. Hertenberger ¹¹¹ L. Hervas ³⁷ M. E. Hesping ¹⁰²
 N. P. Hessey ^{162a} J. Hessler ¹¹² M. Hidaoui ^{36b} N. Hidic ¹³⁶ E. Hill ¹⁶¹ S. J. Hillier ²¹ J. R. Hinds ¹⁰⁹
 F. Hinterkeuser ²⁵ M. Hirose ¹²⁷ S. Hirose ¹⁶³ D. Hirschbuehl ¹⁷⁷ T. G. Hitchings ¹⁰³ B. Hiti ⁹⁵ J. Hobbs ¹⁵¹
 R. Hobincu ^{29e} N. Hod ¹⁷⁵ A. M. Hodges ¹⁶⁸ M. C. Hodgkinson ¹⁴⁵ B. H. Hodgkinson ¹²⁹ A. Hoecker ³⁷
 D. D. Hofer ¹⁰⁸ J. Hofer ¹⁶⁹ M. Holzbock ³⁷ L. B. A. H. Hommels ³³ V. Homsak ¹²⁹ B. P. Honan ¹⁰³ J. J. Hong ⁶⁸
 T. M. Hong ¹³² B. H. Hooberman ¹⁶⁸ W. H. Hopkins ⁶ M. C. Hoppesch ¹⁶⁸ Y. Horii ¹¹³ M. E. Horstmann ¹¹²
 S. Hou ¹⁵⁴ M. R. Housenga ¹⁶⁸ A. S. Howard ⁹⁵ J. Howarth ⁵⁹ J. Hoya ⁶ M. Hrabovsky ¹²⁵ T. Hryna'ova ⁴
 P. J. Hsu ⁶⁵ S.-C. Hsu ¹⁴² T. Hsu ⁶⁶ M. Hu ^{18a} Q. Hu ⁶² S. Huang ³³ X. Huang ^{14,114c} Y. Huang ¹³⁶
 Y. Huang ^{114b} Y. Huang ¹⁰² Y. Huang ¹⁴ Z. Huang ⁶⁶ Z. Hubacek ¹³⁵ M. Huebner ²⁵ F. Huegging ²⁵
 T. B. Huffman ¹²⁹ M. Hufnagel Maranha De Faria ^{83a} C. A. Hugli ⁴⁸ M. Huhtinen ³⁷ S. K. Huiberts ¹⁷
 R. Hulskens ¹⁰⁶ C. E. Hultquist ^{18a} N. Huseynov ^{12,w} J. Huston ¹⁰⁹ J. Huth ⁶¹ R. Hyneman ⁷ G. Iacobucci ⁵⁶
 G. Iakovidis ^{27b} L. Iconomidou-Fayard ⁶⁶ J. P. Iddon ³⁷ P. Iengo ^{172a,72b} R. Iguchi ¹⁵⁹ Y. Iiyama ¹⁵⁹ T. Iizawa ¹⁵⁹
 Y. Ikegami ⁸⁴ D. Iliadis ¹⁵⁸ N. Illic ¹⁶¹ H. Imam ^{36a} G. Inacio Goncalves ^{83d} S. A. Infante Cabanas ^{140c}
 T. Ingebretsen Carlson ^{47a,47b} J. M. Inglis ⁹⁶ G. Introzzi ^{73a,73b} M. Iodice ^{77a} V. Ippolito ^{75a,75b} R. K. Irwin ⁹⁴
 M. Ishino ¹⁵⁹ W. Islam ¹⁷⁶ C. Issever ¹⁹ S. Istin ^{22a,x} K. Itabashi ⁸⁴ H. Ito ¹⁷⁴ R. Iuppa ^{78a,78b} A. Ivina ¹⁷⁵
 V. Izzo ^{72a} P. Jacka ¹³⁴ P. Jackson ¹ P. Jain ⁴⁸ K. Jakobs ⁵⁴ T. Jakoubek ¹⁷⁵ J. Jamieson ⁵⁹ W. Jang ¹⁵⁹
 S. Jankovych ¹³⁶ M. Javurkova ¹⁰⁵ P. Jawahar ¹⁰³ L. Jeanty ¹²⁶ J. Jejelava ^{155a,y} P. Jenni ^{54,z} C. E. Jessiman ³⁵
 C. Jia ^{143a} H. Jia ¹⁷⁰ J. Jia ¹⁵¹ X. Jia ^{14,114c} Z. Jia ^{114a} C. Jiang ⁵² Q. Jiang ^{64b} S. Jiggins ⁴⁸
 M. Jimenez Ortega ¹⁶⁹ J. Jimenez Pena ¹³ S. Jin ^{114a} A. Jinaru ^{29b} O. Jinnouchi ¹⁴¹ P. Johansson ¹⁴⁵ K. A. Johns ⁷
 J. W. Johnson ¹³⁹ F. A. Jolly ⁴⁸ D. M. Jones ¹⁵² E. Jones ⁴⁸ K. S. Jones ⁸ P. Jones ³³ R. W. L. Jones ⁹³
 T. J. Jones ⁹⁴ H. L. Joos ^{55,37} R. Joshi ¹²² J. Jovicevic ¹⁶ X. Ju ^{18a} J. J. Junggeburth ³⁷ T. Junkermann ^{63a}
 A. Juste Rozas ^{13,u} M. K. Juzek ⁸⁷ S. Kabana ^{140e} A. Kaczmarska ⁸⁷ M. Kado ¹¹² H. Kagan ¹²² M. Kagan ¹⁴⁹
 A. Kahn ¹³¹ C. Kahra ¹⁰² T. Kaji ¹⁵⁹ E. Kajomovitz ¹⁵⁶ N. Kakati ¹⁷⁵ N. Kakoty ¹³ I. Kalaitzidou ⁵⁴ S. Kandel ⁸
 N. J. Kang ¹³⁹ D. Kar ^{34g} K. Karava ¹²⁹ E. Karentzos ²⁵ O. Karkout ¹¹⁷ S. N. Karpov ³⁹ Z. M. Karpova ³⁹
 V. Kartvelishvili ⁹³ A. N. Karyukhin ³⁸ E. Kasimi ¹⁵⁸ J. Katzy ⁴⁸ S. Kaur ³⁵ K. Kawade ¹⁴⁶ M. P. Kawale ¹²³
 C. Kawamoto ⁸⁹ T. Kawamoto ⁶² E. F. Kay ³⁷ F. I. Kaya ¹⁶⁴ S. Kazakos ¹⁰⁹ V. F. Kazanin ³⁸ J. M. Keaveney ^{34a}
 R. Keeler ¹⁷¹ G. V. Kehris ⁶¹ J. S. Keller ³⁵ J. J. Kempster ¹⁵² O. Kepka ¹³⁴ J. Kerr ^{162b} B. P. Kerridge ¹³⁷
 B. P. Kerševan ⁹⁵ L. Keszeghova ^{30a} R. A. Khan ¹³² A. Khanov ¹²⁴ A. G. Kharlamov ³⁸ T. Kharlamova ³⁸
 E. E. Khoda ¹⁴² M. Kholodenko ^{133a} T. J. Khoo ¹⁹ G. Khoriauli ¹⁷² Y. Khoulaki ^{36a} J. Khubua ^{155b,aa}

- Y. A. R. Khwaira¹³⁰ B. Kibirige,^{34g} D. Kim⁶ D. W. Kim^{47a,47b} Y. K. Kim⁴⁰ N. Kimura⁹⁸ M. K. Kingston⁵⁵
 A. Kirchhoff⁵⁵ C. Kirlfel²⁵ F. Kirlfel²⁵ J. Kirk¹³⁷ A. E. Kiryunin¹¹² S. Kita¹⁶³ O. Kivernyk²⁵ M. Klassen¹⁶⁴
 C. Klein³⁵ L. Klein¹⁷² M. H. Klein⁴⁵ S. B. Klein⁵⁶ U. Klein⁹⁴ A. Klimentov^{27b} T. Klioutchnikova³⁷
 P. Kluit¹¹⁷ S. Kluth¹¹² E. Kneringer⁷⁹ T. M. Knight¹⁶¹ A. Knue⁴⁹ M. B. Knuesel^{27a} M. Kobel⁵⁰
 D. Kobylanski¹⁷⁵ S. F. Koch¹²⁹ M. Kocian¹⁴⁹ P. Kodyš¹³⁶ D. M. Koeck¹²⁶ T. Koffas³⁵ O. Kolay⁵⁰
 I. Koletsou⁴ T. Komarek⁸⁷ K. Köneke⁵⁵ A. X. Y. Kong¹ T. Kono¹²¹ N. Konstantinidis⁹⁸ P. Kontaxakis⁵⁶
 B. Konya¹⁰⁰ R. Kopeliansky⁴² S. Kopermy^{86a} K. Korcyl⁸⁷ K. Kordas^{158,ab} A. Korn⁹⁸ S. Korn⁵⁵
 I. Korolkov¹³ N. Korotkova³⁸ B. Kortman¹¹⁷ O. Kortner¹¹² S. Kortner¹¹² W. H. Kostecka¹¹⁸ M. Kostov^{30a}
 V. V. Kostyukhin¹⁴⁷ A. Kotsokechagia³⁷ A. Kotwal⁵¹ A. Koulouris³⁷ A. Kourkoumeli-Charalampidi^{73a,73b}
 C. Kourkoumelis⁹ E. Kourlitis¹¹² O. Kovanda¹²⁶ R. Kowalewski¹⁷¹ W. Kozanecki¹²⁶ A. S. Kozhin³⁸
 V. A. Kramarenko³⁸ G. Kramberger⁹⁵ P. Kramer²⁵ M. W. Krasny¹³⁰ A. Krasznahorkay¹⁰⁵ A. C. Kraus¹¹⁸
 J. W. Kraus¹⁷⁷ J. A. Kremer⁴⁸ N. B. Krengel¹⁴⁷ T. Kresse⁵⁰ L. Kretschmann¹⁷⁷ J. Kretzschmar⁹⁴ K. Kreul¹⁹
 P. Krieger¹⁶¹ K. Krizka²¹ K. Kroeninger⁴⁹ H. Kroha¹¹² J. Kroll¹³⁴ J. Kroll¹³¹ K. S. Krowppman¹⁰⁹
 U. Kruchonak³⁹ H. Krüger²⁵ N. Krumnack⁸¹ M. C. Kruse⁵¹ O. Kuchinskaia³⁹ S. Kuday^{3a} S. Kuehn³⁷
 R. Kuesters⁵⁴ T. Kuhl⁴⁸ V. Kukhtin³⁹ Y. Kulchitsky³⁹ S. Kuleshov^{140d,140b} J. Kull¹ M. Kumar^{34g}
 N. Kumari⁴⁸ P. Kumari^{162b} A. Kupco¹³⁴ T. Kupfer⁴⁹ A. Kupich³⁸ O. Kuprash⁵⁴ H. Kurashige⁸⁵
 L. L. Kurchaninov^{162a} O. Kurdysh⁴ Y. A. Kurochkin³⁸ A. Kurova³⁸ M. Kuze¹⁴¹ A. K. Kvam¹⁰⁵ J. Kvita¹²⁵
 N. G. Kyriacou¹⁰⁸ C. Lacasta¹⁶⁹ F. Lacava^{75a,75b} H. Lacker¹⁹ D. Lacour¹³⁰ N. N. Lad⁹⁸ E. Ladygin³⁹
 A. Lafarge⁴¹ B. Laforge¹³⁰ T. Lagouri¹⁷⁸ F. Z. Lahbab^{36a} S. Lai⁵⁵ J. E. Lambert¹⁷¹ S. Lammers⁶⁸
 W. Lampl⁷ C. Lampoudis^{158,ab} G. Lamprinoudis¹⁰² A. N. Lancaster¹¹⁸ E. Lanç^{27b} U. Landgraf⁵⁴
 M. P. J. Landon⁹⁶ V. S. Lang⁵⁴ O. K. B. Langrekken¹²⁸ A. J. Lankford¹⁶⁵ F. Lanni³⁷ K. Lantzsch²⁵
 A. Lanza^{73a} M. Lanzac Berrocal¹⁶⁹ J. F. Laporte¹³⁸ T. Lari^{71a} D. Larsen¹⁷ L. Larson¹¹ F. Lasagni Manghi^{24b}
 M. Lassnig³⁷ S. D. Lawlor¹⁴⁵ R. Lazaridou¹⁷³ M. Lazzaroni^{71a,71b} H. D. M. Le¹⁰⁹ E. M. Le Boulicaut¹⁷⁸
 L. T. Le Pottier^{18a} B. Leban^{24b,24a} F. Ledroit-Guillon⁶⁰ T. F. Lee^{162b} L. L. Leeuw^{34c} M. Lefebvre¹⁷¹
 C. Leggett^{18a} G. Lehmann Miotti³⁷ M. Leigh⁵⁶ W. A. Leight¹⁰⁵ W. Leinonen¹¹⁶ A. Leisos^{158,ac}
 M. A. L. Leite^{83c} C. E. Leitgeb¹⁹ R. Leitner¹³⁶ K. J. C. Leney⁴⁵ T. Lenz²⁵ S. Leone^{74a} C. Leonidopoulos⁵²
 A. Leopold¹⁵⁰ J. H. Lepage Bourbonnais³⁵ R. Les¹⁰⁹ C. G. Lester³³ M. Levchenko³⁸ J. Levéque⁴
 L. J. Levinson¹⁷⁵ G. Levirini^{24b,24a} M. P. Lewicki⁸⁷ C. Lewis¹⁴² D. J. Lewis⁴ L. Lewitt¹⁴⁵ A. Li¹⁷ B. Li^{143a}
 C. Li¹⁰⁸ C.-Q. Li¹¹² H. Li^{143a} H. Li¹⁰³ H. Li¹⁵ H. Li⁶² H. Li^{143a} J. Li^{144a} K. Li¹⁴ L. Li^{144a} R. Li¹⁷⁸
 S. Li^{14,114c} S. Li^{144b,144a} T. Li⁵ X. Li¹⁰⁶ Z. Li¹⁵⁹ Z. Li^{14,114c} Z. Li⁶² S. Liang^{14,114c} Z. Liang¹⁴
 M. Liberatore¹³⁸ B. Liberti^{76a} K. Lie^{64c} J. Lieber Marin^{83e} H. Lien⁶⁸ H. Lin¹⁰⁸ S. F. Lin¹⁵¹ L. Linden¹¹¹
 R. E. Lindley⁷ J. H. Lindon³⁷ J. Ling⁶¹ E. Lipeles¹³¹ A. Lipniacka¹⁷ A. Lister¹⁷⁰ J. D. Little⁶⁸ B. Liu¹⁴
 B. X. Liu^{114b} D. Liu^{144b,144a} E. H. L. Liu²¹ J. K. K. Liu¹²⁰ K. Liu^{144b} K. Liu^{144b,144a} M. Liu⁶² M. Y. Liu⁶²
 P. Liu¹⁴ Q. Liu^{144b,142,144a} X. Liu⁶² X. Liu^{143a} Y. Liu^{114b,114c} Y. L. Liu^{143a} Y. W. Liu⁶² Z. Liu^{66,ad}
 S. L. Lloyd⁹⁶ E. M. Lobodzinska⁴⁸ P. Loch⁷ E. Lodhi¹⁶¹ T. Lohse¹⁹ K. Lohwasser¹⁴⁵ E. Loiacono⁴⁸
 J. D. Lomas²¹ J. D. Long⁴² I. Longarini¹⁶⁵ R. Longo¹⁶⁸ A. Lopez Solis¹³ N. A. Lopez-canelas⁷
 N. Lorenzo Martinez⁴ A. M. Lory¹¹¹ M. Losada^{119a} G. Löschecke Centeno¹⁵² X. Lou^{47a,47b} X. Lou^{14,114c}
 A. Lounis⁶⁶ P. A. Love⁹³ G. Lu^{14,114c} M. Lu⁶⁶ S. Lu¹³¹ Y. J. Lu¹⁵⁴ H. J. Lubatti¹⁴² C. Luci^{75a,75b}
 F. L. Lucio Alves^{114a} F. Luehring⁶⁸ B. S. Lunday¹³¹ O. Lundberg¹⁵⁰ J. Lunde³⁷ N. A. Luongo⁶ M. S. Lutz³⁷
 A. B. Lux²⁶ D. Lynn^{27b} R. Lysak¹³⁴ V. Lysenko¹³⁵ E. Lytken¹⁰⁰ V. Lyubushkin³⁹ T. Lyubushkina³⁹
 M. M. Lyukova¹⁵¹ M. Firdaus M. Soberi⁵² H. Ma^{27b} K. Ma⁶² L. L. Ma^{143a} W. Ma⁶² Y. Ma¹²⁴
 J. C. MacDonald¹⁰² P. C. Machado De Abreu Farias^{83e} R. Madar⁴¹ T. Madula⁹⁸ J. Maeda⁸⁵ T. Maeno^{27b}
 P. T. Mafa^{34c,ae} H. Maguire¹⁴⁵ V. Maiboroda⁶⁶ A. Maio^{133a,133b,133d} K. Maj^{86a} O. Majersky⁴⁸ S. Majewski¹²⁶
 R. Makhmanazarov³⁸ N. Makovec⁶⁶ V. Maksimovic¹⁶ B. Malaescu¹³⁰ J. Malamant¹²⁸ Pa. Malecki⁸⁷
 V. P. Maleev³⁸ F. Malek^{60,af} M. Mali⁹⁵ D. Malito⁹⁷ U. Mallik^{80,aa} A. Maloizel⁵ S. Maltezos¹⁰
 A. Malvezzi Lopes^{83d} S. Malyukov³⁹ J. Mamuzic¹³ G. Mancini⁵³ M. N. Mancini²⁸ G. Manco^{73a,73b}
 J. P. Mandalia⁹⁶ S. S. Mandarry¹⁵² I. Mandić⁹⁵ L. Manhaes de Andrade Filho^{83a} I. M. Maniatis¹⁷⁵
 J. Manjarres Ramos⁹¹ D. C. Mankad¹⁷⁵ A. Mann¹¹¹ T. Manoussos³⁷ M. N. Mantinan⁴⁰ S. Manzoni³⁷
 L. Mao^{144a} X. Mapekula^{34c} A. Marantis¹⁵⁸ R. R. Marcelo Gregorio⁹⁶ G. Marchiori⁵ M. Marcisovsky¹³⁴
 C. Marcon^{71a} E. Maricic¹⁶ M. Marinescu⁴⁸ S. Marium⁴⁸ M. Marjanovic¹²³ A. Markhoos⁵⁴ M. Markovitch⁶⁶
 M. K. Maroun¹⁰⁵ G. T. Marsden¹⁰³ E. J. Marshall⁹³ Z. Marshall^{18a} S. Marti-Garcia¹⁶⁹ J. Martin⁹⁸
 T. A. Martin¹³⁷ V. J. Martin⁵² B. Martin dit Latour¹⁷ L. Martinelli^{75a,75b} M. Martinez^{13,u} P. Martinez Agullo¹⁶⁹
 V. I. Martinez Outschoorn¹⁰⁵ P. Martinez Suarez¹³ S. Martin-Haugh¹³⁷ G. Martinovicova¹³⁶ V. S. Martoiu^{29b}
 A. C. Martyniuk⁹⁸ A. Marzin³⁷ D. Mascione^{78a,78b} L. Masetti¹⁰² J. Masik¹⁰³ A. L. Maslenikov³⁹
 S. L. Mason⁴² P. Massarotti^{72a,72b} P. Mastrandrea^{74a,74b} A. Mastroberardino^{44b,44a} T. Masubuchi¹²⁷
 T. T. Mathew¹²⁶ J. Matousek¹³⁶ D. M. Mattern⁴⁹ J. Maurer^{29b} T. Maurin⁵⁹ A. J. Maury⁶⁶ B. Maček⁹⁵
 C. Mavungu Tsava¹⁰⁴ D. A. Maximov³⁸ A. E. May¹⁰³ E. Mayer⁴¹ R. Mazini^{34g} I. Maznas¹¹⁸ S. M. Mazza¹³⁹
 E. Mazzeo^{71a,71b} J. P. Mc Gowan¹⁷¹ S. P. Mc Kee¹⁰⁸ C. A. Mc Lean⁶ C. C. McCracken¹⁷⁰ E. F. McDonald¹⁰⁷

- A. E. McDougall ¹¹⁷ L. F. Mcelhinney ⁹³ J. A. Mcfayden ¹⁵² R. P. McGovern ¹³¹ R. P. Mckenzie ^{34g}
 T. C. McLachlan ⁴⁸ D. J. McLaughlin ⁹⁸ S. J. McMahon ¹³⁷ C. M. Mcpartland ⁹⁴ R. A. McPherson ^{171,o}
 S. Mehlhase ¹¹¹ A. Mehta ⁹⁴ D. Melini ¹⁶⁹ B. R. Mellado Garcia ^{34g} A. H. Melo ⁵⁵ F. Meloni ⁴⁸
 A. M. Mendes Jacques Da Costa ¹⁰³ L. Meng ⁹³ S. Menke ¹¹² M. Mentink ³⁷ E. Meoni ^{44b,44a} G. Mercado ¹¹⁸
 S. Merianos ¹⁵⁸ C. Merlassino ^{69a,69c} C. Meroni ^{71a,71b} J. Metcalfe ⁶ A. S. Mete ⁶ E. Meuser ¹⁰² C. Meyer ⁶⁸
 J-P. Meyer ¹³⁸ Y. Miao ^{114a} R. P. Middleton ¹³⁷ M. Mihovilovic ⁶⁶ L. Mijović ⁵² G. Mikenberg ¹⁷⁵
 M. Mikesikova ¹³⁴ M. Mikuž ⁹⁵ H. Mildner ¹⁰² A. Milic ³⁷ D. W. Miller ⁴⁰ E. H. Miller ¹⁴⁹ L. S. Miller ³⁵
 A. Milov ¹⁷⁵ D. A. Milstead ^{47a,47b} T. Min ^{114a} A. A. Minaenko ³⁸ I. A. Minashvili ^{155b} A. I. Mincer ¹²⁰ B. Mindur ^{86a}
 M. Mineev ³⁹ Y. Mino ⁸⁹ L. M. Mir ¹³ M. Miralles Lopez ⁵⁹ M. Mironova ^{18a} M. C. Missio ¹¹⁶ A. Mitra ¹⁷³
 V. A. Mitsou ¹⁶⁹ Y. Mitsumori ¹¹³ O. Miu ¹⁶¹ P. S. Miyagawa ⁹⁶ T. Mkrtchyan ^{63a} M. Mlinarevic ⁹⁸
 T. Mlinarevic ⁹⁸ M. Mlynarikova ³⁷ S. Mobius ²⁰ M. H. Mohamed Farook ¹¹⁵ A. F. Mohammed ^{14,114c}
 S. Mohapatra ⁴² S. Mohiuddin ¹²⁴ G. Mokgatitswane ^{34g} L. Moleri ¹⁷⁵ U. Molinatti ¹²⁹ L. G. Mollier ²⁰
 B. Mondal ¹⁴⁷ S. Mondal ¹³⁵ K. Mönig ⁴⁸ E. Monnier ¹⁰⁴ L. Monsonis Romero ¹⁶⁹ J. Montejo Berlingen ¹³
 A. Montella ^{47a,47b} M. Montella ¹²² F. Montereali ^{77a,77b} F. Monticelli ⁹² S. Monzani ^{69a,69c} A. Morancho Tarda ⁴³
 N. Morange ⁶⁶ A. L. Moreira De Carvalho ⁴⁸ M. Moreno Llácer ¹⁶⁹ C. Moreno Martinez ⁵⁶ J. M. Moreno Perez ^{23b}
 P. Morettini ^{57b} S. Morgenstern ³⁷ M. Morii ⁶¹ M. Morinaga ¹⁵⁹ M. Moritsu ⁹⁰ F. Morodei ^{75a,75b}
 P. Moschovakos ³⁷ B. Moser ⁵⁴ M. Mosidze ^{155b} T. Moskalets ⁴⁵ P. Moskvitina ¹¹⁶ J. Moss ³² P. Moszkowicz ^{86a}
 A. Moussa ^{36d} Y. Moyal ¹⁷⁵ H. Moyano Gomez ¹³ E. J. W. Moyse ¹⁰⁵ O. Mtintsilana ^{34g} S. Muanza ¹⁰⁴
 M. Mucha ²⁵ J. Mueller ¹³² R. Müller ³⁷ G. A. Mullier ¹⁶⁷ A. J. Mullin ³³ J. J. Mullin ⁵¹ A. E. Mulski ⁶¹
 D. P. Mungo ¹⁶¹ D. Munoz Perez ¹⁶⁹ F. J. Munoz Sanchez ¹⁰³ W. J. Murray ^{173,137} M. Muškinja ⁹⁵ C. Mwewa ⁴⁸
 A. G. Myagkov ^{38,k} A. J. Myers ⁸ G. Myers ¹⁰⁸ M. Myska ¹³⁵ B. P. Nachman ^{18a} K. Nagai ¹²⁹ K. Nagano ⁸⁴
 R. Nagasaka ¹⁵⁹ J. L. Nagle ^{27b,ag} E. Nagy ¹⁰⁴ A. M. Nairz ³⁷ Y. Nakahama ⁸⁴ K. Nakamura ⁸⁴ K. Nakkalil ⁵
 H. Nanjo ¹²⁷ E. A. Narayanan ⁴⁵ Y. Narukawa ¹⁵⁹ I. Naryshkin ³⁸ L. Nasella ^{71a,71b} S. Nasri ^{119b} C. Nass ²⁵
 G. Navarro ^{23a} J. Navarro-Gonzalez ¹⁶⁹ A. Nayaz ¹⁹ P. Y. Nechaeva ³⁸ S. Nechaeva ^{24b,24a} F. Nechansky ¹³⁴
 L. Nedic ¹²⁹ T. J. Neep ²¹ A. Negri ^{73a,73b} M. Negrini ^{24b} C. Nellist ¹¹⁷ C. Nelson ¹⁰⁶ K. Nelson ¹⁰⁸
 S. Nemecek ¹³⁴ M. Nessi ^{37,ah} M. S. Neubauer ¹⁶⁸ J. Newell ⁹⁴ P. R. Newman ²¹ Y. W. Y. Ng ¹⁶⁸ B. Ngair ^{119a}
 H. D. N. Nguyen ¹¹⁰ J. D. Nichols ¹²³ R. B. Nickerson ¹²⁹ R. Nicolaïdou ¹³⁸ J. Nielsen ¹³⁹ M. Niemeyer ⁵⁵
 J. Niermann ³⁷ N. Nikiforou ³⁷ V. Nikolaenko ^{38,k} I. Nikolic-Audit ¹³⁰ P. Nilsson ^{27b} I. Ninca ⁴⁸ G. Ninio ¹⁵⁷
 A. Nisati ^{75a} N. Nishi ² R. Nisius ¹¹² N. Nitika ^{69a,69c} J-E. Nitschke ⁵⁰ E. K. Nkadameng ^{34b} T. Nobe ¹⁵⁹
 T. Nommensen ¹⁵³ M. B. Norfolk ¹⁴⁵ B. J. Norman ³⁵ M. Noury ^{36a} J. Novak ⁹⁵ T. Novak ⁹⁵ R. Novotny ¹³⁵
 L. Nozka ¹²⁵ K. Ntekas ¹⁶⁵ N. M. J. Nunes De Moura Junior ^{83b} J. Ocariz ¹³⁰ A. Ochi ⁸⁵ I. Ochoa ^{133a}
 S. Oerde ^{48,ai} J. T. Offermann ⁴⁰ A. Ogrodnik ¹³⁶ A. Oh ¹⁰³ C. C. Ohm ¹⁵⁰ H. Oide ⁸⁴ M. L. Ojeda ³⁷
 Y. Okumura ¹⁵⁹ L. F. Oleiro Seabra ^{133a} I. Oleksiyuk ⁵⁶ G. Oliveira Correa ¹³ D. Oliveira Damazio ^{27b}
 J. L. Oliver ¹⁶⁵ Ö. Ö. Öncel ⁵⁴ A. P. O'Neill ²⁰ A. Onofre ^{133a,133e,aj} P. U. E. Onyisi ¹¹ M. J. Oreglia ⁴⁰
 D. Orestano ^{77a,77b} R. Orlandini ^{77a,77b} R. S. Orr ¹⁶¹ L. M. Osojnak ¹³¹ Y. Osumi ¹¹³ G. Otero y Garzon ³¹
 H. Otono ⁹⁰ G. J. Ottino ^{18a} M. Ouchrif ^{36d} F. Ould-Saada ¹²⁸ T. Ovsiannikova ¹⁴² M. Owen ⁵⁹ R. E. Owen ¹³⁷
 V. E. Ozcan ^{22a} F. Ozturk ⁸⁷ N. Ozturk ⁸ S. Ozturk ⁸² H. A. Pacey ¹²⁹ K. Pachal ^{162a} A. Pacheco Pages ¹³
 C. Padilla Aranda ¹³ G. Padovano ^{75a,75b} S. Pagan Griso ^{18a} G. Palacino ⁶⁸ A. Palazzo ^{70a,70b} J. Pampel ²⁵
 J. Pan ¹⁷⁸ T. Pan ^{64a} D. K. Panchal ¹¹ C. E. Pandini ¹¹⁷ J. G. Panduro Vazquez ¹³⁷ H. D. Pandya ¹ H. Pang ¹³⁸
 P. Pani ⁴⁸ G. Panizzo ^{69a,69c} L. Panwar ¹³⁰ L. Paolozzi ⁵⁶ S. Parajuli ¹⁶⁸ A. Paramonov ⁶ C. Paraskevopoulos ⁵³
 D. Paredes Hernandez ^{64b} A. Pareti ^{73a,73b} K. R. Park ⁴² T. H. Park ¹¹² F. Parodi ^{57b,57a} J. A. Parsons ⁴²
 U. Parzefall ⁵⁴ B. Pascual Dias ⁴¹ L. Pascual Dominguez ¹⁰¹ E. Pasqualucci ^{75a} S. Passaggio ^{57b} F. Pastore ⁹⁷
 P. Patel ⁸⁷ U. M. Patel ⁵¹ J. R. Pater ¹⁰³ T. Pauly ³⁷ F. Pauwels ¹³⁶ C. I. Pazos ¹⁶⁴ M. Pedersen ¹²⁸ R. Pedro ^{133a}
 S. V. Peleganchuk ³⁸ O. Penc ³⁷ E. A. Pender ⁵² S. Peng ¹⁵ G. D. Penn ¹⁷⁸ K. E. Penski ¹¹¹ M. Penzin ³⁸
 B. S. Peralva ^{83d} A. P. Pereira Peixoto ¹⁴² L. Pereira Sanchez ¹⁴⁹ D. V. Perepelitsa ^{27b,ag} G. Perera ¹⁰⁵
 E. Perez Codina ^{162a} M. Perganti ¹⁰ H. Pernegger ³⁷ S. Perrella ^{75a,75b} O. Perrin ⁴¹ K. Peters ⁴⁸ R. F. Y. Peters ¹⁰³
 B. A. Petersen ³⁷ T. C. Petersen ⁴³ E. Petit ¹⁰⁴ V. Petousis ¹³⁵ A. R. Petri ^{71a,71b} C. Petridou ^{158,ab} T. Petru ¹³⁶
 A. Petrukhin ¹⁴⁷ M. Pettee ^{18a} A. Petukhov ⁸² K. Petukhova ³⁷ R. Pezoa ^{140f} L. Pezzotti ^{24b,24a} G. Pezzullo ¹⁷⁸
 L. Pfaffenbichler ³⁷ A. J. Pfleger ³⁷ T. M. Pham ¹⁷⁶ T. Pham ¹⁰⁷ P. W. Phillips ¹³⁷ G. Piacquadio ¹⁵¹ E. Pianori ^{18a}
 F. Piazza ¹²⁶ R. Piegaia ³¹ D. Pietreanu ^{29b} A. D. Pilkington ¹⁰³ M. Pinamonti ^{69a,69c} J. L. Pinfold ²
 B. C. Pinheiro Pereira ^{133a} J. Pinol Bel ¹³ A. E. Pinto Pinoargote ¹³⁰ L. Pintucci ^{69a,69c} K. M. Piper ¹⁵²
 A. Pirttikoski ⁵⁶ D. A. Pizzi ³⁵ L. Pizzimento ^{64b} A. Plebani ³³ M.-A. Pleier ^{27b} V. Pleskot ¹³⁶ E. Plotnikova ³⁹
 G. Poddar ⁹⁶ R. Poettgen ¹⁰⁰ L. Poggiali ¹³⁰ S. Polacek ¹³⁶ G. Polesello ^{73a} A. Poley ¹⁴⁸ A. Polini ^{24b}
 C. S. Pollard ¹⁷³ Z. B. Pollock ¹²² E. Pompa Pacchi ¹²³ N. I. Pond ⁹⁸ D. Ponomarenko ⁶⁸ L. Pontecorvo ³⁷
 S. Popa ^{29a} G. A. Popeneiciu ^{29d} A. Poreba ³⁷ D. M. Portillo Quintero ^{162a} S. Pospisil ¹³⁵ M. A. Postill ¹⁴⁵
 P. Postolache ^{29c} K. Potamianos ¹⁷³ P. A. Potepa ^{86a} I. N. Potrap ³⁹ C. J. Potter ³³ H. Potti ¹⁵³ J. Poveda ¹⁶⁹
 M. E. Pozo Astigarraga ³⁷ R. Pozzi ³⁷ A. Prades Ibanez ^{76a,76b} J. Pretel ¹⁷¹ D. Price ¹⁰³ M. Primavera ^{70a}
 L. Primomo ^{69a,69c} M. A. Principe Martin ¹⁰¹ R. Privara ¹²⁵ T. Procter ^{86b} M. L. Proffitt ¹⁴² N. Proklova ¹³¹

- K. Prokofiev ^{64c} G. Proto ¹¹² J. Proudfoot ⁶ M. Przybycien ^{86a} W. W. Przygoda ^{86b} A. Psallidas ⁴⁶
 J. E. Puddefoot ¹⁴⁵ D. Pudzha ⁵³ D. Pyatiizbyantseva ¹¹⁶ J. Qian ¹⁰⁸ R. Qian ¹⁰⁹ D. Qichen ¹⁰³ Y. Qin ¹³
 T. Qiu ⁵² A. Quadt ⁵⁵ M. Queitsch-Maitland ¹⁰³ G. Quetant ⁵⁶ R. P. Quinn ¹⁷⁰ G. Rabanal Bolanos ⁶¹
 D. Rafanoharana ⁵⁴ F. Raffaeli ^{76a,76b} F. Ragusa ^{71a,71b} J. L. Rainbolt ⁴⁰ J. A. Raine ⁵⁶ S. Rajagopalan ^{27b}
 E. Ramakoti ³⁹ L. Rambelli ^{57b,57a} I. A. Ramirez-Berend ³⁵ K. Ran ^{48,114c} D. S. Rankin ¹³¹ N. P. Rapheeha ^{34g}
 H. Rasheed ^{29b} D. F. Rassloff ^{63a} A. Rastogi ^{18a} S. Rave ¹⁰² S. Ravera ^{57b,57a} B. Ravina ³⁷ I. Ravinovich ¹⁷⁵
 M. Raymond ³⁷ A. L. Read ¹²⁸ N. P. Readioff ¹⁴⁵ D. M. Rebuzzi ^{73a,73b} A. S. Reed ¹¹² K. Reeves ²⁸
 J. A. Reidelsturz ¹⁷⁷ D. Reikher ¹²⁶ A. Rej ⁴⁹ C. Rembser ³⁷ H. Ren ⁶² M. Renda ^{29b} F. Renner ⁴⁸
 A. G. Rennie ⁵⁹ A. L. Rescia ⁴⁸ S. Resconi ^{71a} M. Ressegotti ^{57b,57a} S. Rettie ³⁷ W. F. Rettie ³⁵ E. Reynolds ^{18a}
 O. L. Rezanova ³⁹ P. Reznicek ¹³⁶ H. Riani ^{36d} N. Ribaric ⁵¹ E. Ricci ^{78a,78b} R. Richter ¹¹² S. Richter ^{47a,47b}
 E. Richter-Was ^{86b} M. Ridel ¹³⁰ S. Ridouani ^{36d} P. Rieck ¹²⁰ P. Riedler ³⁷ E. M. Riefel ^{47a,47b} J. O. Rieger ¹¹⁷
 M. Rijssenbeek ¹⁵¹ M. Rimoldi ³⁷ L. Rinaldi ^{24b,24a} P. Rincke ¹⁶⁷ G. Ripellino ¹⁶⁷ I. Riu ¹³
 J. C. Rivera Vergara ¹⁷¹ F. Rizatdinova ¹²⁴ E. Rizvi ⁹⁶ B. R. Roberts ^{18a} S. S. Roberts ¹³⁹ D. Robinson ³³
 M. Robles Manzano ¹⁰² A. Robson ⁵⁹ A. Rocchi ^{76a,76b} C. Roda ^{74a,74b} S. Rodriguez Bosca ³⁷
 Y. Rodriguez Garcia ^{23a} A. M. Rodriguez Vera ¹¹⁸ S. Roe ³⁷ J. T. Roemer ³⁷ O. Røhne ¹²⁸ R. A. Rojas ³⁷
 C. P. A. Roland ¹³⁰ A. Romaniouk ⁷⁹ E. Romano ^{73a,73b} M. Romano ^{24b} A. C. Romero Hernandez ¹⁶⁸
 N. Rompotis ⁹⁴ L. Roos ¹³⁰ S. Rosati ^{75a} B. J. Rosser ⁴⁰ E. Rossi ¹²⁹ E. Rossi ^{72a,72b} L. P. Rossi ⁶¹ L. Rossini ⁵⁴
 R. Rosten ¹²² M. Rotaru ^{29b} B. Rottler ⁵⁴ D. Rousseau ⁶⁶ D. Rousseau ⁴⁸ S. Roy-Garand ¹⁶¹ A. Rozanov ¹⁰⁴
 Z. M. A. Rozario ⁵⁹ Y. Rozen ¹⁵⁶ A. Rubio Jimenez ¹⁶⁹ V. H. Ruelas Rivera ¹⁹ T. A. Ruggeri ¹ A. Ruggiero ¹²⁹
 A. Ruiz-Martinez ¹⁶⁹ A. Rummler ³⁷ Z. Rurikova ⁵⁴ N. A. Rusakovich ³⁹ H. L. Russell ¹⁷¹ G. Russo ^{75a,75b}
 J. P. Rutherford ⁷ S. Rutherford Colmenares ³³ M. Rybar ¹³⁶ P. Rybczynski ^{86a} A. Ryzhov ⁴⁵
 J. A. Sabater Iglesias ⁵⁶ H.F-W. Sadrozinski ¹³⁹ F. Safai Tehrani ^{75a} S. Saha ¹ M. Sahinsoy ⁸² B. Sahoo ¹⁷⁵
 A. Saibel ¹⁶⁹ B. T. Saifuddin ¹²³ M. Saimpert ¹³⁸ G. T. Saito ^{83c} M. Saito ¹⁵⁹ T. Saito ¹⁵⁹ A. Sala ^{71a,71b}
 A. Salnikov ¹⁴⁹ J. Salt ¹⁶⁹ A. Salvador Salas ¹⁵⁷ F. Salvatore ¹⁵² A. Salzburger ³⁷ D. Sammel ⁵⁴ E. Sampson ⁹³
 D. Sampsonidis ^{158,ab} D. Sampsonidou ¹²⁶ J. Sánchez ¹⁶⁹ V. Sanchez Sebastian ¹⁶⁹ H. Sandaker ¹²⁸ C. O. Sander ⁴⁸
 J. A. Sandesara ¹⁷⁶ M. Sandhoff ¹⁷⁷ C. Sandoval ^{23b} L. Sanfilippo ^{63a} D. P. C. Sankey ¹³⁷ T. Sano ⁸⁹ A. Sansoni ⁵³
 L. Santi ³⁷ C. Santoni ⁴¹ H. Santos ^{133a,133b} A. Santra ¹⁷⁵ E. Sanzani ^{24b,24a} K. A. Saoucha ^{88b}
 J. G. Saraiva ^{133a,133d} J. Sardain ⁷ O. Sasaki ⁸⁴ K. Sato ¹⁶³ C. Sauer ³⁷ E. Sauvan ⁴ P. Savard ^{161,d} R. Sawada ¹⁵⁹
 C. Sawyer ¹³⁷ L. Sawyer ⁹⁹ C. Sbarra ^{24b} A. Sbrizzi ^{24b,24a} T. Scanlon ⁹⁸ J. Schaarschmidt ¹⁴² U. Schäfer ¹⁰²
 A. C. Schaffer ^{66,45} D. Schaile ¹¹¹ R. D. Schamberger ¹⁵¹ C. Scharf ¹⁹ M. M. Schefer ²⁰ V. A. Schegelsky ³⁸
 D. Scheirich ¹³⁶ M. Schernau ^{140e} C. Scheulen ⁵⁶ C. Schiavi ^{57b,57a} M. Schioppa ^{44b,44a} B. Schlag ¹⁴⁹
 S. Schlenker ³⁷ J. Schmeing ¹⁷⁷ E. Schmidt ¹¹² M. A. Schmidt ¹⁷⁷ K. Schmieden ¹⁰² C. Schmitt ¹⁰² N. Schmitt ¹⁰²
 S. Schmitt ⁴⁸ L. Schoeffel ¹³⁸ A. Schoening ^{63b} P. G. Scholer ³⁵ E. Schopf ¹⁴⁷ M. Schott ²⁵ S. Schramm ⁵⁶
 T. Schroer ⁵⁶ H-C. Schultz-Coulon ^{63a} M. Schumacher ⁵⁴ B. A. Schumm ¹³⁹ Ph. Schune ¹³⁸ H. R. Schwartz ¹³⁹
 A. Schwartzman ¹⁴⁹ T. A. Schwarz ¹⁰⁸ Ph. Schwemling ¹³⁸ R. Schwienhorst ¹⁰⁹ F. G. Sciacca ²⁰ A. Sciandra ^{27b}
 G. Sciolla ²⁸ F. Scuri ^{74a} C. D. Sebastiani ³⁷ K. Sedlaczek ¹¹⁸ S. C. Seidel ¹¹⁵ A. Seiden ¹³⁹ B. D. Seidlitz ⁴²
 C. Seitz ⁴⁸ J. M. Seixas ^{83b} G. Sekhniaidze ^{72a} L. Selem ⁶⁰ N. Semprini-Cesari ^{24b,24a} A. Semushin ¹⁷⁹
 D. Sengupta ⁵⁶ V. Senthilkumar ¹⁶⁹ L. Serin ⁶⁶ M. Sessa ¹²³ F. Sforza ^{57b,57a} A. Sfyrla ⁵⁶
 Q. Sha ¹⁴ E. Shabalina ⁵⁵ H. Shaddix ¹¹⁸ A. H. Shah ³³ R. Shaheen ¹⁵⁰ J. D. Shahinian ¹³¹ M. Shamim ³⁷
 L. Y. Shan ¹⁴ M. Shapiro ^{18a} A. Sharma ³⁷ A. S. Sharma ¹⁷⁰ P. Sharma ^{27b} P. B. Shatalov ³⁸ K. Shaw ¹⁵²
 S. M. Shaw ¹⁰³ Q. Shen ^{144a} D. J. Sheppard ¹⁴⁸ P. Sherwood ⁹⁸ L. Shi ⁹⁸ X. Shi ¹⁴ S. Shimizu ⁸⁴
 C. O. Shimmin ¹⁷⁸ I. P. J. Shipsey ^{129,aa} S. Shirabe ⁹⁰ M. Shiyakova ^{39,ak} M. J. Shochet ⁴⁰ D. R. Shope ¹²⁸
 B. Shrestha ¹²³ S. Shrestha ^{122,al} I. Shreyber ³⁹ M. J. Shroff ¹⁷¹ P. Sicho ¹³⁴ A. M. Sickles ¹⁶⁸
 E. Sideras Haddad ^{34g,166} A. C. Sidley ¹¹⁷ A. Sidoti ^{24b} F. Siegert ⁵⁰ Dj. Sijacki ¹⁶ F. Sili ⁹² J. M. Silva ⁵²
 I. Silva Ferreira ^{83b} M. V. Silva Oliveira ^{27b} S. B. Silverstein ^{47a} S. Simion ⁶⁶ R. Simonello ³⁷ E. L. Simpson ¹⁰³
 H. Simpson ¹⁵² L. R. Simpson ⁶ S. Simsek ⁸² S. Sindhu ⁵⁵ P. Sinervo ¹⁶¹ S. N. Singh ²⁸ S. Singh ^{27b} S. Sinha ⁴⁸
 S. Sinha ¹⁰³ M. Sioli ^{24b,24a} K. Sioulas ⁹ I. Siral ³⁷ E. Sitnikova ⁴⁸ J. Sjölin ^{47a,47b} A. Skaf ⁵⁵ E. Skorda ²¹
 P. Skubic ¹²³ M. Slawinska ⁸⁷ I. Slazyk ¹⁷ V. Smakhtin ¹⁷⁵ B. H. Smart ¹³⁷ S. Yu. Smirnov ^{140b} Y. Smirnov ⁸²
 L. N. Smirnova ^{38,k} O. Smirnova ¹⁰⁰ A. C. Smith ⁴² D. R. Smith ¹⁶⁵ J. L. Smith ¹⁰³ M. B. Smith ³⁵ R. Smith ¹⁴⁹
 H. Smitmanns ¹⁰² M. Smizanska ⁹³ K. Smolek ¹³⁵ P. Smolyanskiy ¹³⁵ A. A. Snesarev ³⁹ H. L. Snoek ¹¹⁷
 S. Snyder ^{27b} R. Sobie ^{171,o} A. Soffer ¹⁵⁷ C. A. Solans Sanchez ³⁷ E. Yu. Soldatov ³⁹ U. Soldevila ¹⁶⁹
 A. A. Solodkov ^{34g} S. Solomon ²⁸ A. Soloshenko ³⁹ K. Solovieva ⁵⁴ O. V. Solovyanov ⁴¹ P. Sommer ⁵⁰
 A. Sonay ¹³ A. Sopczak ¹³⁵ A. L. Sopio ⁵² F. Sopkova ^{30b} J. D. Sorenson ¹¹⁵ I. R. Sotarriba Alvarez ¹⁴¹
 V. Sothilingam ^{63a} O. J. Soto Sandoval ^{140c,140b} S. Sottocornola ⁶⁸ R. Soualah ^{88a} Z. Soumami ³⁶ D. South ⁴⁸
 N. Soybelman ¹⁷⁵ S. Spagnolo ^{70a,70b} M. Spalla ¹¹² D. Sperlich ⁵⁴ B. Spisso ^{72a,72b} D. P. Spiteri ⁵⁹ L. Splendori ¹⁰⁴
 M. Spousta ¹³⁶ E. J. Staats ³⁵ R. Stamen ^{63a} E. Stanecka ⁸⁷ W. Stanek-Maslouska ⁴⁸ M. V. Stange ⁵⁰
 B. Stanislause ^{18a} M. M. Stanitzki ⁴⁸ B. Stapf ⁴⁸ E. A. Starchenko ³⁸ G. H. Stark ¹³⁹ J. Stark ⁹¹ P. Staroba ¹³⁴
 P. Starovoitov ^{88b} R. Staszewski ⁸⁷ G. Stavropoulos ⁴⁶ A. Stefl ³⁷ P. Steinberg ^{27b} B. Stelzer ^{148,162a}

- H. J. Stelzer¹³² O. Stelzer-Chilton^{162a} H. Stenzel⁵⁸ T. J. Stevenson¹⁵² G. A. Stewart³⁷ J. R. Stewart¹²⁴
 M. C. Stockton³⁷ G. Stoica^{29b} M. Stolarski^{133a} S. Stonjek¹¹² A. Straessner⁵⁰ J. Strandberg¹⁵⁰
 S. Strandberg^{47a,47b} M. Stratmann¹⁷⁷ M. Strauss¹²³ T. Streblner¹⁰⁴ P. Strizenec^{30b} R. Ströhmer¹⁷²
 D. M. Strom¹²⁶ R. Stroynowski⁴⁵ A. Strubig^{47a,47b} S. A. Stucci^{27b} B. Stugu¹⁷ J. Stupak¹²³ N. A. Styles⁴⁸
 D. Su¹⁴⁹ S. Su⁶² X. Su^{30a} D. Suchy¹³¹ K. Sugizaki³⁸ V. V. Sulin³⁸ M. J. Sullivan⁹⁴ D. M. S. Sultan¹²⁹
 L. Sultanaliyeva³⁸ S. Sultansoy^{3b} S. Sun¹⁷⁶ W. Sun¹⁴ O. Sunneborn Gudnadottir¹⁶⁷ N. Sur¹⁰⁰ M. R. Sutton¹⁵²
 H. Suzuki¹⁶³ M. Svatos¹³⁴ P. N. Swallow³³ M. Swiatlowski^{162a} T. Swirski¹⁷² I. Sykora^{30a} M. Sykora¹³⁶
 T. Sykora¹³⁶ D. Ta¹⁰² K. Tackmann^{48,ai} A. Taffard¹⁶⁵ R. Tafirout^{162a} Y. Takubo⁸⁴ M. Talby¹⁰⁴
 A. A. Talyshев³⁸ K. C. Tam^{64b} N. M. Tamir¹⁵⁷ A. Tanaka¹⁵⁹ J. Tanaka¹⁵⁹ R. Tanaka⁶⁶ M. Tanasini¹⁵¹
 Z. Tao¹⁷⁰ S. Tapia Araya^{140f} S. Tapprogge¹⁰² A. Tarek Abouelfadl Mohamed¹⁰⁹ S. Tarem¹⁵⁶ K. Tariq¹⁴
 G. Tarna^{29b} G. F. Tartarelli^{71a} M. J. Tartarin⁹¹ P. Tas¹³⁶ M. Tasevsky¹³⁴ E. Tassi^{44b,44a} A. C. Tate¹⁶⁸
 G. Tateno¹⁵⁹ Y. Tayalati^{36e,am} G. N. Taylor¹⁰⁷ W. Taylor^{162b} A. S. Tegetmeier⁹¹ P. Teixeira-Dias⁹⁷
 J. J. Teoh¹⁶¹ K. Terashi¹⁵⁹ J. Terron¹⁰¹ S. Terzo¹³ M. Testa⁵³ R. J. Teuscher^{161,o} A. Thaler⁷⁹ O. Theiner⁵⁶
 T. Theveneaux-Pelzer¹⁰⁴ D. W. Thomas⁹⁷ J. P. Thomas²¹ E. A. Thompson^{18a} P. D. Thompson²¹ E. Thomson¹³¹
 R. E. Thornberry⁴⁵ C. Tian⁶² Y. Tian⁵⁶ V. Tikhomirov⁸² Yu. A. Tikhonov³⁹ S. Timoshenko³⁸ D. Timoshyn¹³⁶
 E. X. L. Ting¹ P. Tipton¹⁷⁸ A. Tishelman-Charny^{27b} K. Todome¹⁴¹ S. Todorova-Nova¹³⁶ S. Todt⁵⁰
 L. Toffolin^{69a,69c} M. Togawa⁸⁴ J. Tojo⁹⁰ S. Tokár^{30a} O. Toldaiev⁶⁸ G. Tolkachev¹⁰⁴ M. Tomoto^{84,113}
 L. Tompkins^{149,an} E. Torrence¹²⁶ H. Torres⁹¹ E. Torró Pastor¹⁶⁹ M. Toscani³¹ C. Toscirci⁴⁰ M. Tost¹¹
 D. R. Tovey¹⁴⁵ T. Trefzger¹⁷² P. M. Tricarico¹³ A. Tricoli^{27b} I. M. Trigger^{162a} S. Trincaz-Duvoud¹³⁰
 D. A. Trischuk²⁸ A. Tropina³⁹ L. Truong^{34c} M. Trzebinski⁸⁷ A. Trzupek⁸⁷ F. Tsai¹⁵¹ M. Tsai¹⁰⁸
 A. Tsiamis¹⁵⁸ P. V. Tsiareshka³⁹ S. Tsigaridas^{162a} A. Tsirigotis^{158,ac} V. Tsiskaridze¹⁶¹ E. G. Tskhadadze^{155a}
 M. Tsopoulou¹⁵⁸ Y. Tsujikawa⁸⁹ I. I. Tsukerman³⁸ V. Tsulaia^{18a} S. Tsuno⁸⁴ K. Tsuri¹²¹ D. Tsybychev¹⁵¹
 Y. Tu^{64b} A. Tudorache^{29b} V. Tudorache^{29b} S. Turchikhin^{57b,57a} I. Turk Cakir^{3a} R. Turra^{71a} T. Turtuvshin^{39,ao}
 P. M. Tuts⁴² S. Tzamarias^{158,ab} E. Tzovara¹⁰² Y. Uematsu⁸⁴ F. Ukegawa¹⁶³ P. A. Ulloa Poblete^{140c,140b}
 E. N. Umaka^{27b} G. Unal³⁷ A. Undrus^{27b} G. Unel¹⁶⁵ J. Urban^{30b} P. Urrejola^{140a} G. Usai⁸ R. Ushioda¹⁶⁰
 M. Usman¹¹⁰ F. Ustuner⁵² Z. Uysal⁸² V. Vacek¹³⁵ B. Vachon¹⁰⁶ T. Vafeiadis³⁷ A. Vaitkus⁹⁸
 C. Valderanis¹¹¹ E. Valdes Santurio^{47a,47b} M. Valente³⁷ S. Valentineti^{24b,24a} A. Valero¹⁶⁹ E. Valiente Moreno¹⁶⁹
 A. Vallier⁹¹ J. A. Valls Ferrer¹⁶⁹ D. R. Van Arneman¹¹⁷ T. R. Van Daalen¹⁴² A. Van Der Graaf⁴⁹
 H. Z. Van Der Schyf^{34g} P. Van Gemmeren⁶ M. Van Rijnbach³⁷ S. Van Stroud⁹⁸ I. Van Vulpen¹¹⁷ P. Vana¹³⁶
 M. Vanadia^{76a,76b} U. M. Vande Voorde¹⁵⁰ W. Vandelli³⁷ E. R. Vandewall¹²⁴ D. Vannicola¹⁵⁷ L. Vannoli⁵³
 R. Vari^{75a} E. W. Varnes⁷ C. Varni^{18b} D. Varouchas⁶⁶ L. Varriale¹⁶⁹ K. E. Varvell¹⁵³ M. E. Vasile^{29b}
 L. Vaslin⁸⁴ M. D. Vassilev¹⁴⁹ A. Vasyukov³⁹ L. M. Vaughan¹²⁴ R. Vavricka¹³⁶ T. Vazquez Schroeder¹³
 J. Veatch³² V. Vecchio¹⁰³ M. J. Veen¹⁰⁵ I. Velisek^{27b} I. Velkovska⁹⁵ L. M. Veloce¹⁶¹ F. Veloso^{133a,133c}
 S. Veneziano^{75a} A. Ventura^{70a,70b} S. Ventura Gonzalez¹³⁸ A. Verbytskyi¹¹² M. Verducci^{74a,74b} C. Vergis⁹⁶
 M. Verissimo De Araujo^{83b} W. Verkerke¹¹⁷ J. C. Vermeulen¹¹⁷ C. Vernieri¹⁴⁹ M. Vessella¹⁶⁵ M. C. Vetterli^{148,d}
 A. Vgenopoulos¹⁰² N. Viaux Maira^{140f} T. Vickey¹⁴⁵ O. E. Vickey Boeriu¹⁴⁵ G. H. A. Viehhauser¹²⁹ L. Vigani^{63b}
 M. Vigl¹¹² M. Villa^{24b,24a} M. Villaplana Perez¹⁶⁹ E. M. Villhauer⁵² E. Vilucchi⁵³ M. G. Vincter³⁵ A. Visibile,
 C. Vittori³⁷ I. Vivarelli^{24b,24a} E. Voevodina¹¹² F. Vogel¹¹¹ J. C. Voigt⁵⁰ P. Vokac¹³⁵ Yu. Volkotrub^{86b}
 E. Von Toerne²⁵ B. Vormwald³⁷ K. Vorobev⁵¹ M. Vos¹⁶⁹ K. Voss¹⁴⁷ M. Vozak³⁷ L. Vozdecky¹²³
 N. Vranjes¹⁶ M. Vranjes Milosavljevic¹⁶ M. Vreeswijk¹¹⁷ N. K. Vu^{144b,144a} R. Vuillermet³⁷ O. Vujinovic¹⁰²
 I. Vukotic⁴⁰ I. K. Vyas³⁵ J. F. Wack³³ S. Wada¹⁶³ C. Wagner¹⁴⁹ J. M. Wagner^{18a} W. Wagner¹⁷⁷ S. Wahdan¹⁷⁷
 H. Wahlberg⁹² C. H. Waits¹²³ J. Walder¹³⁷ R. Walker¹¹¹ W. Walkowiak¹⁴⁷ A. Wall¹³¹ E. J. Wallin¹⁰⁰
 T. Wamorkar^{18a} A. Z. Wang¹³⁹ C. Wang¹⁰² C. Wang¹¹ H. Wang^{18a} J. Wang^{64c} P. Wang¹⁰³ P. Wang⁹⁸
 R. Wang⁶¹ R. Wang⁶ S. M. Wang¹⁵⁴ S. Wang¹⁴ T. Wang⁶² T. Wang⁶² W. T. Wang⁸⁰ W. Wang¹⁴
 X. Wang¹⁶⁸ X. Wang^{144a} X. Wang⁴⁸ Y. Wang^{114a} Y. Wang⁶² Z. Wang¹⁰⁸ Z. Wang^{144b} Z. Wang¹⁰⁸
 C. Wanotayaroj⁸⁴ A. Warburton¹⁰⁶ A. L. Warnerbring¹⁴⁷ N. Warrack⁵⁹ S. Waterhouse⁹⁷ A. T. Watson²¹
 H. Watson⁵² M. F. Watson²¹ E. Watton⁵⁹ G. Watts¹⁴² B. M. Waugh⁹⁸ J. M. Webb⁵⁴ C. Weber^{27b}
 H. A. Weber¹⁹ M. S. Weber²⁰ S. M. Weber^{63a} C. Wei⁶² Y. Wei⁵⁴ A. R. Weidberg¹²⁹ E. J. Weik¹²⁰
 J. Weingarten⁴⁹ C. Weiser⁵⁴ C. J. Wells⁴⁸ T. Wenaus^{27b} B. Wendland⁴⁹ T. Wengler³⁷ N. S. Wenke,
 N. Wermes²⁵ M. Wessels^{63a} A. M. Wharton⁹³ A. S. White⁶¹ A. White⁸ M. J. White¹ D. Whiteson¹⁶⁵
 L. Wickremasinghe¹²⁷ W. Wiedenmann¹⁷⁶ M. Wielers¹³⁷ R. Wierda¹⁵⁰ C. Wiglesworth⁴³ H. G. Wilkens³⁷
 J. J. H. Wilkinson³³ D. M. Williams⁴² H. H. Williams¹³¹ S. Williams³³ S. Willocq¹⁰⁵ B. J. Wilson¹⁰³
 D. J. Wilson¹⁰³ P. J. Windischhofer⁴⁰ F. I. Winkel³¹ F. Winklmeier¹²⁶ B. T. Winter⁵⁴ M. Wittgen,
 M. Wobisch⁹⁹ T. Wojtkowski⁶⁰ Z. Wolffs¹¹⁷ J. Wollrath³⁷ M. W. Wolter⁸⁷ H. Wolters^{133a,133c} M. C. Wong¹³⁹
 E. L. Woodward⁴² S. D. Worm⁴⁸ B. K. Wosiek⁸⁷ K. W. Woźniak⁸⁷ S. Wozniewski⁵⁵ K. Wright⁵⁹ C. Wu¹⁶¹
 C. Wu²¹ J. Wu¹⁵⁹ M. Wu^{114b} M. Wu¹¹⁶ S. L. Wu¹⁷⁶ S. Wu¹⁴ X. Wu⁶² Y. Wu⁶² Z. Wu⁴
 J. Wuerzinger¹¹² T. R. Wyatt¹⁰³ B. M. Wynne⁵² S. Xella⁴³ L. Xia^{114a} M. Xia¹⁵ M. Xie⁶² A. Xiong¹²⁶
 J. Xiong^{18a} D. Xu¹⁴ H. Xu⁶² L. Xu⁶² R. Xu¹³¹ T. Xu¹⁰⁸ Y. Xu¹⁴² Z. Xu⁵² Z. Xu^{114a} B. Yabsley¹⁵³

S. Yacoob^{34a} Y. Yamaguchi⁸⁴ E. Yamashita¹⁵⁹ H. Yamauchi¹⁶³ T. Yamazaki^{18a} Y. Yamazaki⁸⁵ S. Yan⁵⁹
 Z. Yan¹⁰⁵ H. J. Yang^{144a,144b} H. T. Yang⁶² S. Yang⁶² T. Yang^{64c} X. Yang³⁷ X. Yang¹⁴ Y. Yang¹⁵⁹
 Y. Yang⁶² W-M. Yao^{18a} C. L. Yardley¹⁵² J. Ye¹⁴ S. Ye^{27b} X. Ye⁶² Y. Yeh⁹⁸ I. Yeletskikh³⁹ B. Yeo^{18b}
 M. R. Yexley⁹⁸ T. P. Yildirim¹²⁹ P. Yin⁴² K. Yorita¹⁷⁴ C. J. S. Young³⁷ C. Young¹⁴⁹ N. D. Young¹²⁶ Y. Yu⁶²
 J. Yuan^{14,114c} M. Yuan¹⁰⁸ R. Yuan^{144b,144a} L. Yue⁹⁸ M. Zaazoua⁶² B. Zabinski⁸⁷ I. Zahir^{36a} A. Zaio,
 Z. K. Zak⁸⁷ T. Zakareishvili¹⁶⁹ S. Zambito⁵⁶ J. A. Zamora Saa^{140d} J. Zang¹⁵⁹ D. Zanzi⁵⁴ R. Zanzotteri^{71a,71b}
 O. Zaplatilek¹³⁵ C. Zeitnitz¹⁷⁷ H. Zeng¹⁴ J. C. Zeng¹⁶⁸ D. T. Zenger, Jr.²⁸ O. Zenin³⁸ T. Ženiš^{30a} S. Zenz⁹⁶
 D. Zerwas⁶⁶ M. Zhai^{14,114c} D. F. Zhang¹⁴⁵ G. Zhang¹⁴ J. Zhang^{143a} J. Zhang⁶ K. Zhang^{14,114c} L. Zhang⁶²
 L. Zhang^{114a} P. Zhang^{14,114c} R. Zhang¹⁷⁶ S. Zhang⁹¹ T. Zhang¹⁵⁹ X. Zhang^{144a} Y. Zhang¹⁴² Y. Zhang⁹⁸
 Y. Zhang⁶² Y. Zhang^{114a} Z. Zhang^{18a} Z. Zhang^{143a} Z. Zhang⁶⁶ H. Zhao¹⁴² T. Zhao^{143a} Y. Zhao³⁵
 Z. Zhao⁶² Z. Zhao⁶² A. Zhemchugov³⁹ J. Zheng^{114a} K. Zheng¹⁶⁸ X. Zheng⁶² Z. Zheng¹⁴⁹ D. Zhong¹⁶⁸
 B. Zhou¹⁰⁸ H. Zhou⁷ N. Zhou^{144a} Y. Zhou¹⁵ Y. Zhou^{114a} Y. Zhou⁷ C. G. Zhu^{143a} J. Zhu¹⁰⁸ X. Zhu,^{144b}
 Y. Zhu^{144a} Y. Zhu⁶² X. Zhuang¹⁴ K. Zhukov⁶⁸ N. I. Zimine³⁹ J. Zinsser^{63b} M. Ziolkowski¹⁴⁷ L. Živković¹⁶
 A. Zoccoli^{24b,24a} K. Zoch⁶¹ T. G. Zorbas¹⁴⁵ O. Zormpa⁴⁶ and L. Zwalski³⁷

(ATLAS Collaboration)

¹Department of Physics, University of Adelaide, Adelaide, Australia²Department of Physics, University of Alberta, Edmonton AB, Canada^{3a}Department of Physics, Ankara University, Ankara, Türkiye^{3b}Division of Physics, TOBB University of Economics and Technology, Ankara, Türkiye⁴LAPP, Université Savoie Mont Blanc, CNRS/IN2P3, Annecy, France⁵APC, Université Paris Cité, CNRS/IN2P3, Paris, France⁶High Energy Physics Division, Argonne National Laboratory, Argonne, Illinois, USA⁷Department of Physics, University of Arizona, Tucson, Arizona, USA⁸Department of Physics, University of Texas at Arlington, Arlington, Texas, USA⁹Physics Department, National and Kapodistrian University of Athens, Athens, Greece¹⁰Physics Department, National Technical University of Athens, Zografou, Greece¹¹Department of Physics, University of Texas at Austin, Austin, Texas, USA¹²Institute of Physics, Azerbaijan Academy of Sciences, Baku, Azerbaijan¹³Institut de Física d'Altes Energies (IFAE), Barcelona Institute of Science and Technology, Barcelona, Spain¹⁴Institute of High Energy Physics, Chinese Academy of Sciences, Beijing, China¹⁵Physics Department, Tsinghua University, Beijing, China¹⁶Institute of Physics, University of Belgrade, Belgrade, Serbia¹⁷Department for Physics and Technology, University of Bergen, Bergen, Norway^{18a}Physics Division, Lawrence Berkeley National Laboratory, Berkeley, California, USA^{18b}University of California, Berkeley, California, USA¹⁹Institut für Physik, Humboldt Universität zu Berlin, Berlin, Germany²⁰Albert Einstein Center for Fundamental Physics and Laboratory for High Energy Physics, University of Bern, Bern, Switzerland²¹School of Physics and Astronomy, University of Birmingham, Birmingham, United Kingdom^{22a}Department of Physics, Bogazici University, Istanbul, Türkiye^{22b}Department of Physics Engineering, Gaziantep University, Gaziantep, Türkiye^{22c}Department of Physics, Istanbul University, Istanbul, Türkiye^{23a}Facultad de Ciencias y Centro de Investigaciones, Universidad Antonio Nariño, Bogotá, Colombia^{23b}Departamento de Física, Universidad Nacional de Colombia, Bogotá, Colombia^{24a}Dipartimento di Fisica e Astronomia A. Righi, Università di Bologna, Bologna, Italy^{24b}INFN Sezione di Bologna, Italy²⁵Physikalisch-es Institut, Universität Bonn, Bonn, Germany²⁶Department of Physics, Boston University, Boston, Massachusetts, USA^{27a}Department of Physics, University of Colorado Boulder, Colorado, USA^{27b}Physics Department, Brookhaven National Laboratory, Upton, New York, USA²⁸Department of Physics, Brandeis University, Waltham, Massachusetts, USA^{29a}Transilvania University of Brasov, Brasov, Romania^{29b}Horia Hulubei National Institute of Physics and Nuclear Engineering, Bucharest, Romania^{29c}Department of Physics, Alexandru Ioan Cuza University of Iasi, Iasi, Romania^{29d}National Institute for Research and Development of Isotopic and Molecular Technologies, Physics Department, Cluj-Napoca, Romania^{29e}National University of Science and Technology Politehnica, Bucharest, Romania^{29f}West University in Timisoara, Timisoara, Romania

- ^{29g}*Faculty of Physics, University of Bucharest, Bucharest, Romania*
- ^{30a}*Faculty of Mathematics, Physics and Informatics, Comenius University, Bratislava, Slovak Republic*
- ^{30b}*Department of Subnuclear Physics, Institute of Experimental Physics of the Slovak Academy of Sciences, Kosice, Slovak Republic*
- ³¹*Universidad de Buenos Aires, Facultad de Ciencias Exactas y Naturales, Departamento de Física, y CONICET, Instituto de Física de Buenos Aires (IFIBA), Buenos Aires, Argentina*
- ³²*California State University, California, USA*
- ³³*Cavendish Laboratory, University of Cambridge, Cambridge, United Kingdom*
- ^{34a}*Department of Physics, University of Cape Town, Cape Town, South Africa*
- ^{34b}*iThemba Labs, Western Cape, South Africa*
- ^{34c}*Department of Mechanical Engineering Science, University of Johannesburg, Johannesburg, South Africa*
- ^{34d}*National Institute of Physics, University of the Philippines Diliman (Philippines), South Africa*
- ^{34e}*University of South Africa, Department of Physics, Pretoria, South Africa*
- ^{34f}*University of Zululand, KwaDlangezwa, South Africa*
- ^{34g}*School of Physics, University of the Witwatersrand, Johannesburg, South Africa*
- ³⁵*Department of Physics, Carleton University, Ottawa, Ontario, Canada*
- ^{36a}*Faculté des Sciences Ain Chock, Université Hassan II de Casablanca, Morocco*
- ^{36b}*Faculté des Sciences, Université Ibn-Tofail, Kénitra, Morocco*
- ^{36c}*Faculté des Sciences Semlalia, Université Cadi Ayyad, LPHEA-Marrakech, Morocco*
- ^{36d}*LPMR, Faculté des Sciences, Université Mohamed Premier, Oujda, Morocco*
- ^{36e}*Faculté des sciences, Université Mohammed V, Rabat, Morocco*
- ^{36f}*Institute of Applied Physics, Mohammed VI Polytechnic University, Ben Guerir, Morocco*
- ³⁷*CERN, Geneva, Switzerland*
- ³⁸*Affiliated with an institute formerly covered by a cooperation agreement with CERN*
- ³⁹*Affiliated with an international laboratory covered by a cooperation agreement with CERN*
- ⁴⁰*Enrico Fermi Institute, University of Chicago, Chicago, Illinois, USA*
- ⁴¹*LPC, Université Clermont Auvergne, CNRS/IN2P3, Clermont-Ferrand, France*
- ⁴²*Nevis Laboratory, Columbia University, Irvington, New York, USA*
- ⁴³*Niels Bohr Institute, University of Copenhagen, Copenhagen, Denmark*
- ^{44a}*Dipartimento di Fisica, Università della Calabria, Rende, Italy*
- ^{44b}*INFN Gruppo Collegato di Cosenza, Laboratori Nazionali di Frascati, Italy*
- ⁴⁵*Physics Department, Southern Methodist University, Dallas, Texas, USA*
- ⁴⁶*National Centre for Scientific Research “Demokritos”, Agia Paraskevi, Greece*
- ^{47a}*Department of Physics, Stockholm University, Sweden*
- ^{47b}*Oskar Klein Centre, Stockholm, Sweden*
- ⁴⁸*Deutsches Elektronen-Synchrotron DESY, Hamburg and Zeuthen, Germany*
- ⁴⁹*Fakultät Physik, Technische Universität Dortmund, Dortmund, Germany*
- ⁵⁰*Institut für Kern- und Teilchenphysik, Technische Universität Dresden, Dresden, Germany*
- ⁵¹*Department of Physics, Duke University, Durham, North Carolina, USA*
- ⁵²*SUPA—School of Physics and Astronomy, University of Edinburgh, Edinburgh, United Kingdom*
- ⁵³*INFN e Laboratori Nazionali di Frascati, Frascati, Italy*
- ⁵⁴*Physikalisches Institut, Albert-Ludwigs-Universität Freiburg, Freiburg, Germany*
- ⁵⁵*II. Physikalisches Institut, Georg-August-Universität Göttingen, Göttingen, Germany*
- ⁵⁶*Département de Physique Nucléaire et Corpusculaire, Université de Genève, Genève, Switzerland*
- ^{57a}*Dipartimento di Fisica, Università di Genova, Genova, Italy*
- ^{57b}*INFN Sezione di Genova, Italy*
- ⁵⁸*II. Physikalisches Institut, Justus-Liebig-Universität Giessen, Giessen, Germany*
- ⁵⁹*SUPA - School of Physics and Astronomy, University of Glasgow, Glasgow, United Kingdom*
- ⁶⁰*LPSC, Université Grenoble Alpes, CNRS/IN2P3, Grenoble INP, Grenoble, France*
- ⁶¹*Laboratory for Particle Physics and Cosmology, Harvard University, Cambridge, Massachusetts, USA*
- ⁶²*Department of Modern Physics and State Key Laboratory of Particle Detection and Electronics, University of Science and Technology of China, Hefei, China*
- ^{63a}*Kirchhoff-Institut für Physik, Ruprecht-Karls-Universität Heidelberg, Heidelberg, Germany*
- ^{63b}*Physikalisches Institut, Ruprecht-Karls-Universität Heidelberg, Heidelberg, Germany*
- ^{64a}*Department of Physics, Chinese University of Hong Kong, Shatin, N.T., Hong Kong, China*
- ^{64b}*Department of Physics, University of Hong Kong, Hong Kong, China*
- ^{64c}*Department of Physics and Institute for Advanced Study, Hong Kong University of Science and Technology, Clear Water Bay, Kowloon, Hong Kong, China*
- ⁶⁵*Department of Physics, National Tsing Hua University, Hsinchu, Taiwan*
- ⁶⁶*IJCLab, Université Paris-Saclay, CNRS/IN2P3, 91405, Orsay, France*

- ⁶⁷*Centro Nacional de Microelectrónica (IMB-CNM-CSIC), Barcelona, Spain*
⁶⁸*Department of Physics, Indiana University, Bloomington, Indiana, USA*
^{69a}*INFN Gruppo Collegato di Udine, Sezione di Trieste, Udine, Italy*
^{69b}*ICTP, Trieste, Italy*
^{69c}*Dipartimento Politecnico di Ingegneria e Architettura, Università di Udine, Udine, Italy*
^{70a}*INFN Sezione di Lecce, Italy*
^{70b}*Dipartimento di Matematica e Fisica, Università del Salento, Lecce, Italy*
^{71a}*INFN Sezione di Milano, Italy*
^{71b}*Dipartimento di Fisica, Università di Milano, Milano, Italy*
^{72a}*INFN Sezione di Napoli, Italy*
^{72b}*Dipartimento di Fisica, Università di Napoli, Napoli, Italy*
^{73a}*INFN Sezione di Pavia, Italy*
^{73b}*Dipartimento di Fisica, Università di Pavia, Pavia, Italy*
^{74a}*INFN Sezione di Pisa, Italy*
^{74b}*Dipartimento di Fisica E. Fermi, Università di Pisa, Pisa, Italy*
^{75a}*INFN Sezione di Roma, Italy*
^{75b}*Dipartimento di Fisica, Sapienza Università di Roma, Roma, Italy*
^{76a}*INFN Sezione di Roma Tor Vergata, Italy*
^{76b}*Dipartimento di Fisica, Università di Roma Tor Vergata, Roma, Italy*
^{77a}*INFN Sezione di Roma Tre, Italy*
^{77b}*Dipartimento di Matematica e Fisica, Università Roma Tre, Roma, Italy*
^{78a}*INFN-TIFPA, Italy*
^{78b}*Università degli Studi di Trento, Trento, Italy*
⁷⁹*Universität Innsbruck, Department of Astro and Particle Physics, Innsbruck, Austria*
⁸⁰*University of Iowa, Iowa City, Iowa, USA*
⁸¹*Department of Physics and Astronomy, Iowa State University, Ames, Iowa, USA*
⁸²*Istinye University, Sarıyer, İstanbul, Türkiye*
^{83a}*Departamento de Engenharia Elétrica, Universidade Federal de Juiz de Fora (UFJF), Juiz de Fora, Brazil*
^{83b}*Universidade Federal do Rio De Janeiro COPPE/EE/IF, Rio de Janeiro, Brazil*
^{83c}*Instituto de Física, Universidade de São Paulo, São Paulo, Brazil*
^{83d}*Rio de Janeiro State University, Rio de Janeiro, Brazil*
^{83e}*Federal University of Bahia, Bahia, Brazil*
⁸⁴*KEK, High Energy Accelerator Research Organization, Tsukuba, Japan*
⁸⁵*Graduate School of Science, Kobe University, Kobe, Japan*
^{86a}*AGH University of Krakow, Faculty of Physics and Applied Computer Science, Krakow, Poland*
^{86b}*Marian Smoluchowski Institute of Physics, Jagiellonian University, Krakow, Poland*
⁸⁷*Institute of Nuclear Physics Polish Academy of Sciences, Krakow, Poland*
^{88a}*Khalifa University of Science and Technology, Abu Dhabi, United Arab Emirates*
^{88b}*University of Sharjah, Sharjah, United Arab Emirates*
⁸⁹*Faculty of Science, Kyoto University, Kyoto, Japan*
⁹⁰*Research Center for Advanced Particle Physics and Department of Physics, Kyushu University, Fukuoka, Japan*
⁹¹*L2IT, Université de Toulouse, CNRS/IN2P3, UPS, Toulouse, France*
⁹²*Instituto de Física La Plata, Universidad Nacional de La Plata and CONICET, La Plata, Argentina*
⁹³*Physics Department, Lancaster University, Lancaster, United Kingdom*
⁹⁴*Oliver Lodge Laboratory, University of Liverpool, Liverpool, United Kingdom*
⁹⁵*Department of Experimental Particle Physics, Jožef Stefan Institute and Department of Physics, University of Ljubljana, Ljubljana, Slovenia*
⁹⁶*Department of Physics and Astronomy, Queen Mary University of London, London, United Kingdom*
⁹⁷*Department of Physics, Royal Holloway University of London, Egham, United Kingdom*
⁹⁸*Department of Physics and Astronomy, University College London, London, United Kingdom*
⁹⁹*Louisiana Tech University, Ruston, Louisiana, USA*
¹⁰⁰*Fysiska institutionen, Lunds universitet, Lund, Sweden*
¹⁰¹*Departamento de Física Teorica C-15 and CIAFF, Universidad Autónoma de Madrid, Madrid, Spain*
¹⁰²*Institut für Physik, Universität Mainz, Mainz, Germany*
¹⁰³*School of Physics and Astronomy, University of Manchester, Manchester, United Kingdom*
¹⁰⁴*CPPM, Aix-Marseille Université, CNRS/IN2P3, Marseille, France*
¹⁰⁵*Department of Physics, University of Massachusetts, Amherst, Massachusetts, USA*
¹⁰⁶*Department of Physics, McGill University, Montreal QC, Canada*
¹⁰⁷*School of Physics, University of Melbourne, Victoria, Australia*
¹⁰⁸*Department of Physics, University of Michigan, Ann Arbor, Michigan, USA*

- ¹⁰⁹Department of Physics and Astronomy, *Michigan State University*, East Lansing, Michigan, USA
¹¹⁰Group of Particle Physics, *University of Montreal*, Montreal QC, Canada
¹¹¹Fakultät für Physik, *Ludwig-Maximilians-Universität München*, München, Germany
¹¹²Max-Planck-Institut für Physik (Werner-Heisenberg-Institut), München, Germany
¹¹³Graduate School of Science and Kobayashi-Maskawa Institute, *Nagoya University*, Nagoya, Japan
^{114a}Department of Physics, *Nanjing University*, Nanjing, China
^{114b}School of Science, Shenzhen Campus of Sun Yat-sen University, China
^{114c}University of Chinese Academy of Science (UCAS), Beijing, China
¹¹⁵Department of Physics and Astronomy, *University of New Mexico*, Albuquerque, New Mexico, USA
¹¹⁶Institute for Mathematics, Astrophysics and Particle Physics, *Radboud University/Nikhef*, Nijmegen, Netherlands
¹¹⁷Nikhef National Institute for Subatomic Physics and University of Amsterdam, Amsterdam, Netherlands
¹¹⁸Department of Physics, *Northern Illinois University*, DeKalb, Illinois, USA
^{119a}New York University Abu Dhabi, Abu Dhabi, United Arab Emirates
^{119b}United Arab Emirates University, Al Ain, United Arab Emirates
¹²⁰Department of Physics, *New York University*, New York, New York, USA
¹²¹Ochanomizu University, Otsuka, Bunkyo-ku, Tokyo, Japan
¹²²Ohio State University, Columbus, Ohio, USA
¹²³Homer L. Dodge Department of Physics and Astronomy, *University of Oklahoma*, Norman, Oklahoma, USA
¹²⁴Department of Physics, *Oklahoma State University*, Stillwater, Oklahoma, USA
¹²⁵Palacký University, Joint Laboratory of Optics, Olomouc, Czech Republic
¹²⁶Institute for Fundamental Science, *University of Oregon*, Eugene, Oregon, USA
¹²⁷Graduate School of Science, *University of Osaka*, Osaka, Japan
¹²⁸Department of Physics, *University of Oslo*, Oslo, Norway
¹²⁹Department of Physics, *Oxford University*, Oxford, United Kingdom
¹³⁰LPNHE, Sorbonne Université, Université Paris Cité, CNRS/IN2P3, Paris, France
¹³¹Department of Physics, *University of Pennsylvania*, Philadelphia, Pennsylvania, USA
¹³²Department of Physics and Astronomy, *University of Pittsburgh*, Pittsburgh, Pennsylvania, USA
^{133a}Laboratório de Instrumentação e Física Experimental de Partículas—LIP, Lisboa, Portugal
^{133b}Departamento de Física, Faculdade de Ciências, *Universidade de Lisboa*, Lisboa, Portugal
^{133c}Departamento de Física, *Universidade de Coimbra*, Coimbra, Portugal
^{133d}Centro de Física Nuclear da *Universidade de Lisboa*, Lisboa, Portugal
^{133e}Departamento de Física, Escola de Ciências, *Universidade do Minho*, Braga, Portugal
^{133f}Departamento de Física Teórica y del Cosmos, Universidad de Granada, Granada (Spain), Portugal
^{133g}Departamento de Física, *Instituto Superior Técnico*, Universidade de Lisboa, Lisboa, Portugal
¹³⁴Institute of Physics of the Czech Academy of Sciences, Prague, Czech Republic
¹³⁵Czech Technical University in Prague, Prague, Czech Republic
¹³⁶Charles University, Faculty of Mathematics and Physics, Prague, Czech Republic
¹³⁷Particle Physics Department, *Rutherford Appleton Laboratory*, Didcot, United Kingdom
¹³⁸IRFU, CEA, Université Paris-Saclay, Gif-sur-Yvette, France
¹³⁹Santa Cruz Institute for Particle Physics, *University of California Santa Cruz*, Santa Cruz, California, USA
^{140a}Departamento de Física, Pontifícia Universidad Católica de Chile, Santiago, Chile
^{140b}Millennium Institute for Subatomic physics at high energy frontier (SAPHIR), Santiago, Chile
^{140c}Instituto de Investigación Multidisciplinario en Ciencia y Tecnología, y Departamento de Física, *Universidad de La Serena*, Chile
^{140d}Universidad Andres Bello, Department of Physics, Santiago, Chile
^{140e}Instituto de Alta Investigación, *Universidad de Tarapacá*, Arica, Chile
^{140f}Departamento de Física, *Universidad Técnica Federico Santa María*, Valparaíso, Chile
¹⁴¹Department of Physics, *Institute of Science*, Tokyo, Japan
¹⁴²Department of Physics, *University of Washington*, Seattle, Washington, USA
^{143a}Institute of Frontier and Interdisciplinary Science and Key Laboratory of Particle Physics and Particle Irradiation (MOE), *Shandong University*, Qingdao, China
^{143b}School of Physics, Zhengzhou University, China
^{144a}State Key Laboratory of Dark Matter Physics, School of Physics and Astronomy, *Shanghai Jiao Tong University*, Key Laboratory for Particle Astrophysics and Cosmology (MOE), SKLPPC, Shanghai, China
^{144b}State Key Laboratory of Dark Matter Physics, Tsung-Dao Lee Institute, *Shanghai Jiao Tong University*, Shanghai, China
¹⁴⁵Department of Physics and Astronomy, *University of Sheffield*, Sheffield, United Kingdom
¹⁴⁶Department of Physics, *Shinshu University*, Nagano, Japan
¹⁴⁷Department Physik, *Universität Siegen*, Siegen, Germany
¹⁴⁸Department of Physics, *Simon Fraser University*, Burnaby BC, Canada
¹⁴⁹SLAC National Accelerator Laboratory, Stanford, California, USA

- ¹⁵⁰Department of Physics, Royal Institute of Technology, Stockholm, Sweden
¹⁵¹Departments of Physics and Astronomy, Stony Brook University, Stony Brook, New York, USA
¹⁵²Department of Physics and Astronomy, University of Sussex, Brighton, United Kingdom
¹⁵³School of Physics, University of Sydney, Sydney, Australia
¹⁵⁴Institute of Physics, Academia Sinica, Taipei, Taiwan
^{155a}E. Andronikashvili Institute of Physics, Iv. Javakhishvili Tbilisi State University, Tbilisi, Georgia
^{155b}High Energy Physics Institute, Tbilisi State University, Tbilisi, Georgia
^{155c}University of Georgia, Tbilisi, Georgia
¹⁵⁶Department of Physics, Technion, Israel Institute of Technology, Haifa, Israel
¹⁵⁷Raymond and Beverly Sackler School of Physics and Astronomy, Tel Aviv University, Tel Aviv, Israel
¹⁵⁸Department of Physics, Aristotle University of Thessaloniki, Thessaloniki, Greece
¹⁵⁹International Center for Elementary Particle Physics and Department of Physics, University of Tokyo, Tokyo, Japan
¹⁶⁰Graduate School of Science and Technology, Tokyo Metropolitan University, Tokyo, Japan
¹⁶¹Department of Physics, University of Toronto, Toronto, Ontario, Canada
^{162a}TRIUMF, Vancouver BC, Canada
^{162b}Department of Physics and Astronomy, York University, Toronto, Ontario, Canada
¹⁶³Division of Physics and Tomonaga Center for the History of the Universe, Faculty of Pure and Applied Sciences, University of Tsukuba, Tsukuba, Japan
¹⁶⁴Department of Physics and Astronomy, Tufts University, Medford, Massachusetts, USA
¹⁶⁵Department of Physics and Astronomy, University of California Irvine, Irvine, California, USA
¹⁶⁶University of West Attica, Athens, Greece
¹⁶⁷Department of Physics and Astronomy, University of Uppsala, Uppsala, Sweden
¹⁶⁸Department of Physics, University of Illinois, Urbana, Illinois, USA
¹⁶⁹Instituto de Física Corpuscular (IFIC), Centro Mixto Universidad de Valencia—CSIC, Valencia, Spain
¹⁷⁰Department of Physics, University of British Columbia, Vancouver BC, Canada
¹⁷¹Department of Physics and Astronomy, University of Victoria, Victoria BC, Canada
¹⁷²Fakultät für Physik und Astronomie, Julius-Maximilians-Universität Würzburg, Würzburg, Germany
¹⁷³Department of Physics, University of Warwick, Coventry, United Kingdom
¹⁷⁴Waseda University, Tokyo, Japan
¹⁷⁵Department of Particle Physics and Astrophysics, Weizmann Institute of Science, Rehovot, Israel
¹⁷⁶Department of Physics, University of Wisconsin, Madison, Wisconsin, USA
¹⁷⁷Fakultät für Mathematik und Naturwissenschaften, Fachgruppe Physik, Bergische Universität Wuppertal, Wuppertal, Germany
¹⁷⁸Department of Physics, Yale University, New Haven, Connecticut, USA
¹⁷⁹Yerevan Physics Institute, Yerevan, Armenia

^aAlso at Department of Physics, King's College London, London, United Kingdom.^bAlso at Institute of Physics, Azerbaijan Academy of Sciences, Baku, Azerbaijan.^cAlso at Imam Mohammad Ibn Saud Islamic University, Saudi Arabia.^dAlso at TRIUMF, Vancouver BC, Canada.^eAlso at Department of Physics, University of Thessaly, Greece.^fAlso at An-Najah National University, Nablus, Palestine.^gAlso at Department of Physics, University of Fribourg, Fribourg, Switzerland.^hAlso at Department of Physics, Westmont College, Santa Barbara, USA.ⁱAlso at Departament de Fisica de la Universitat Autònoma de Barcelona, Barcelona, Spain.^jAlso at University of Sienna, Italy.^kAlso at Affiliated with an institute formerly covered by a cooperation agreement with CERN.^lAlso at The Collaborative Innovation Center of Quantum Matter (CICQM), Beijing, China.^mAlso at Faculty of Physics, Sofia University, 'St. Kliment Ohridski', Sofia, Bulgaria.ⁿAlso at Università di Napoli Parthenope, Napoli, Italy.^oAlso at Institute of Particle Physics (IPP), Canada.^pAlso at Department of Physics, Bolu Abant Izzet Baysal University, Bolu, Türkiye.^qAlso at Faculty of Physics, University of Bucharest, Romania.^rAlso at Borough of Manhattan Community College, City University of New York, New York NY, USA.^sAlso at National Institute of Physics, University of the Philippines Diliman (Philippines), Philippines.^tAlso at Department of Financial and Management Engineering, University of the Aegean, Chios, Greece.^uAlso at Institutio Catalana de Recerca i Estudis Avancats, ICREA, Barcelona, Spain.^vAlso at Henan University, China.^wAlso at CMD-AC UNEC Research Center, Azerbaijan State University of Economics (UNEC), Azerbaijan.^xAlso at Yeditepe University, Physics Department, Istanbul, Türkiye.^yAlso at Institute of Theoretical Physics, Ilia State University, Tbilisi, Georgia.

^zAlso at CERN, Geneva, Switzerland.

^{aa}Deceased.

^{ab}Also at Center for Interdisciplinary Research and Innovation (CIRI-AUTH), Thessaloniki, Greece.

^{ac}Also at Hellenic Open University, Patras, Greece.

^{ad}Also at Department of Modern Physics and State Key Laboratory of Particle Detection and Electronics, University of Science and Technology of China, Hefei, China.

^{ae}Also at Department of Mathematical Sciences, University of South Africa, Johannesburg, South Africa.

^{af}Also at Department of Physics, Stellenbosch University, South Africa.

^{ag}Also at University of Colorado Boulder, Department of Physics, Colorado, USA.

^{ah}Also at Département de Physique Nucléaire et Corpusculaire, Université de Genève, Genève, Switzerland.

^{ai}Also at Institut für Experimentalphysik, Universität Hamburg, Hamburg, Germany.

^{aj}Also at Centre of Physics of the Universities of Minho and Porto (CF-UM-UP), Portugal.

^{ak}Also at Institute for Nuclear Research and Nuclear Energy (INRNE) of the Bulgarian Academy of Sciences, Sofia, Bulgaria.

^{al}Also at Washington College, Chestertown, MD, USA.

^{am}Also at Institute of Applied Physics, Mohammed VI Polytechnic University, Ben Guerir, Morocco.

^{an}Also at Department of Physics, Stanford University, Stanford CA, USA.

^{ao}Also at Institute of Physics and Technology, Mongolian Academy of Sciences, Ulaanbaatar, Mongolia.